Acta Pharm. Sci. Vol 55 No: 1. 2017
DOI: 10.23893/1307-2080.APS.0551

Molecular Modelling and Activity Analysis of Mycobacterium tuberculosis DNA Gyrase B ATPase Active Site

Barkın Berk[1]*, Zafer Şahin[1]

[1] İstanbul Medipol University, School of Pharmacy, 34810, İstanbul, Turkey.

ABSTRACT

Computer-based algorithms and statistical techniques such as receiver operating characteristic (ROC) curves are increasingly used for the design of new ligands. X-ray crystallographic data and homology models allow examining the interactions between ligands and biomacromolecules using different algorithms and techniques. DNA gyrase enzyme inhibition is an alternative approach to clinical antimicrobial therapy for multi-drug resistant *Mycobacterium tuberculosis* (MT).

In this study, different datasets were created by enriching 1,442,716 compounds using known DNA GyrB ATPase inhibiting molecules. HTVS was performed on a previously designed homology model of MT DNA GyrB ATPase active site and true-positive scores were verified using ROC curves. Furthermore, 11 molecules with high scores were tested for their activity and the compound with the 5-(4-aminophenoxy)-2-(3-aminophenyl)-2,3-dihydro-1*H*-isoindole-1,3-dione structure was found to have similar activities to standard novobiocin. Finally, molecular interaction field and distance/interaction probability analyses were performed on the pose to identify new probable active derivatives of this compound.

Keywords: HTVS, ROC curves, Docking, *Mycobacterium tuberculosis*, DNA Gyrase B ATPase

INTRODUCTION

According to the World Health Organization (WHO), on average, 8 to 10 million people are exposed to tuberculosis (TB) every year and this number is still increasing. Pulmonary tuberculosis originating from *Mycobacterium tuberculosis* (MT) is one of the major causes of death in patients infected with the hu-

*Corresponding author: Barkın Berk
E-mail address: bberk@medipol.edu.tr

man immunodeficiency virus. Clinically, the most common problem concerning tuberculosis is its 'multidrug resistance' since there is no regime or new drug that can overcome this resistance[1].

Mycobacterium is an organism which has its own idiosyncratic family, Mycobacteriaceae with 140 well-defined and investigated species[2]. Of the species of this family that have spread over wide areas, *M. tuberculosis*, *M. bovis, M. africanum*, and *M. microti* are responsible for the development of tuberculosis, and *M. leprae* and its subspecies are responsible for the development of leprosy[3].

The genome structure of MT consists of 4,411,529 base pairs and 4,000 genes providing this species with various and rapid coding capacity and ease of adaptation to the development of multidrug resistance unlike any other subspecies of the same family[4]. There are two different approaches to seeking a treatment option for multi-drug resistant tuberculosis (MDR-TB). The first is to find and validate new biomacromolecular targets in the biochemical pathways of MT or test molecules with known structures over validated targets that have not previously been tested for MDR-TB. However, this is not the first preference due to the fast adaptation capacity of MT. The second approach involves an exploration of new compounds including tetracycline, cephalosporin and quinolone ring systems and further investigation of existing and validated targets [5].

DNA gyrase is a type of topoisomerase II, introducing supercoils to DNA using ATP hydrolyse energy. It is constructed by GyrA and GyrB subunits, which merge to form the heterodimer A_2B_2 structure. The amino terminal of the GyrB subunit (43kDa) is responsible for ATPase activity and the carboxy-terminal (47kDa) facilitates the interaction between protein A and DNA. Together, GyrA and GyrB break and reunite DNA. In this process, GyrB utilises the energy released from ATP hydrolyse at the N-terminal[6]. With this function, either the DNA or ATP binding cavities can be blocked by inhibitors for the termination of growth; therefore, DNA gyrase of MT has become a precious dual target for the treatment of MDR-TB.

Fluoroquinolones, DNA binding cavity inhibitors, are the only group of DNA gyrase inhibitors that are clinically used. However, along with rapid bacterial resistance, fluoroquinolones present with serious side effects and toxicity[7]. Therefore, the catalytic domain (ATPase) of GyrB N-terminal has become a popular topic of research[8].

In general, a computer-assisted drug design follows ligand- and structure-based methodologies, in which ligand libraries are virtually screened using various techniques. In the past few decades, these designs have led to the development

of successful drug molecules including dorzolamide, imatinib and raltegravir [9-14]. Although various valuable crystal structures of the DNA gyrase of MT have been proposed to enlighten its working mechanism [15-17], none has so far demonstrated the interaction between major inhibitor novobiocin and the catalytic domain (ATPase) of GyrB. Previously, we designed a homology model of MT DNA GyrB ATPase active site using the crystal structure of the 43K ATPase domain of *Thermus thermophilus* gyrase B in complex with novobiocin (RSCB Pdb id; 1KIJ) as a template and maintaining novobiocin and water in the hydrophobic pocket, which are assumed to be important for the ligand activity [18].

In the present study, we prepared various datasets for the enrichment of 1,442,716 compounds from the ZINC database using known DNA GyrB ATPase active molecules and performed high throughput virtual screening (HTVS) with different docking protocols to evaluate the role of water molecules in the ligand-binding cavity. In addition, the evaluation of docking scores using ROC curves allowed us to verify the true positive binders that can be used as cores in future studies. Moreover, eleven molecules with the highest score were tested using the MT gyrase supercoiling assay against the novobiocin standard for inhibitor activities. Finally, we identified molecular interaction fields (MIF) and performed a distance/interaction probability analysis on the active ligand to investigate how new probable active derivatives can be produced from the core.

METHODOLOGY

Materials

The dataset used in this study is a pre-prepared subset of the ZINC data bank, 'clean-leads-subset (# 11)' (logP values < 3.5, molecular weight < 350, rotational number of bonds £7 and 1.442.716 compounds,). The compounds selected for biological testing were purchased from Molport Chemicals (Latvia) with 99.5% minimum purity and used after confirming the results of the LC-MS/MS and elemental analysis supplied by the dealer.

The preparation of the protein structure and ligands, trial and test sets, grid files, docking and scoring were performed using algorithms from the Maestro modules (Schrodinger Inc, USA). For the preparation of ROC curves and interaction graphics, the Molecular Operating Environment (MOE) software (Chemical Computing Group Inc., Canada) was used and the MIF analysis was performed in the GRID 22c software (Molecular Discovery Inc, UK).

The biological activities were tested using the MT gyrase supercoiling assay (Inspiralis Inc. UK, MTS001 and MTS002) and novobiocin as the reference standard (CAS, 1476-53-5, AppliChem, Germany).

Homology modelling and preparation of protein structure

The homology model used in this study was simulated using the crystallographic structure of *Thermus thermophilus* Gyrase B 43k ATPase domain in a complex form with novobiocin (Pdb id; 1KIJ, resolution; 2.30 A°). This structure was chosen due to its 43% sequence similarity (Basic Local Alignment Search Tool, E value: 2e-77) to the MT DNA GyrB sequence of the UniProtKB database (UniProtKB/Swiss-Prot P0C5C5). During modelling, various water molecules which were assumed to be responsible for ligand-protein interactions were maintained as recommended in previous research[19]. Furthermore, the protein preparation wizard from the workflows menu of Maestro was utilised for hydrogen insertion, rotamer adjustment and H-bond optimization using the parameters of Optimized Potentials for Liquid Simulations (OPLS 2005) force field.

Preparation of trial and test sets

Initially, the 'clean-leads-subset (# 11)' with the characteristics given above were downloaded from the ZINC database in the sdf format. This dataset was enriched with 29 DNA gyrase ATPase site ligands, the activity of which had previously been proven. The ligands were prepared using the LigPrep module of Maestro (Schrodinger Inc.) by generating possible ionization (pH 7±2) and tautomeric states. Duplicated structures and salt forms were eliminated. During the course of the study, the enriched dataset was used as a whole as the 'test set' and randomly selected 11,000 plus 29 active compounds were used as the 'trial set'.

Preparation of grid files

All the grid files for the MT DNA gyrase ATPase active sites were prepared using the Maestro Glide-Receptor Grid Generation tool. A receptor-binding pocket was defined by taking 6 A° surrounding area of novobiocin as the centroid. During preparation, the original ligand was excluded and a scaling factor of 1.0 and a partial charge cut-off of 0.25 were used as the parameters for the Van der Walls radius-scaling factor. Using these parameters, two different grid files were prepared;

- Unrestricted (positioning all the compounds based on the original ligand being the centroid)
- Restricted with ASP 79 and/or HOH 539 (either making bond with ASP 79 and/or HOH 539 or defining the position of ligands based on the position of HOH 539)

Trial set docking, scoring and ROC curves

The trial set was docked using Glide HTVS, SP and XP protocols in the unrestricted and restricted grid files. The basic settings for HTVS, SP and XP algorithms were set as; treating the receptor as rigid and the ligands as flexible, dock-

ing without using a core pattern comparison algorithm, using the constraints from grid files if needed, writing 100,000 poses per docking run and performing a post-docking minimization on the top five poses. The glide docking score was used as the principal score parameter. Then, the results were transferred to the MOE software in the sdf format, re-opened, lined up in an ascending manner corresponding to the maximum docking score for each compound and evaluated using ROC curves with SVL scripts in MOE.

Test set, docking, scoring and ROC curves

The test set was docked using the Glide HTVS methodology and restricted grid files. Then, to reduce the computer load, 240,000 molecules with the highest score were re-docked following the SP protocol and rescored in place by the XP algorithm. For experimental consistency, the basic settings for HTVS, SP and XP algorithms and the steps followed for the evaluation of ROC curves were kept the same as those used for the trial set.

Biological activity

Eleven compounds were tested with the MT gyrase supercoiling assay at the concentrations of 1 mg/20, 50, 100 μL using novobiocin as the reference standard for comparison purposes. Furthermore, the most active compound, 5-(4-aminophenoxy)-2-(3-aminophenyl)-2,3-dihydro-1*H*-isoindole-1,3-dione (10), was re-evaluated in the concentration range of 0.1to 2 mg/100 μL (2.8-57 mM) compared to the same concentrations of novobiocin (1.6-32 mM).

DNA gyrase supercoiling assays were performed according to the manufacturer's instructions and analysed by monitoring the conversion of relaxed pBR322 plasmid to its supercoiled form using DNA gel electrophoresis. Essentially, 1 U of either *E. coli* or *S. aureus* DNA gyrase was first diluted in a 5×gyrase buffer and incubated in an assay buffer (35 mM Tris HCl at pH 7.5, 24 mM KCl, 4 mM MgCl 2, 2 mM DTT, 1.8 mM spermidine, 1 mM ATP, 6.5% w/v glycerol, and 0.1 mg/mL BSA) with 0.5 μg of pBR322 plasmid and compound dilutions at 37 °C for 30 min. Reactions were stopped with the addition of stop dye (40% sucrose, 100 mM Tris HCl at pH 7.5, 1 mM EDTA, and 0.5 mg/mL bromophenol blue) and loaded onto TAE agarose gel (1%). Gels were visualised using a gel documentation system (Bio-Rad ChemiDoc). Since high levels of dimethyl sulfoxide (DMSO) are known to affect DNA gyrase activity, titration was used to determine the minimum amount of DMSO to be used in the assays, and 5% DMSO (with negligible or no effect on gyrase) was chosen to dilute the compounds[20].

MIF and distance/interaction probability analysis

The maximum scoring docking pose of 5-(4-aminophenoxy)-2-(3-

aminophenyl)-2,3-dihydro-1*H*-isoindole-1,3-dione (10) was converted to the pdb format and re-opened in the greater user interface of GRID 22c (Molecular Discovery Inc, England). During grid manufacturing process, automatic settings were used for loading, file correction and site marking around ligands. The calculations were run using the following; R-NH_2 (including unbounded electrons), R_1R_2NH (including unbounded electrons), $CONH_2$, ROR, RCOR, R-OH, Ph-OH, water and hydrophobic probes and charges were kept the same. All visualisations were performed in the MOE software. The distance/interaction probability analysis was conducted using the 'Ligand-receptor contacts (visualisation+scoring) svl'.

RESULTS AND DISCUSSION

Trial set docking, scoring and ROC curves

The enriched trial set was docked to the homology model and scored using HTVS, SP and XP algorithms with both unrestricted and restricted grid files. During this process, the native ligand novobiocin was docked to its original position smoothly (RMSD 0.83-0.85 A°) showing similarities and interactions with the original x-ray crystallographic data.

A weakness of the docking program is related to the scoring functions. In this study, we used maximum docking scores for ROC curves to evaluate accuracy powers in discriminating interaction patterns. The ROC curves used in these experiments are plots of the true positive rate (sensitivity) against the false positive rate (specificity) for different possible cut points. They show the trade-off between sensitivity and specificity where any increase in sensitivity is accompanied by a decrease in specificity. The closer any curve follows first the left-hand and then the top border of the ROC space, the higher the accuracy is. The accuracy of our tests depended on how the groups being tested were separated into those with and without experimental activity. Accuracy is measured by the area under the ROC curve. An area of 1 represents a perfect test and an area of 0.5 indicates a poor test. Similar to the regression analysis, when an area approaches 1, the power of discrimination increases. Table 1 presents the area under curve (AUC) values of the grid files for each algorithm.

Table 1: Area under curve values of the trial set using restricted and unrestricted grid files according to HTVS, SP and XP protocols

	Area under curve values from ROC	
	Unrestricted grid file	Restricted grid file
HTVS	0.73206	0.74175
SP	0.7763	0.79532
XP	0.7871	0.8010

The clear steady increase shown in Table 1 indicates that using a restricted grid file restricted with ASP 79 and/or HOH 539 or by defining the position of ligand based on the position of HOH 539 both gave better results in terms of ligand positioning during docking and successfully discriminated false positives. In the light of these results, we decided to continue with the restricted grid file for the further evaluation of the test set.

Test set docking, scoring and ROC curves

Based on the ROC evaluated AUC from the trial set, deciding on further dockings restricted to certain bonding to ASP 79 and/or HOH 539 is a challenge since it is virtually essential to eliminate all the water molecules. The reason for this is that in some docking algorithms such as molecular dynamic and induced fit in which both the receptor and the ligands are flexible to a certain degree, the free water molecules can easily cause various problems. This is why in this study we kept the receptor rigid and the ligand flexible. In addition, previous crystallographic data showed that bonding with ASP 79 through bridging water exactly in this position facilitates further interactions[18].

In the test set, over a million compounds were processed during docking calculations and AUC was reduced only by 2%. Then, to decrease the process time and computer load after HTVS, we decided to have a cut-off point for 240,000

	AUC values	ROC
HTVS	0.7198	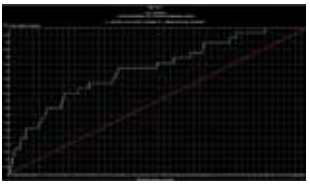
SP	0.7500	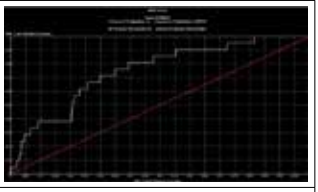
XP	0.7828	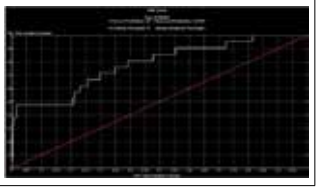

Figure 1: Area under curve and ROC curves of the test set using the restricted grid file and the HTVS, SP and XP protocols

compounds with high scores and further docked and rescored them with SP and XP protocols. Figure 1 shows the AUC and ROC values for each protocol using the grid file restricted with ASP 79 and/or HOH 539.

Of the 239,737 compounds scored by the XP algorithm using the chosen grid file, 12 with the highest score were sorted in descending order with ZINC database codes and evaluated for biological activity (Figure 2). The reason for selecting the top 12 compounds was that Compound 13 was the first active compound after the docking procedure and had the following structure; methyl 3-{[(4-[(3,4-dichlorobenzyl)oxy]-1H-indazol-3-yl)methyl]amino}cyclohexanecarboxylate. This active structure of Compound 13 has also been reported in previous studies[21,22].

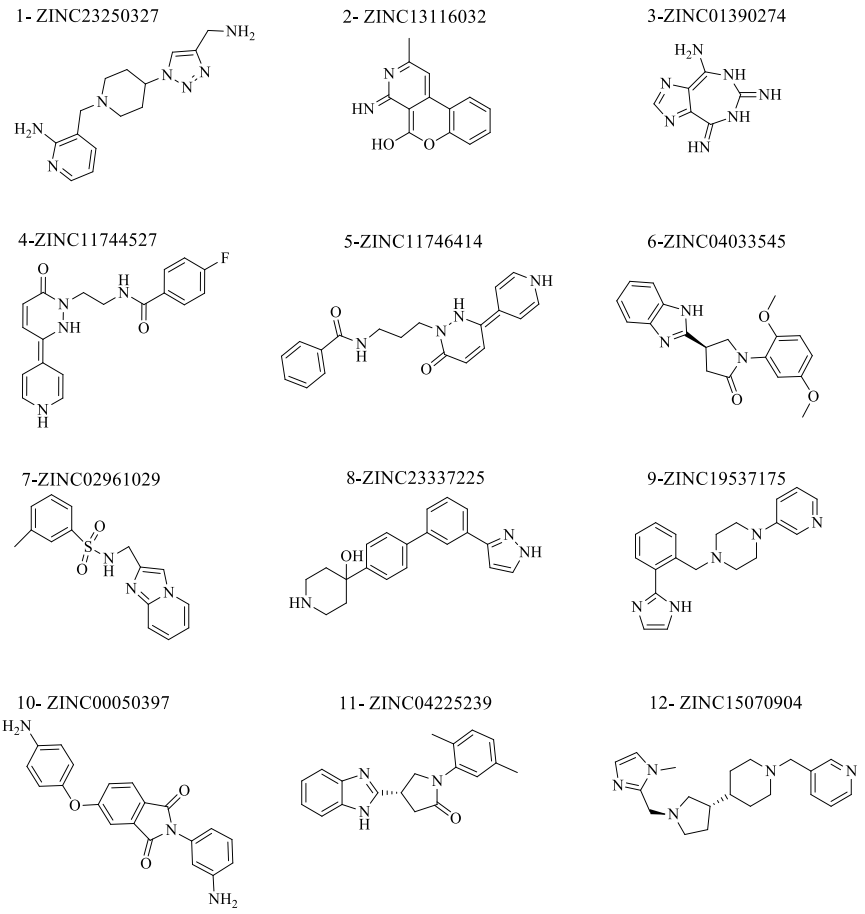

Figure 2: Compounds of the test set that scored highest using the XP algorithm.

Biological activity

Compound 2 was synthesized with <95% purity and thus was discarded from biological testing. The remaining eleven compounds were tested against standard novobiocin with the MT gyrase supercoiling assay at the concentrations of 1 mg/20μL, 1 mg/50μL and 1 mg/100μL (w/v). Among all compounds, only Compound 10 with the 5-(4-aminophenoxy)-2-(3-aminophenyl)-2,3-dihydro-1*H*-izoindole-1,3-dione structure showed a similar inhibitor activity compared to the standard. The results of gel electrophoresis at 1 mg/100μL concentration of each compound are given in Figure 3.

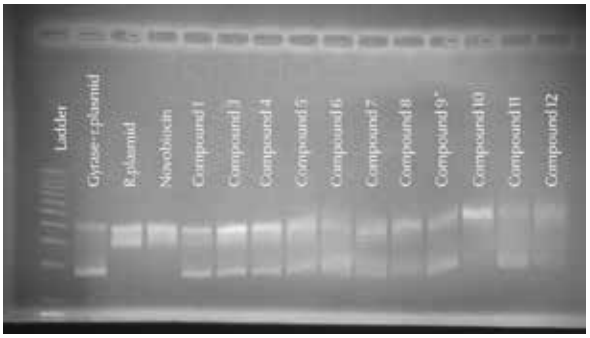

Figure 3: Results of gel electrophoresis with 1 mg/100μL (w/v) dilution super-coiled (Gyrase+r. plasmid), relaxed (r. plasmid) Novobiocin (r. plasmid+gyrase+novobiocin)

Additional analyses for the activity of Compound 10 were performed in decreasing order within a concentration rage of 0.1 to 2 mg/100 μL (2.8-57 mM) compared to the same concentrations of novobiocin (1.6-32 mM) (Figure 4). The results clearly showed that Compound 10 had similar effectiveness to the standard and needed further evaluation as a core.

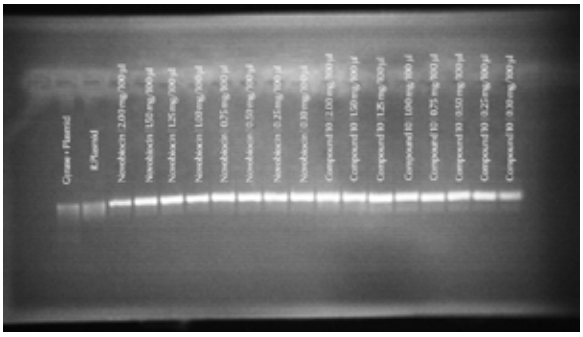

Figure 4: Efficiency scale of increasing concentrations of novobiocin and Compound 10 in the existence of gyrase super-coiled and relaxed plasmid (Gyrase + Plasmid).

MIF and distance/interaction probability analysis

The MIF analysis between the homology model and Compound 10 based on the selected probes of GRID 22c demonstrated that ROR and RCOR probes were not effective. The visualisations of R-NH_2 (including unbounded electrons), R_1R_2NH (including unbounded electrons), $CONH_2$, R-OH, Ph-OH, water and hydrophobic probes are presented in Figure 5.

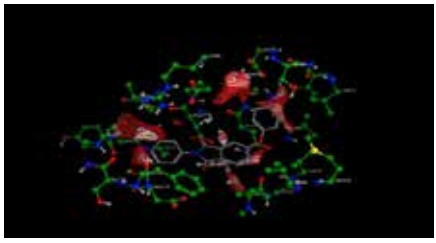

R-NH_2 (red) and R_1R_2NH (white)

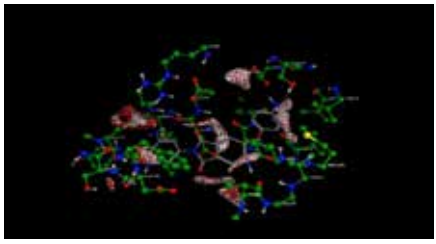

R-OH (red) and Ph-OH (white)

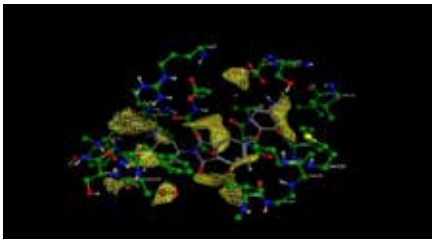

H_2O (yellow)

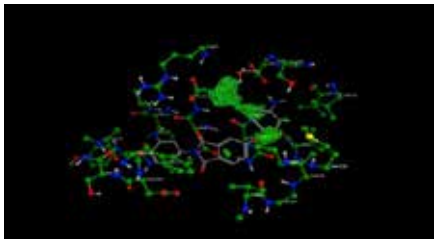

Hydrophobic (green)

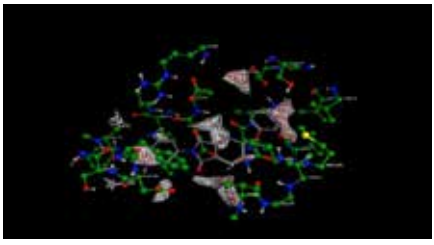

$CONH_2$

Figure 5: MIFs of Compound 10 with different probes

H-bond and hydrophobic interaction distances and probabilities between Compound 10 and the homology model were examined using the 'Ligand-receptor contacts (visualisation+scoring)' svl in the MOE software based on Bohm's similar calculation algorithm (Figure 6).

Both primary amine groups belonging to the phenoxy and phenyl substituents of Compound 10 were susceptible to the H-bonds with ASP 79 and 55 at a percentage of 81 (distance (d):2.7A^o) and 22 (d: 3.4A^o), respectively. Furthermore, hy-

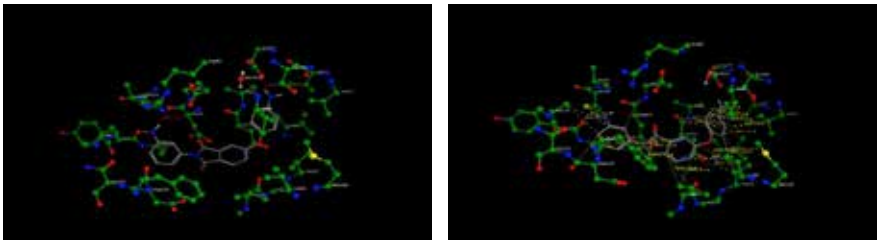

Figure 6: H-bond and hydrophobic interaction distances and probabilities between Compound 10 and the homology model (H-bonds: left-white, hydrophobic interactions: right-yellow)

drophobic interaction tendencies were observed between the ligands' aromatic groups and the active site. The first was between the 4-aminophenyl group and the surrounding Asp 55, Phe 109, Ser, 111 and Ala 11 amino acids. The second interaction was between the central isoindole ring and the surrounding Phe 109, Val 113, Val 123 (81-89%, d: 4.4-4.6 A°)). Finally, the 3-aminophenyl group and the surrounding Ala 53, Ile 84, Val 125 and Val 171 were found to have a hydrophobic interaction(81-92%, d: 4.3-4.6 A°).

The MIF analysis showed that the 4-aminophenyl group fits into the hydrophobic pocket surrounded by Val; 49, 77, 125, 171, Ile 84 and Arg 92. The same site controls the condensed phenyl part of the isoindole ring providing an angle between the ether bridge and the 4-aminophenyl group. The 3- aminophenyl group interacts with Ala 59, Ser 111 and Asp 110 alpha carbons on the loop site of a protein. Therefore, the most appropriate structures for the hydrophobic pocket appear to be the aromatic ones. The substituted amines, hydroxyl or the amide functional group seemed to facilitate better interactions than the primary amine of the phenyl group. The distance between the isoindole ring and the 4-aminophenoxy group should be maximum 1.4 A°. Ether bridge is not actually a requirement for receptor-ligand interaction. Furthermore, the 4^{th} carbon of the isoindole ring can be converted to nitrogen for more suitable interactions. In addition, we suggest that amino substation on the 3^{rd} carbon of the phenyl group should be re-located to the 4^{th} and 5^{th} positions to increase the activity. The attachment of probable hydrogen bonding groups to the phenyl ring appears to be suitable for accurate bonding with Asp55. The results indicate that preserving the isoindole ring system is important for modifications to the ring system and for hydrophobic stabilisation with the surrounding amino acids.

The results of this study showed that ROC curves can be effectively used for the correction of scoring functions not only in x-ray crystallographic data, but also in homology models. For future work, we are planning to use the results of MIF and interaction probability to design new isoindole derivatives, which may be beneficial for DNA gyrase B ATPase inhibition.

ACKNOWLEDGEMENT

This work was financially supported by the Scientific and Technological Research Council of Turkey (TÜBİTAK), Grant Number: SBAG-110S017.

REFERENCES

1. Tomioka, H.; Namba, K., [Development of Antituberculous Drugs: Current Status and Future Prospects]. *Kekkaku : [Tuberculosis]* **2006**, *81* (12), 753-774.

2. Us, D.; Berk, B.; Gurdal, E., et al., Mannich Base Derivatives of 3-Hydroxy-6-Methyl-4h-Pyran-4-One with Antimicrobial Activity. *Turk. J. Chem.* **2010**, *34* (3), 447-456.

3. Katoch, V. M., Infections Due to Non-Tuberculous Mycobacteria (Ntm). *Indian J. Med. Res.* **2004**, *120* (4), 290-304.

4. Cole, S. T.; Brosch, R.; Parkhill, J., et al., Deciphering the Biology of Mycobacterium Tuberculosis from The Complete Genome Sequence. *Nature* **1998**, *393* (6685), 537-544.

5. Khisimuzi, M.; Zhenkun, M., Mycobacterium Tuberculosis DNA Gyrase as a Target for Drug Discovery. *Infect. Disord. Drug Targets* **2007**, *7* (2), 159-168.

6. Maxwell, A., DNA Gyrase as a Drug Target. *Trends Microbiol.* **1997**, *5* (3), 102-109.

7. Leone, R.; Venegoni, M.; Motola, D., et al., Adverse Drug Reactions Related to the Use of Fluoroquinolone Antimicrobials: An Analysis of Spontaneous Reports and Fluoroquinolone Consumption Data from Three Italian Regions. *Drug Safety* **2003**, *26* (2), 109-120.

8. Us, D.; Gurdal, E.; Berk, B., et al., 4h-Pyran-4-One Derivatives:; Leading Molecule for Preparation of Compounds with Antimycobacterial Potential. *Turk. J. Chem.* **2009**, *33* (6), 803-812.

9. McInnes, C., Virtual Screening Strategies in Drug Discovery. *Curr. Opin. Chem. Biol.* **2007**, *11* (5), 494-502.

10. Greer, J.; Erickson, J. W.; Baldwin, J. J.; Varney, M. D., Application of the Three-Dimensional Structures of Protein Target Molecules in Structure-Based Drug Design. *J. Med. Chem.* **1994**, *37* (8), 1035-1054.

11. Gubernator, K.; Bèohm, H.-J., *Structure-Based Ligand Design*. Wiley-VCH: Weinheim ; New York, **1998**; p xiv, 153 p.

12. Capdeville, R.; Buchdunger, E.; Zimmermann, J.; Matter, A., Glivec (Sti571, Imatinib), a Rationally Developed, Targeted Anticancer Drug. *Nat. Rev. Drug Discov.* **2002**, *1* (7), 493-502.

13. Kroemer, R. T., Structure-Based Drug Design: Docking and Scoring. *Curr. Protein Sept. Sci.* **2007**, *8* (4), 312-328.

14. Rester, U., From Virtuality to Reality - Virtual Screening in Lead Discovery and Lead Optimization: A Medicinal Chemistry Perspective. *Curr. Opin. Drug Discov. Devel.* **2008**, *11* (4), 559-568.

15. Blower, T. R.; Williamson, B. H.; Kerns, R. J.; Berger, J. M., Crystal Structure and Stability of Gyrase-Fluoroquinolone Cleaved Complexes from Mycobacterium Tuberculosis. *Proc. Natl. Acad. Sci. U S A* **2016**, *113* (7), 1706-1713.

16. Agrawal, A.; Roue, M.; Spitzfaden, C., et al., Mycobacterium Tuberculosis DNA Gyrase Atpase Domain Structures Suggest a Dissociative Mechanism That Explains How Atp Hydrolysis Is Coupled to Domain Motion. *Biochem. J.* **2013**, *456* (2), 263-273.

17. Shirude, P. S.; Madhavapeddi, P.; Tucker, J. A., et al., Aminopyrazinamides: Novel and Specific Gyrb Inhibitors That Kill Replicating and Nonreplicating Mycobacterium Tuberculosis. *ACS Chem. Biol.* **2013**, *8* (3), 519-523.

18. Lamour, V.; Hoermann, L.; Jeltsch, J. M., et al., An Open Conformation of the Thermus Thermophilus Gyrase B Atp-Binding Domain. *J. Biol. Chem.* **2002**, *277* (21), 18947-18953.

19. Berk, B.; Us, D.; Oktem, S., et al., Molecular Modeling and Antimycobacterial Studies of Mannich Bases: 5-Hydroxy-2-Methyl-4h-Pyran-4-Ones. *Turk. J. Chem.* **2011**, *35* (2), 317-330.

20. Maxwell, A.; Burton, N. P.; O'Hagan, N., High-Throughput Assays for DNA Gyrase and Other Topoisomerases. *Nucleic Acids Res.* **2006**, *34* (15), e104.

21. Tanitame, A.; Oyamada, Y.; Ofuji, K., et al., Design, Synthesis and Structure-Activity Relationship Studies of Novel Indazole Analogues as DNA Gyrase Inhibitors with Gram-Positive Antibacterial Activity. *Bioorg. Med. Chem. Lett.* **2004**, *14* (11), 2857-2862.

22. Tanitame, A.; Oyamada, Y.; Ofuji, K., et al., Potent DNA Gyrase Inhibitors; Novel 5-Vinylpyrazole Analogues with Gram-Positive Antibacterial Activity. *Bioorg. Med. Chem. Lett.* **2004**, *14* (11), 2863-2866.

(Received 25 September 2016; accepted 11 October 2016)

Acta Pharm. Sci. Vol 55 No: 1. 2017
DOI: 10.23893/1307-2080.APS.0552

Biorelevant and Quality Control Dissolution Method Development and Validation of Quetiapine Fumarate Tablets

Muhsina Taskeen[1], Mamatha Tirunagari [1*], Husna. K Qureshi[2]

[1] Department of Quality Assurance, Sultan – Ul –Uloom College of Pharmacy, Road No: 3, Banjara Hills, Hyderabad – 500034, Telangana State, India.
[2] Bojjam Narasimhulu Pharmacy College for Women, Saidabad, Hyderabad – 500059, Telangana State, India.

ABSTRACT

The aim of this study was to develop and validate Biorelevant and Quality control dissolution method for poorly water soluble drug Quetiapine Fumarate (QF). The Ultra Violet spectrophotometric method developed was based on the direct estimation method using 248 nm as λmax. The method was validated according to International Conference on Harmonization (ICH) guidelines which include precision, specificity, accuracy and linearity. The Biorelevant dissolution medium i.e., Blank Fed State Simulated Intestinal Fluid (FeSSIF) and Quality control dissolution medium i.e., 0.1N Hydro Chloric acid were selected on the basis of solubility studies. Stability studies were performed in respective dissolution mediums and the sample solutions were found to be stable for 2 days. The corresponding Biorelevant and Quality control dissolution profiles were constructed and the selected brands showed more than 85% drug release within 20 min. Thus, the proposed Biorelevant and Quality control dissolution methods can be used successfully.

Keywords: Biorelevant, Dissolution, Quetiapine fumarate, UV spectrophotometry, Validation.

INTRODUCTION

Dissolution is a required performance test for solid dosage forms, transdermal patches and suspensions. It is also only test that measures the rate of *in vitro* drug release as a function of time, which can reflect either reproducibility of the product manufacturing process or, in limited cases, *in vivo* drug release. It is an important tool in drug development and quality control [1]. Dissolution

*Corresponding Author: Mamatha Tirunagari
E-Mail address: tmamatha12@gmail.com

test that can predict the *in vivo* performance of drug products are usually called biorelevant dissolution tests. These tests can be used to guide formulation development, to identify food effects on the dissolution and bioavailability of orally administered drugs, and to identify solubility limitations and stability issues[2]. Chemically quetiapine fumarate is 2-[-2(4-Dibenzo [b,f] [1.4] thiazepin-11-yl-1-piperazinyl) ethoxy] ethanol fumarate salt.[3] (Shown in Figure 1)

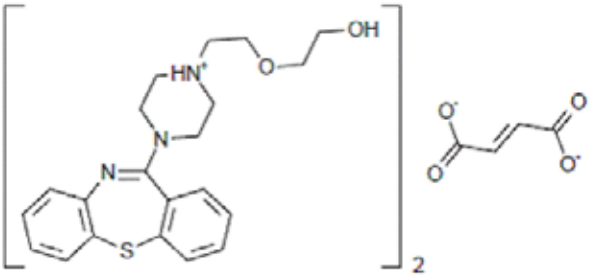

Figure 1. Chemical structure of Quetiapine fumarate.

Its molecular formula is $2(C_{21}H_{25}N_3O_2S).C_4H_4O_4$. QF appears as white crystalline solid and can be stored at room temperature[4]. It is an atypical antipsychotic drug, used in the treatment of psychosis associated with Parkinson's disease, chronic schizophrenia[5] and bipolar disorders[6]. The dibenzothiazepine structure with two basic nitrogen atoms is responsible for its higher solubility under acidic conditions. At a pH above 4, the water solubility is poor; towards pH 2, an increase in solubility is noticeable. Due to its poor solubility over the physiological pH range but because of its high permeability, quetiapine is classified as a Biopharmaceutics Classification System class II drug.[7]Quetiapine's antipsychotic activity is likely due to a combination of antagonism at D2 receptors in the mesolimbic pathway and 5HT2A receptors in the frontal cortex. Antagonism at D2 receptors relieves positive symptoms while antagonism at 5HT2A receptors relieves negative symptoms of schizophrenia.[8] In the present investigation an attempt was made to develop and validate a simple Biorelevant and quality control dissolution method for QF with greater precision and accuracy.

MATERIALS AND METHODS

Materials

Quetiapine fumarate pure drug was received as a gift sample for analyzing using UV spectrophotometry technique.[9, 10, 11] Sodium Chloride, Glacial Acetic acid, Sodium taurocholate, lecithin, methylene blue, hydrochloric acid (HCl) and Sodium hydroxide pellets were procured from SD Fine Chem LTD (Mumbai). All reagents and solvents used were of Analytical grade. The commercial products

of QF that is Quitipin®, Qutan®, Quel® were procured from local drug stores. Dissolution apparatus USP type II (USP model: TDT-06P, Electrolabs, India) and UV Spectrophotometer (UV model 1700, Shimadzu, Japan) were used.

Methods

Solubility Studies

Solubility data was used as the basis for the selection of the best solvent for dissolution of Quetiapine fumarate tablets. It was expressed as amount of drug dissolved. For equilibrium solubility studies, excess of the drug was placed in 25 ml beakers containing different media: Distilled water, 0.1N HCl (pH 1.2), pH 4.5 Acetate buffer, pH 6.5 Phosphate buffer, pH 7.4 Phosphate buffer and Blank Fed State Simulated Intestinal Fluid (FeSSIF). The samples were gently rotated in water bath shaker at 37 ± 0.5°C for 24 h. An aliquot (2 ml) was removed from each beaker after 24 h and filtered using 0.45 μm syringe filter. 1 ml of filtered samples were diluted with corresponding medium and analyzed by UV spectrophotometry at corresponding λ_{max}.

Stability studies

Stability studies were performed by preparing solutions of pure drug mixture and commercial products of the drug and preserving it for 2 days. An accurately weighed quantity of pure drug and tablet powder were dissolved in sufficient quantity of 0.1N HCl and Blank FeSSIF to get the final stock concentration. An aliquot of these stock solutions was diluted with 0.1N HCl and Blank FeSSIF to get the final concentration of 10 μg/ml. All the solutions were prepared in three replicates. The solutions were kept at 37 ± 0.5 °C for 1 h under light shaking, later being left at room temperature for 48 h. Aliquots of samples were analyzed spectrophotometrically after 1 h, 24 h and 48 h.[12]

Preparation of 0.1N HCl

Conc. HCl (85 ml) was dissolved in 1 L of distilled water to get 0.1N HCl solution.

Preparation of blank fed state simulated intestinal fluid (FeSSIF)

Blank FeSSIF (pH 5.0) was prepared by dissolving 11.874 g of sodium chloride, 8.65 g (8.238 ml) of glacial acetic acid and 4.04 g of sodium hydroxide pellets in 1 L of distilled water.

Preparation of fed state simulated intestinal fluid

FeSSIF was prepared by dissolving 8.25 g of sodium taurocholate in 250 ml of blank FeSSIF, 29.54 ml of a solution containing 100 mg/ml lecithin in methylene chloride is added to form an emulsion, and then methylene chloride is

eliminated under vacuum until a clear, micellar solution having no perceptible odor of methylene chloride is obtained. After cooling to room temperature, the volume is adjusted to 1 L with blank FeSSIF.

Quality Control Dissolution Method Development and Validation

UV Method Development & Determination of λ max

An accurately weighed quantity of QF was dissolved in suitable volume of 0.1N HCl to prepare the stock solution. An aliquot from this stock solution was diluted with 0.1N HCl to get a final concentration of 10µg/ml. All solutions were prepared in three replicates. The above solutions were scanned in the range of 200-400 nm in 1.0cm cell against 0.1N HCl and spectra were recorded to determine the λ_{max} of the drug. Figure 2 shows the UV absorption spectra of QF.

Preparation of standard solutions and calibration curve

Stock solution of QF was prepared by dissolving an accurately weighed quantity of QF in 0.1N HCl. From the stock solution various concentrations i.e., 1, 2, 3, 4, 5, 6, 7, 10, 15, 20 and 25 µg/ml were prepared. All solutions were scanned in wavelength range of 200-400 nm. The absorbance was plotted against the respective concentrations to obtain the calibration curve. The spectrum showing linearity of QF is given in Figure 3. The calibration data is shown in Table 3 and curve in Figure 4.

Validation Parameters

Validation of the proposed methods was carried out for its linearity & range, accuracy, specificity and precision according to ICH guidelines.[13, 14]

Linearity and Range

For the determination of linearity of QF in commercial products, sample solutions of different concentrations were prepared. The stock solution of QF for all the three brands were prepared by dissolving required amount of QF in suitable volume of 0.1N HCl. The solution was sonicated for 10 min and then filtered through Whatman filter paper. The solutions were further diluted to get concentrations in range of 1 – 25 µg/ml.

The absorbance of the above solutions was measured at 248 nm. A graph of absorbance v/s concentration was plotted and correlation coefficient is calculated. The linearity data for all the three brands is presented in Table 4. The graphs were constructed as concentration v/s absorbance and depicted in Figure 5 to Figure 7.

Acceptance criteria: Correlation coefficient should be within 0.997 – 0.999.

Accuracy

The accuracy was determined by performing recovery studies at three different concentration levels i.e., 50%, 100%, 150% in triplicate. The individual recovery and mean recovery values were calculated and are shown in Table 5 to 7 for all three brands.

Preparation of sample solutions:

Sample preparation of 50%: Tablet powder equivalent to 50 mg of QF and 25 mg of QF Active Pharmaceutical Ingredient were taken in 100 ml volumetric flask. Sufficient quantity of 0.1N HCl was added and sonicated to dissolve it and the volume was made up to the mark. Then the solution was filtered through Whatman filter paper and appropriate dilutions of 5, 10 and 15 µg/ml were prepared. The absorbance of final solutions was measured at 248 nm.

Sample preparation of 100%: Tablet powder equivalent to 50 mg of QF and 50 mg of QF API were taken in 100 ml volumetric flask. Sufficient quantity of 0.1N HCl was added and sonicated to dissolve it and the volume was made up to the mark. Then the solution was filtered through Whatman filter paper and appropriate dilutions of 5, 10 and 15 µg/ml were prepared. The absorbance of final solutions was measured at 248 nm.

Sample preparation of 150%: Tablet powder equivalent to 50 mg of QF and 75 mg of QF API were taken in 100 ml volumetric flask. Sufficient quantity of 0.1N HCl was added and sonicated to dissolve it and the volume was made up to the mark. Then the solution was filtered through Whatman filter paper and appropriate dilutions of 5, 10 and 15 µg/ml were prepared. The absorbance of final solutions was measured at 248 nm.

The absorbance of the standard solutions of 50%, 100% and 150% were measured. From this individual recovery and mean recovery values were calculated.

Acceptance criteria: The % recovery for each level should be between 98.0 to 102.0%.

Specificity

The specificity of test method was established by comparing the spectra of the sample solutions of same concentration of pure drug and commercial products. The similarity in spectra was shown in Figure 8.

Precision

The precision was determined by studying repeatability and intermediate precision. The stock solution of QF for all the three brands were prepared by dissolv-

ing an accurately weighed quantity of QF in sufficient volume of 0.1N HCl and sonicated for 10 min. The sample solution was then filtered through Whatman filter paper. The solution was further diluted to get 5 and 10 µg/ml solutions. All dilutions were prepared in triplicate.

Repeatability

To check repeatability, the samples of concentrations 5 µg/ml and 10 µg/ml were analyzed at 248 nm on same day and under same experimental conditions. % RSD was calculated and is shown in Table 8.

Intermediate precision (Interday and Intraday precision)

The interday precision was determined by analyzing the sample solutions of concentration 5 µg/ml and 10 µg/ml at 248 nm on different days under same experimental conditions. % RSD was calculated is shown in Table 9.

The intraday precision was determined by analyzing the sample solutions of concentration 5 µg/ml and 10 µg/ml at 248 nm, in two different laboratories on the same day. % RSD was calculated is shown in Table 10.

Quality Control Dissolution Method Development

The best dissolution medium was selected on the basis of the solubility studies. Various dissolution conditions were tested for the development of a suitable dissolution method for the dissolution of QF tablets. The following dissolution conditions were selected and the analytical method used was UV spectrophotometry.

Medium: 0.1N HCl

Volume : 900 ml

Apparatus: USP Type II (Paddle Apparatus)

RPM: 50

Temperature: 37 ± 0.5 °C

Time interval: 10, 20, 30, 45 min.

Preparation of test solution

A tablet was placed in each vessel of the six dissolution vessels of the tablet Dissolution Tester USP (Electrolab, India) containing 0.1N HCl dissolution medium after testing sink conditions. A 5 ml aliquot of the sample was withdrawn at 10, 20, 30, 45 min intervals replacing 5 ml of dissolution medium each time. The samples were filtered through Whatman filter paper.

Analysis of the dissolution samples

The filtered dissolution samples were analyzed spectrophotometrically and % drug release was calculated and shown in Table 11. The graph of percentage drug release versus time is shown in Figure 9.

Acceptance criteria: All the 6 tablets must show % drug release of more than 85%.

Biorelevant Dissolution Method Development

Based on solubility and stability studies the dissolution parameters includes Blank FeSSIF (900 ml) as medium in USP Type II (Paddle Apparatus) with 50 RPM maintained at temperature of 37 ± 0.5°C. A tablet was placed in each vessel of the six dissolution vessels after testing sink conditions. A 5 ml aliquot of the sample was withdrawn at 10, 20, 30, 45 min intervals replacing 5 ml of dissolution medium each time. The samples were filtered through Whatman filter paper. The Biorelevant dissolution samples were analyzed by UV spectrophotometry and % drug release was calculated and shown in Table 11. The graph of % drug release vs. time is shown in Figure 10.

Acceptance criteria: All the 6 tablets must show % drug release of more than 85%.

RESULTS AND DISCUSSION

Solubility studies

The solubility studies were performed in different media by placing excess of drug in the medium and gently shaking it for 1 h. The samples were collected and analyzed spectrophotometrically after 24 h. The results of solubility studies are given in Table 1. The drug is found to be soluble in 0.1N HCl and Blank FeSSIF. So it was selected as dissolution medium.

Solvent	Solubility (mg/ml)
Distilled water	3.3
0.1N HCl	35.6
Acetate buffer pH 4.5	5.8
Phosphate buffer pH 6.8	2.1
Phosphate buffer pH 7.4	1.3
Blank FeSSIF	9.2

Table 1. Solubility data of QF in different media

Stability Studies

The stability studies were performed by analyzing sample solution of concentration 10 µg/ml prepared by appropriate dilutions from the stock solution of pure drug and tablet formulations of QF and preserving for 2 days. All samples were prepared in triplicate, the results of stability studies are given in Table 2. It was found that the sample solutions of QF are stable for 48 h at room temperature.

Absorbance											
Stability data of QF in 0.1N HCl						Stability data of QF in Blank FeSSIF					
Pure drug			Commercial product			Pure drug			Commercial product		
1 h	24 h	48 h	1 h	24 h	48 h	1 h	24 h	48 h	1 h	24 h	48 h
0.474	0.481	0.487	0.409	0.411	0.415	0.355	0.359	0.348	0.463	0.467	0.471
0.477	0.486	0.491	0.413	0.414	0.417	0.356	0.361	0.369	0.465	0.467	0.469
0.474	0.482	0.490	0.410	0.409	0.412	0.358	0.363	0.368	0.461	0.465	0.473

Table 2. Stability data of QF in 0.1N HCl and Blank FeSSIF

UV Method Development and Determination of λ_{max}

Diluted samples of concentration 10 µg/ml were prepared in triplicate from standard solution of QF. The samples were scanned in the range of 200-400 nm in 1.0 cm cell against 0.1N HCl. Figure 2 shows the UV absorption spectrum of QF. λ_{max} of QF was found to be 248 nm.

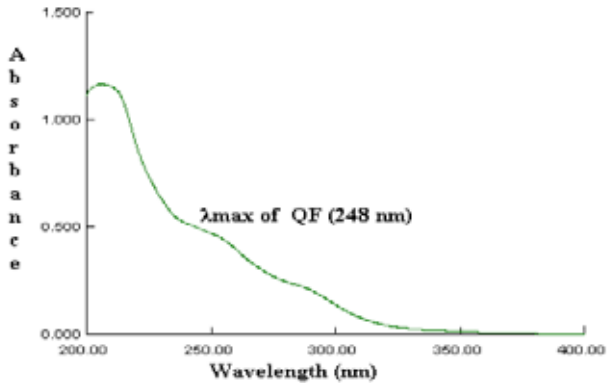

Figure 2. UV absorption spectrum of Quetiapine fumarate

The calibration curves of QF in 0.1 N HCl were constructed and were found to be linear. Beer's law was obeyed in the concentration range of 1 to 25 µg/ml for QF in 0.1 N HCl. The UV spectrum for the linearity of QF is shown in Figure 3 and the calibration curve is shown in Figure 4 with data given in Table 3.

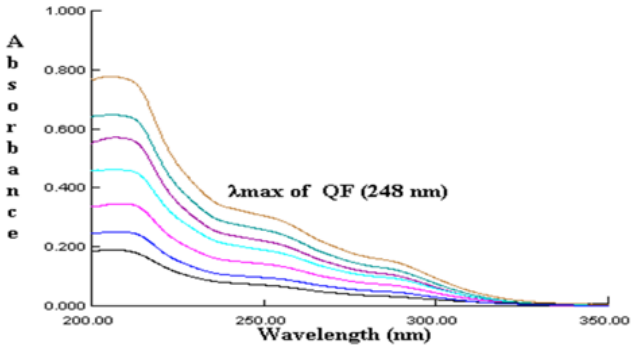

Figure 3. Linearity of QF at different concentration levels

Serial No.	Concentration (µg/ml)	Absorbance (Mean ± SD)
1	1	0.072 ± 0.02
2	2	0.098 ± 0.02
3	3	0.144 ± 0.01
4	4	0.193 ± 0.04
5	5	0.234 ± 0.02
6	6	0.272 ± 0.02
7	7	0.342 ± 0.01
8	10	0.479 ± 0.05
9	15	0.688 ± 0.02
10	20	0.902 ± 0.01
11	25	1.161 ± 0.04

Table 3. Result of Calibration data for QF

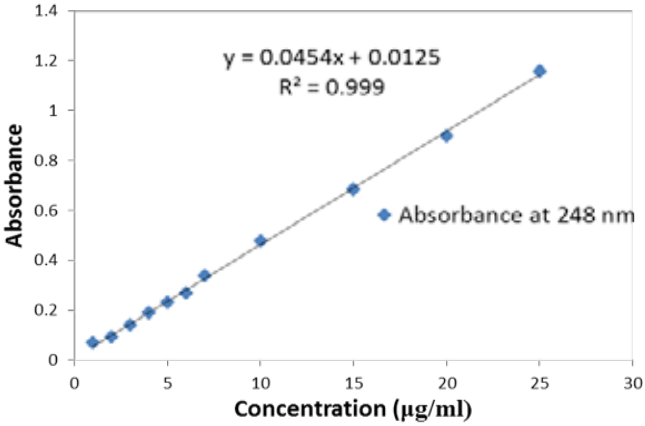

Figure 4. Calibration curve of QF Pure drug

VALIDATION

Linearity and Range

The proposed method was found to linear in the range of 1 - 25 µg/ml for the three brands.The graphs were constructed as concentration vs. absorbance and are depicted in Figure 5, 6 & 7. The linearity data is given in Table 4 for QF in all the three brands.

Beer's law was obeyed in concentration range of 1 µg/ml to 25 µg/ml for Quitipin®, Qutan®&Quel®.

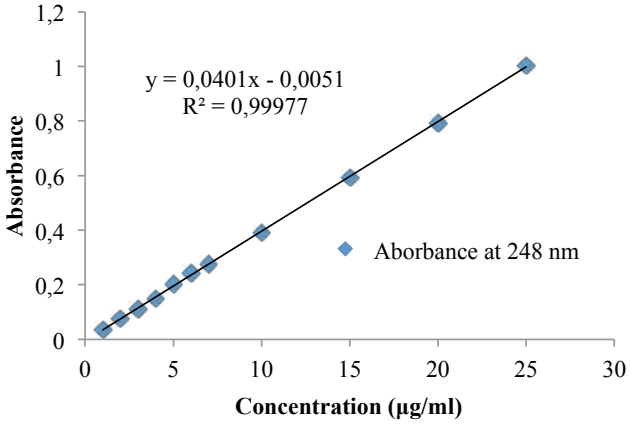

Figure 5. Linearity curve of QF in Quitipin®

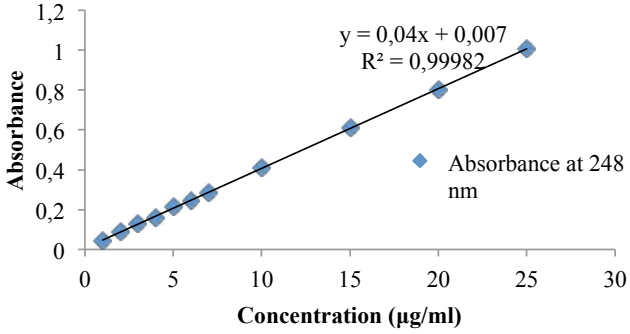

Figure 6. Linearity curve of QF in Qutan®

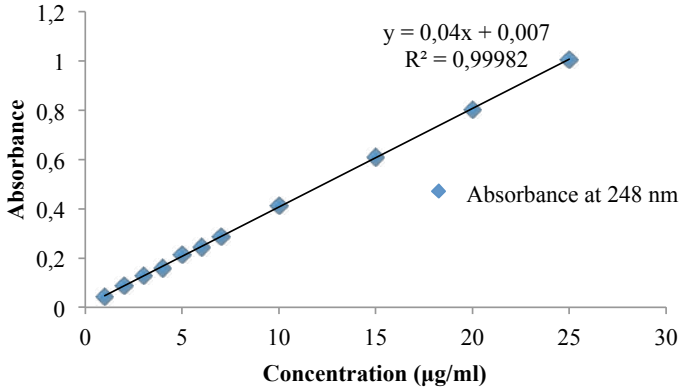

Figure 7. Linearity curve of QF in Quel®

Serial No.	Concentration (µg/ml)	Absorbance (Mean ± SD)		
		Quitipin®	Qutan®	Quel®
1	1	0.035 ± 0.01	0.044 ± 0.03	0.044 ± 0.02
2	2	0.077 ± 0.01	0.087 ± 0.02	0.081 ± 0.02
3	3	0.112 ± 0.02	0.130 ± 0.02	0.128 ± 0.01
4	4	0.150 ± 0.04	0.160 ± 0.04	0.163 ± 0.02
5	5	0.203 ± 0.02	0.214 ± 0.02	0.198 ± 0.04
6	6	0.242 ± 0.02	0.244 ± 0.01	0.245 ± 0.01
7	7	0.276 ± 0.01	0.286 ± 0.01	0.290 ± 0.03
8	10	0.392 ± 0.04	0.412 ± 0.02	0.410 ± 0.05
9	15	0.593 ± 0.03	0.611 ± 0.05	0.624 ± 0.04
10	20	0.793 ± 0.01	0.804 ± 0.03	0.822 ± 0.02
11	25	1.004 ± 0.02	1.006 ± 0.02	1.016 ± 0.01

Table 4. Results for the linearity reading of QF in Quitipin®, Qutan®&Quel®

Accuracy

The recovery studies were performed for QF at three different concentration levels i.e., 50%, 100%, 150% in triplicate. The individual recovery and mean recovery values were calculated and are shown in Table 5 to 7 for all the three brands. The % recovery was under the acceptance criteria of 98% to 102%. Thus, the method is accurate.

% Conc. at specific levels	Amount added (mg)	Amount recovered (mg)	% recovery	Mean recovery ± SD
50%	25	25.22	100.90	100.50 ± 0.61
	25	24.95	99.80	
	25	25.20	100.80	
100%	50	49.80	99.60	99.45 ± 0.21
	50	49.76	99.53	
	50	49.61	99.21	
150%	75	75.62	100.82	100.03 ± 0.70
	75	74.84	99.78	
	75	74.63	99.50	

Table 5. Results of Recovery studies of Quitipin®

% Conc. at specific levels	Amount added (mg)	Amount recovered (mg)	% recovery	Mean recovery ± SD
50%	25	25.00	99.99	100.02 ± 0.07
	25	25.03	100.10	
	25	25.00	99.98	
100%	50	49.43	98.86	99.12 ± 0.40
	50	49.79	99.58	
	50	49.46	98.91	
150%	75	75.02	100.02	100.36 ± 0.47
	75	75.68	100.90	
	75	75.12	100.16	

Table 6. Results of Recovery studies of Qutan®

% Conc. at specific levels	Amount added (mg)	Amount recovered (mg)	% recovery	Mean recovery ± SD
50%	25 25 25	25.03 25.05 25.00	100.12 100.20 99.99	100.10 ± 0.11
100%	50 50 50	50.55 50.50 50.56	101.10 100.99 101.12	101.07 ± 0.07
150%	75 75 75	74.24 74.86 74.92	98.98 99.81 99.89	99.56 ± 0.50

Table 7. Results of Recovery studies of Quel®

Specificity

The method was confirmed to be specific by analyzing samples of pure drug and commercial products. It was observed that there was no interference of the excipients. (Represented in Figure 8)

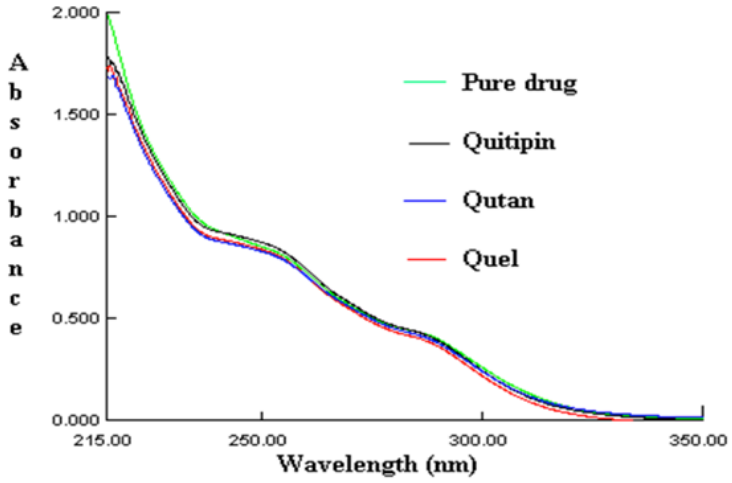

Figure 8. Spectra of pure drug and commercial products

Precision

The precision was determined by Repeatability (Table 8), Inter day (Table 9) and Intraday precision (Table 10) and the % RSD was found to be less than 2% for all the three brands.

The low %RSD values indicate that the method is precise.

Brand	Concentration prepared (µg/ml)	Concentration* (µg/ml)	% RSD
Quitipin®	5 10	5.13 ± 0.04 10.05 ± 0.02	0.74 0.25
Qutan®	5 10	4.78 ± 0.02 10.14 ± 0.07	0.52 0.71
Quel®	5 10	4.64 ± 0.04 9.86 ± 0.09	0.80 0.87

Table 8. Results for Repeatability

Brand	Concentration prepared (µg/ml)	Concentration* (µg/ml)		% RSD	
		Day 1	Day 2	Day 1	Day 2
Quitipin®	5 10	5.13 ± 0.04 10.05±0.02	4.77 ± 0.02 9.55 ± 0.07	0.74 0.25	0.52 0.69
Qutan®	5 10	4.78 ± 0.02 10.14±0.07	5.11 ± 0.03 10.12±0.05	0.52 0.71	0.57 0.51
Quel®	5 10	4.64 ± 0.04 9.86 ± 0.09	4.57 ± 0.04 9.65 ± 0.09	0.80 0.87	0.82 0.96

Table 9. Results for Intermediate Precision (Interday)

Brand	Concentration prepared (µg/ml)	Concentration* (µg/ml)		% RSD	
		Lab 1	Lab 2	Lab 1	Lab 2
Quitipin®	5 10	5.13 ± 0.04 10.05±0.02	5.02 ± 0.04 10.00±0.09	0.74 0.25	0.76 0.86
Qutan®	5 10	4.78 0.02 10.14 0.07	4.83 0.02 9.90 0.05	0.52 0.71	0.52 0.51
Quel®	5 10	4.64 ± 0.04 9.86 ± 0.09	4.85 ± 0.02 9.95 ± 0.05	0.80 0.87	0.50 0.51

Table 10. Results for Intermediate Precision (Intraday)

Quality Control and Biorelevant Dissolution Method Development

The filtered Quality control dissolution samples & Biorelevant dissolution samples were analyzed spectrophotometrically and % drug release was calculated and shown in Table 11.The graph of % drug release versus time is shown in Figure 9 & Figure 10 respectively.By employing the optimized conditions for dissolution, % drug release of more than 85% was achieved within 20 min for all the three brands.

Time (mins)	% Drug release* (Mean ± SD)					
	Dissolution of QF in commercial products			BioRelevant Dissolution of QF in commercial products		
	Qutipin®	Qutan®	Quel®	Qutipin®	Qutan®	Quel®
10	78.66 ± 2.1	77.58 ± 2.5	75.96 ± 4.1	75.4 ± 2.6	72.72 ± 3.1	77.94 ± 2.7
20	93.42 ± 3.2	92.7 ± 3.3	90.18 ± 3.9	86.8 ± 2.1	87.48 ± 3.4	89.28 ± 3.2
30	97.56 ± 2.5	95.04 ± 3.8	94.68 ± 4.6	94.3 ± 3.7	94.14 ± 4.0	96.48 ± 3.7
45	101.2 ± 3.2	100.8 ± 4.1	100.5 ± 3.5	98.92 ± 3.5	98.28 ± 3.6	100.8 ± 2.5

**Average of 6 determinations*

Table 11. Results for Dissolution and Biorelevant Dissolution of commercial products

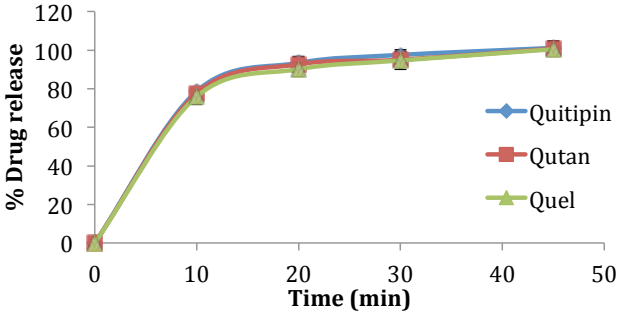

Figure 9. Dissolution profile of QF in commercial products.

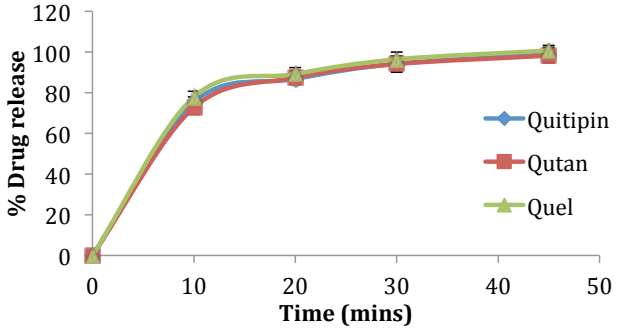

Figure 10. Biorelevant Dissolution profile of QF in commercial products.

CONCLUSION

Biorelevant and quality control dissolution methods were developed and validated. The best dissolution medium selected on the basis of solubility studies for quality control dissolution was 0.1N HCl and the medium for biorelevant dissolution was Blank FeSSIF. The stability studies were performed and the sample solutions were found to be stable for 2 days. The analytical method developed was UV spectrophotometric method involving direct estimation method for QF. The λmax of QF was found to be 248 nm. The method was validated for various parameters like linearity, precision, accuracy and specificity. All the parameters were found to be under the acceptance criteria. The quality control dissolution profile and Biorelevant dissolution profile was obtained by using 900 ml of dissolution medium containing 0.1N HCl and Blank FeSSIF respectively maintained at 37° ± 0.5 °C with paddle apparatus at 50 rpm for 45 min. More than 85% of the drug was released within 20 min. Thus, the methods developed were precise, accurate and reproducible and can be employed as quality control and biorelevant method.

ACKNOWLEDGEMENT:

The authors are thankful to the management of Sultan-ul-Uloom College of Pharmacy for providing necessary facilities to carry out this work.

Declaration of Interest: We do not have any conflict of interest and solely are responsible for content and writing of the paper.

REFERENCES

1. Quingxi, W.; Decheng, M.; John, P. Analytical method selection for drug product dissolution testing. *Dissolution Technol.* **2006**, 8(1), 6-13.

2. Shah. V.P. Dissolution a quality control test vs a bioequivalence test. *Dissolution Technol.* **2006**, 11(1), 1-2.

3. Bhanudas, S. K.; Sanjay, P. Preformulation and formulation studies of novel pH independent controlled release drug delivery system of quetiapine fumarate. *J. Pharm. Res.* **2009**,*2*, 110-119.

4. Valarmathi, R.; Dhivya Dharshini,C. S.; Senthamarai, R.; Farisha Banu, S. Analytical method development of Quetiapine Fumarate in bulk and its Tablet Formulation by simple UV Spectrophotometry. *Int. J. Drug Dev. Res.* **2013,** *5*(1), 366-372.

5. Seeman, P.; Atypical antipsychotics: mechanism of action. *Can J Psychiatry*. **2002,** 47(1), 27–38.

6. Kalyankar, P.; Panade, P.; Lahoti, S. Formulation design and optimization of orodispersible tablets of quetiapine fumarate by sublimation method. *Indian J Pharm Sci.* **2015,** *77*(3), 267-273.

7. Grzegorz Garbacz; Anna Kandzi; Mirko Koziolek; Jarosław Mazgalski; Werner Weitschies. Release characteristics of quetiapine fumarate extended release tablets under biorelevant stress test conditions. *AAPS Pharm. Sci. Tech*. **2014,**15(1), 230–236.

8. Martindale. The complete drug reference, 34th ed.; Pharmaceutical Press, London, **2005**; pp 76.

9. Srihari, G.; Chakravarthi, I. E. Simple spectrophotometric method for determination of Quetiapine fumarate in tablets. *Int. J. Chem. Sci.* **2011**, 9(2), 949-952.

10. Sudarshan Reddy, P.; Ashok Reddy, S.; Karthikvarma, K.; Narasimha Rao, D.; Panjagala Satyanarayana; Naga Raju, T. M. Method development and validation of Quetiapine fumarate bulk and in tablet dosage form by using UV-Spectrophotometry. *Int. J. Pharm & Ind. Res.* **2011,** 1(3), 195–199.

11. Prasanth, V. G.;Susamma Cicy Eapen; Sheeja Velayudhan Kutty; Jyothi T. S. Development and validation of Quetiapine fumarate in pure and pharmaceutical formulation by UV Spectrophotometric method. *Der Pharmacia Sinica.* **2011**, 2(6), 52-58.

12. Rochelle, C.R.; Carolina, L.D.; Lisiane, B.; Ana, M. B.; Pedro, E.H. Development and validation of discriminating method of dissolution for Fosamprenavir tablets based on in vivo data. *J. Pharm. Biomed.* **2011**, 54(1), 439-444.

13. International Conference on Harmonization, Q2 (R1); Draft guidance on Validation of analytical procedures, Federal register; **1997**, 62(96), pp 27463-27467.

14. Jennifer, D., Johannes, K. Pharmaceutical dissolution testing, Taylor and Francis, Indian ed., pp. 352-353.

(Received 04 September 2016; accepted 19 October 2016)

Acta Pharm. Sci. Vol 55 No: 1. 2017
DOI: 10.23893/1307-2080.APS.0553

Novel Benzothiazole Based Imidazole Derivatives as New Cytotoxic Agents Against Glioma (C6) and Liver (HepG2) Cancer Cell Lines

Leyla Yurttaş[1*], Merve Ertaş[2], Gülşen Akalın Çiftçi[3], Halide Edip Temel[3], Şeref Demirayak[2]

[1] Department of Pharmaceutical Chemistry, Faculty of Pharmacy, Anadolu University, 26470 Eskişehir, Turkey
[2] Department of Pharmaceutical Chemistry, School of Pharmacy, Medipol University, 26470 İstanbul, Turkey
[3] Department of Biochemistry, Faculty of Pharmacy, Anadolu University, 26470 Eskişehir, Turkey

ABSTRACT

In this work, some novel *N*-(6-substituted-benzothiazol-2-yl)-2-[[4,5-dimethyl-1-((p-tolyl/4-nitrophenyl)amino)-1*H*-imidazol-2-yl]thio]acetamide derivatives were synthesized and searched for their cytotoxic activities against C6 and HepG2 tumor cells. Among all compounds, the most active compound was determined as compound **7**. It was calculated IC_{50} value about 15.67 µg/mL through C6 tumor cell lines and also compound **2**, **4**, **5**, **6** were observed as good cytotoxic agents against HepG2 tumor cells. Findings about antiproliferative activity studies have encouraged the acquirement of new similar compounds in undergoing studies.

Keywords: Imidazole, Benzothiazole, Cytotoxicity, Antiproliferative Activity

INTRODUCTION

Cancer is the second leading cause of death after heart disease throughout the world. A great amount of anticancer drugs are discovered and still have been designed nowadays for cancer treatment[1]. Today, treatments involving cytotoxic drugs are used in a widespread manner because of increasing in cancer incidence[2]. Compounds containing imidazole and benzothiazole moiety have shown a wide range of biological properties including anticancer, antiviral, antitubercular, antimicrobial, antidiabetic, anti-inflammatory activities. These broad thera-

*Corresponding author: Leyla Yurttaş
E-mail address: lyurttas@anadolu.edu.tr

peutic properties of imidazole and benzothiazole related drugs have encouraged the medicinal chemists in order to synthesize novel chemotherapeutic agents[3-16].

Dr. Malcolm Stevens, a researcher of Cancer Research UK Group at Nottingham University demonstrated the potential of benzothiazole (NSC 674495) and related compounds as anticancer agents. Phortress (NSC 710305) was the lead compound in this work. This lead compound has shown activity against breast tumors, regardless of estrogen receptor status, and against lung, ovarian, colon and renal cancer cells[17].

In a previous study of our research group, synthesized imidazole derivatives showed antiproliferative activity among the sixty tumor cell line, UO-31 derived from renal cancer against tested compound with the growth percentage 69.91 % respectively[18]. Moreover, compounds containing imidazole ring were determined to exhibite high potency anticancer activity against human hepatocellular carcinoma, human colon carcinoma, breast and adeno carcinoma, in recent studies[8,19].

In accordance with these study, *N*-(6-substituted-benzothiazol-2-yl)-2-[[4,5-dimethyl-1-((p-tolyl/4-nitrophenyl)amino)-1*H*-imidazol-2-yl]thio]acetamide derivatives **(2a-j)** were synthesized by two steps and structure of the compounds were clarified by spectroscopic techniques. Cytotoxicity of the compounds was determined by MTT assay against C6 (rat glioma) and HepG2 (human liver) cell lines.

METHODOLOGY

Chemistry

Melting points were determined on d by MP90 digital melting point apparatus (Mettler Toledo, OH) and were uncorrected. Spectroscopic data were recorded on the following instruments: a Bruker Tensor 27 IR spectrophotometer; a ^{1}H NMR (nuclear magnetic resonance) Bruker DPX- 300 FT-NMR spectrometer, ^{13}C NMR, Bruker DPX 75 MHz spectrometer (Bruker Bioscience, Billerica, MA, USA); M+1 peaks were determined by Shimadzu LC/MS ITTOF system (Shimadzu, Tokyo, Japan). Elemental analyses were performed in a Perkin Elmer EAL 240 elemental analyser for C, H and N.

General procedure for the synthesis of final compounds (2a-j)

Firstly, equimolar quantities of **1a** or **1b** (3 mmol) in acetone (35 mL) and equimolar potassium carbonate were stirred and continued to mixing by adding various 2-chloro-*N*-(benzothiazol-2-yl)acetamide derivatives. After completed stirring at room temperature for 3-4 h, the solution was checked by TLC in 1:1

ethanol/EtOAc. The solvent was removed under reduced pressure, and then water (100 mL) and brine added to the residue. The mixture solution was filtered off and air-dried. The obtained solid was dissolved in ethanol and decolorizing activated charcoal was added to solution and boiled finally. After filtering off the charcoal by filter paper, the residue was purified by recrystallization from ethanol (Scheme 1).

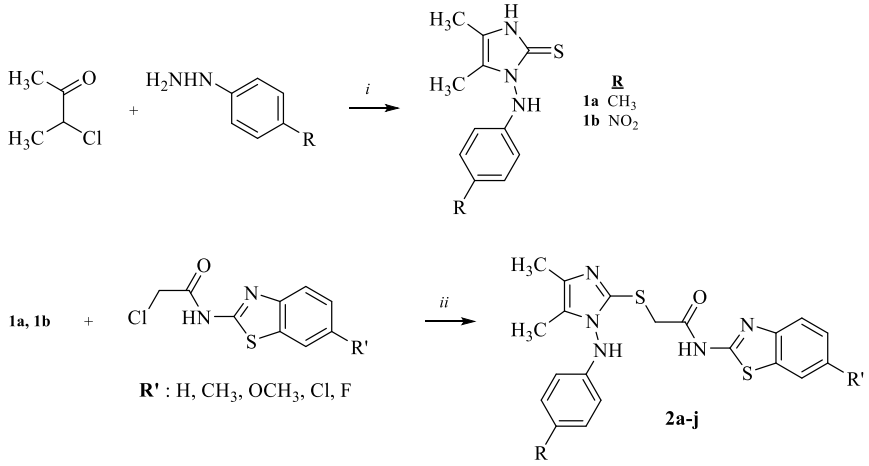

Scheme 1: The synthesis of the compounds. Reactants, reagents, conditions: *i :* AcOH, reflux; *ii :* K_2CO_3, acetone, r.t., 3-4 h.

N-(Benzothiazol-2-yl)-2-[[4,5-dimethyl-1-(p-tolylamino)-1H-imidazol-2-yl]thio]acetamide (2a):

Yield 76 %; mp 178 °C. IR ν_{max} (cm^{-1}): 3250 (N-H), 1689 (C=O), 1598-1375 (C=C, C=N), 1280-1163 (C-N). ^{1}H-NMR (300 MHz, DMSO-d_6, ppm) δ 1.89 (s, 3H, CH_3), 2.07 (s, 3H, CH_3), 2.16 (s, 3H, CH_3), 4.09 (s, 2H, CH_2CO), 6.35 (d, J=8.37 Hz, 2H, Ar-H), 6.99 (d, J=8.25 Hz, 2H, Ar-H), 7.31 (t, J=7.47 Hz, 1H, Ar-H), 7.44 (t, J=7.47 Hz, 1H, Ar-H), 7.75 (d, J=7.92 Hz, 1H, Ar-H), 7.98 (d, J=7.71 Hz, 1H, Ar-H), 9.00 (s, 1H, NH), 12.78 (s, 1H, NH). ^{13}C-NMR (75 MHz, DMSO-d_6, ppm) δ 8.27, 13.56, 20.56, 35.63, 112.69, 121.07, 122.19, 124.03, 125.62, 126.60, 129.46, 130.13, 132.12, 139.85, 145.02, 168.90. For $C_{21}H_{21}N_5OS_2$ calculated: (%) C 59.55, H 5.00, N 16.53; found: (%) C 59.60, H 4.96, N 16.61. HRMS (*m/z*): $[M+H]^+$ calcd: 423.55; found 424.13.

N-(6-Methylbenzothiazol-2-yl)-2-[[4,5-dimethyl-1-(p-tolylamino)-1H-imidazol-2-yl]thio]acetamide (2b):

Yield 72 %; mp 206 °C. IR ν_{max} (cm^{-1}): 3346 (N-H), 1689 (C=O), 1598-1380 (C=C, C=N), 1276-1124 (C-N). ^{1}H-NMR (300 MHz, DMSO-d_6, ppm) δ 1.89 (s, 3H, CH_3),

2.06 (s, 3H, CH_3), 2.16 (s, 3H, CH_3), 2.41 (s, 3H, CH_3), 4.08 (s, 2H, CH_2CO), 6.35 (d, J=8.43 Hz, 2H, Ar-H), 6.99 (d, J=8.10 Hz, 2H, Ar-H), 7.25 (d, J=7.28 Hz, 1H, Ar-H), 7.64 (d, J=8.25 Hz, 1H, Ar-H), 7.77 (d, J=7.92 Hz, 1H, Ar-H), 7.99 (s, 1H, Ar-H), 9.00 (s, 1H, NH), 12.78 (s, 1H, NH). ^{13}C-NMR (75 MHz, DMSO-d_6, ppm) δ 8.27, 13.56, 20.58, 21.44, 35.55, 112.69, 120.73, 121.79, 125.61, 127.93, 129.46, 130.14, 132.10, 133.52, 139.89, 145.01, 168.33. For $C_{22}H_{23}N_5OS_2$ calculated: (%) C 60.39, H 5.30, N 16.00; found: (%) C 60.34, H 5.25, N 16.07. HRMS (*m/z*): $[M+H]^+$ calcd: 437.58; found 438.14.

N-(6-Methoxybenzothiazol-2-yl)-2-[[4,5-dimethyl-1-(p-tolylamino)-1H-imidazol-2-yl]thio]acetamide (2c):

Yield 75 %; mp 224 °C. IR ν_{max} (cm^{-1}): 3289 (N-H), 1670 (C=O), 1602-1398 (C=C, C=N), 1267-1056 (C-N). ^{1}H-NMR (300 MHz, DMSO-d_6, ppm) δ 1.89 (s, 3H, CH_3), 2.06 (s, 3H, CH_3), 2.16 (s, 3H, CH_3), 3.81 (s, 3H, OCH_3), 4.07 (s, 2H, CH_2CO), 6.35 (d, J=8.43 Hz, 2H, Ar-H), 6.97-7.05 (m, 3H, Ar-H), 7.58 (d, J=2.55 Hz, 1H, Ar-H), 7.64 (d, J=8.82 Hz, 1H, Ar-H), 8.98 (s, 1H, NH), 12.65 (s, 1H, NH). ^{13}C-NMR (75 MHz, DMSO-d_6, ppm) δ 8.26, 13.56, 20.58, 35.50, 56.06, 105.21, 112.69, 115.41, 121.70, 125.72, 129.47, 130.14, 132.10, 133.36, 139.88, 145.01, 156.62, 168.16. For $C_{22}H_{23}N_5O_2S_2$ calculated: (%) C 58.26, H 5.11, N 15.44; found: (%) C 58.30, H 5.16, N 15.49. HRMS (*m/z*): $[M+H]^+$ calcd: 453.58; found 454.14.

N-(6-Chlorobenzothiazol-2-yl)-2-[[4,5-dimethyl-1-(p-tolylamino)-1H-imidazol-2-yl]thio]acetamide (2d):

Yield 72 %; mp 214 °C. IR ν_{max} (cm^{-1}): 3288 (N-H), 1697 (C=O), 1546-1400 (C=C, C=N), 1286-1101 (C-N). ^{1}H-NMR (300 MHz, DMSO-d_6, ppm) δ 1.89 (s, 3H, CH_3), 2.06 (s, 3H, CH_3), 2.15 (s, 3H, CH_3), 4.09 (s, 2H, CH_2CO), 6.34 (d, J=8.43 Hz, 2H, Ar-H), 6.98 (d, J=8.13 Hz, 2H, Ar-H), 7.46 (dd, $J_{1,2}$=8.61, 2.22 Hz, 1H, Ar-H), 7.74 (d, J=8.64 Hz, 1H, Ar-H), 8.13 (d, J=2.16 Hz, 1H, Ar-H), 8.99 (s, 1H, NH), 12.89 (s, 1H, NH). ^{13}C-NMR (75 MHz, DMSO-d_6, ppm) δ 8.27, 13.57, 20.58, 35.56, 112.68, 121.93, 122.29, 125.64, 126.96, 128.09, 129.47, 130.13, 132.13, 133.67, 139.80, 145.00, 147.92, 159.10, 168.73. For $C_{21}H_{20}ClN_5OS_2$ calculated: (%) C 55.07, H 4.40, N 15.29; found: (%) C 55.12, H 4.46, N 15.35. HRMS (*m/z*): $[M+H]^+$ calcd: 458.00; found 458.09.

N-(6-Fluorobenzothiazol-2-yl)-2-[[4,5-dimethyl-1-(p-tolylamino)-1H-imidazol-2-yl]thio]acetamide (2e):

Yield 72 %; mp 212 °C. IR ν_{max} (cm^{-1}): 3317, 3286 (N-H), 1689 (C=O), 1543-1398 (C=C, C=N), 1294-1136 (C-N). ^{1}H-NMR (300 MHz, DMSO-d_6, ppm) δ 1.88 (s, 3H, CH_3), 2.06 (s, 3H, CH_3), 2.15 (s, 3H, CH_3), 4.09 (s, 2H, CH_2CO), 6.35 (d, J=8.43 Hz, 2H, Ar-H), 6.98 (d, J=8.16 Hz, 2H, Ar-H), 7.29 (td, $J_{1,2}$=8.70, 2.64

Hz, 1H, Ar-H), 7.76 (q, J=8.70 Hz, 1H, Ar-H), 7.90 (dd, $J_{1,2}$=8.40, 2.67 Hz, 1H, Ar-H), 8.98 (s, 1H, NH), 12.82 (s, 1H, NH). ^{13}C-NMR (75 MHz, DMSO-d_6, ppm) δ 8.27, 13.57, 20.58, 35.51, 108.49, 108.84, 112.69, 114.38, 114.56, 114.89, 122.14, 122.26, 125.63, 129.46, 130.13, 131.13, 139.83, 145.00, 145.74, 157.53, 158.19, 159.33, 160.71, 168.59. For $C_{21}H_{20}FN_5OS_2$ HRMS (*m/z*): $[M+H]^+$ calcd: 441.54; found 442.12.

N-(Benzothiazol-2-yl)-2-{[4,5-dimethyl-1-[(4-nitrophenyl) amino]-1H-imidazol-2-yl]thio}acetamide (2f):

Yield 69 %; mp 126 °C. IR ν_{max} (cm^{-1}): 3323, 3288 (N-H), 1689 (C=O), 1595-1350 (C=C, C=N, NO_2), 1288-1111 (C-N). ^{1}H-NMR (300 MHz, DMSO-d_6, ppm) δ 1.92 (s, 3H, CH_3), 2.08 (s, 3H, CH_3), 4.11 (s, 2H, CH_2CO), 6.56 (d, J=8.61 Hz, 2H, Ar-H), 7.31 (td, $J_{1,2}$=8.10, 1.11 Hz, 1H, Ar-H), 7.44 (td, $J_{1,2}$=7.20, 1.26 Hz, 1H, Ar-H), 7.75 (d, J=7.92 Hz, 1H, Ar-H), 7.96 (d, J=7.23 Hz, 1H, Ar-H), 8.12 (d, J=7.08 Hz, 2H, Ar-H), 10.25 (s, 1H, NH), 12.68 (s, 1H, NH). ^{13}C-NMR (75 MHz, DMSO-d_6, ppm) δ 8.13, 13.57, 35.95, 111.63, 121.08, 122.20, 124.08, 125.48, 126.63, 131.92, 132.67, 139.24, 140.39, 148.97, 152.90, 158.16, 168.12. For $C_{20}H_{18}N_6O_3S_2$ HRMS (*m/z*): $[M+H]^+$ calcd: 454.52; found 455.12.

N-(6-Methylbenzothiazol-2-yl)-2-{[4,5-dimethyl-1-[(4-nitrophenyl) amino]-1H-imidazol-2-yl]thio}acetamide (2g):

Yield 68 %; mp 95 °C. IR ν_{max} (cm^{-1}): 3298 (N-H), 1683 (C=O), 1595-1327 (C=C, C=N, NO_2), 1271-1111 (C-N). ^{1}H-NMR (300 MHz, DMSO-d_6, ppm) δ 1.92 (s, 3H, CH_3), 2.07 (s, 3H, CH_3), 2.40 (s, 3H, CH_3), 4.08 (s, 2H, CH_2CO), 6.55 (t, J=9.27 Hz, 2H, Ar-H), 7.19-7.31 (m, 1H, Ar-H), 7.61 (d, J=8.22 Hz, 1H, Ar-H), 7.74 (s, 1H, Ar-H), 8.07-8.15 (m, 2H, Ar-H), 10.23 (s, 1H, NH), 12.31 (s, 1H, NH). ^{13}C-NMR (75 MHz, DMSO-d_6, ppm) δ 8.13, 13.57, 21.44, 34.04, 36.38, 61.43, 111.66, 117.86, 120.65, 121.27, 121.75, 125.48, 126.62, 126.86, 127.86, 132.65, 132.76, 133.39, 140.36, 153.03, 169.04. For $C_{21}H_{20}N_6O_3S_2$ HRMS (*m/z*): $[M+H]^+$ calcd: 468.55; found 469.12.

N-(6-Methoxybenzothiazol-2-yl)-2-{[4,5-dimethyl-1-[(4-nitrophenyl)amino]-1H-imidazol-2-yl]thio}acetamide (2h):

Yield 67 %; mp 122 °C. IR ν_{max} (cm^{-1}): 3253 (N-H), 1683 (C=O), 1597-1328 (C=C, C=N, NO_2), 1261-1059 (C-N). ^{1}H-NMR (300 MHz, DMSO-d_6, ppm) δ 1.92 (s, 3H, CH_3), 2.08 (s, 3H, CH_3), 3.80 (s, 3H, OCH_3), 4.09 (s, 2H, CH_2CO), 6.55 (d, J=8.52 Hz, 2H, Ar-H), 7.02 (dd, $J_{1,2}$=8.40, 2.58 Hz, 1H, Ar-H), 7.75 (d, J=2.55 Hz, 1H, Ar-H), 7.63 (d, J=7.35 Hz, 1H, Ar-H), 8.11 (d, J=8.40 Hz, 2H, Ar-H), 10.34 (s, 1H, NH), 12.43 (s, 1H, NH). ^{13}C-NMR (75 MHz, DMSO-d_6, ppm) δ 8.15, 13.57, 35.99, 56.08, 105.18, 111.63, 115.39, 121.66, 125.47, 126.62, 132.65, 133.25,

139.24, 140.37, 143.08, 152.95, 156.25, 156.60, 167.88. For $C_{21}H_{20}N_6O_4S_2$ HRMS (*m/z*): $[M+H]^+$ calcd: 484.55; found 485.12.

N-(6-Chlorobenzothiazol-2-yl)-2-{[4,5-dimethyl-1-[(4-nitrophenyl) amino]-1H-imidazol-2-yl]thio}acetamide (2i):

Yield 72 %; mp 115 °C. IR ν_{max} (cm^{-1}): 3254 (N-H), 1683 (C=O), 1595-1328 (C=C, C=N, NO_2), 1288-1053 (C-N). ^{1}H-NMR (300 MHz, DMSO-d_6, ppm) δ 1.92 (s, 3H, CH_3), 2.08 (s, 3H, CH_3), 4.11 (s, 2H, CH_2CO), 6.55 (d, J=8.40 Hz, 2H, Ar-H), 7.45 (dd, $J_{1,2}$=8.61, 2.22 Hz, 1H, Ar-H), 7.73 (d, J=8.67 Hz, 1H, Ar-H), 8.08-8.12 (m, 3H, Ar-H), 10.29 (s, 1H, NH), 12.78 (s, 1H, NH). ^{13}C-NMR (75 MHz, DMSO-d_6, ppm) δ 8.14, 13.57, 35.99, 111.61, 121.92, 122.27, 125.51, 126.60, 126.96, 128.11, 132.69, 133.63, 139.12, 140.36, 152.91, 168.39. For HRMS (*m/z*): $[M+H]^+$ calcd: 488.97; found 489.52.

N-(6-Fluorobenzothiazol-2-yl)-2-{[4,5-dimethyl-1-[(4-nitrophenyl) amino]-1H-imidazol-2-yl]thio}acetamide (2j):

Yield 75 %; mp 121 °C. IR ν_{max} (cm^{-1}): 3282 (N-H), 1683 (C=O), 1597-1328 (C=C, C=N, NO_2), 1267-1051 (C-N). ^{1}H-NMR (300 MHz, DMSO-d_6, ppm) δ 1.93 (s, 3H, CH_3), 2.07 (s, 3H, CH_3), 4.11 (s, 2H, CH_2CO), 6.53-6.59 (m, 2H, Ar-H), 7.28 (td, $J_{1,2}$=9.12, 2.70 Hz, 1H, Ar-H), 7.75 (q, J=9.00 Hz, 1H, Ar-H), 7.88 (dd, J=8.73, 2.67 Hz, 1H, Ar-H), 8.10 (d, J=9.33 Hz, 2H, Ar-H), 10.33 (s, 1H, NH), 12.71 (s, 1H, NH). ^{13}C-NMR (75 MHz, DMSO-d_6, ppm) δ 8.16, 13.57, 35.94, 108.47, 108.83, 111.60, 114.57, 114.89, 122.14, 122.25, 125.52, 126.59, 132.68, 133.08, 139.13, 140.35, 145.70, 152.93, 157.54, 158.17, 160.72, 168.24. For $C_{20}H_{17}FN_6O_3S_2$ HRMS (*m/z*): $[M+H]^+$ calcd: 472.51; found 473.12.

MTT assay

To find cytotoxic activity of the compounds against C6 (rat glioma) and HepG2 (human liver) cell lines according to the reported data, MTT assay (3-(4,5-dimethylthiazol-2-yl)-2,5-diphenyltetrazolium bromide) was performed[20-21]. C6 and HepG2 and cells were cultured in 96-well flat-bottom plates at 37 °C for 24h (2 x 104 cells per well). Then by waiting for 24 h drug incubation, 20 µL MTT solution (5 mg/mL MTT powder in PBS) was added to each well and incubated about 2 h. After dissolving formazan crystals in 200 µL DMSO, the absorbance was read with the aid of ELISA reader (OD570nm). According to medium control, the percentage of viable cells was calculated and for all experiments, measurements were carried out in triplicate[22].

RESULTS AND DISCUSSION

Chemistry

Novel *N*-(6-substituted-benzothiazol-2-yl)-2-[[4,5-dimethyl-1-((p-tolyl/4-nitrophenyl)amino)-1*H*-imidazol-2-yl]thio]acetamide derivatives **(2a-j)** were procured by reacting of *N*-(6-substituted-benzothiazol-2-yl)-2-chloroacetamide derivatives with compounds **(1a-1b)** in the presence of K_2CO_3 in acetone. The synthesized compounds were yielded in a range of % 67-% 76. Melting points of final compounds were calculated between 95 °C and 212 °C. The results of IR spectral analysis showed that characteristic streching bands were observed at 3250 cm^{-1}-3346 cm^{-1} and 1294 cm^{-1}-1051 cm^{-1} in respect of N-H and C-N single bonds, at about 1697 cm^{-1} and 1670 cm^{-1}-1328 cm^{-1} belonging to C=O and C=C, C=N, NO_2 double bonds. In the ^{1}H-NMR spectra of the compounds, peaks of methyl groups hydrogens were observed at between 1.89 ppm and 2.19 ppm whereas protons of N-H were seen at 9.00 ppm and 12.78 ppm range. Aromatic hydrogens and acetyl group hydrogens were seen in order 6.34 ppm-8.15 ppm and 4.08 ppm. ^{13}C-NMR spectroscopic data displayed signals of aliphatic carbons which were assigned at 8.26 ppm-61.43 ppm and signals of aromatic carbons were seen at between 105.18 ppm-169.04 ppm. $[M+H]^+$ peaks of the molecular weights of the compounds were observed at expected values in mass spectroscopy.

Cytotoxicity

Cytotoxicity of compounds **(2a-j)** were evaluated by using MTT assay against C6 (rat glioma) and HepG2 (human liver) tumor cell lines. As shown in Table 1, IC_{50} values were calculated among 15-500 μg/mL values. IC_{50} values of the compounds **5**, **6** and **7** were found values of 16 μg/mL, 19 μg/mL and 15 μg/mL as having high cytotoxic activity because of higher values even more than cisplatin against C6 tumor cell lines. Among all compounds, the most active compound was determined as compound **7**. Its IC_{50} value was calculated as 15.67 μg/mL since that value for cisplatin was defined as 23.0 μg/mL. Compound **8** possessed IC_{50} value greater than 500 μg/mL were considered to be non-toxic. Studies against HepG2 tumor cell lines showed that compound **2**, **4**, **5**, **6** were good cytotoxic agents according to their IC_{50} values in contrast with the value of cisplatin. While these compounds had strongest cytotoxicity, IC_{50} values for compound **8**, **9**, **10** could not be calculated on account of needing high tested concentration as more than 500 μg/mL against HepG2 tumor cells. Accordingly, findings from that cytotoxicity studies displayed that synthesized novel benzothiazole based imidazole derivatives could be considered as new cytotoxic agents.

Table 1. IC_{50} values of the compounds against C6 and HepG2 tumor cell lines

Comp.	C6	HepG2
1	27.0±1.41	50.0±5.0
2	20±2.0	26.33±1.53
3	32.67±6.43	275.0±35.36
4	22.0±3.61	29.33±1.15
5	16.33±2.31	31.67±7.23
6	19.50±2.12	28.67±1.15
7	15.67±2.52	58.33±2.89
8	>500	>500
9	24.33±4.04	>500
10	19.33±2.31	>500
Cisplatin	23.0±1.73	46.67±7.64

REFERENCES

1. Baroniya, S.; Anwer, Z.; Sharma, P. K.; Dudhe, R.; Kumar, N. Recent advancement in imidazole as anti cancer agents: A review. *Pharm. Sin.* **2010**, *1(3),* 172-182.

2. Hoppe-Tichy, T. Current challenges in European oncology pharmacy practice. *J. Oncol. Pharm. Pract*. **2010**, *16*, 9-18.

3. Katritzky, A. R. *Rees. Comprehensive Heterocyclic Chemistry*. **1984**, *5*, 469-498. W. Meyer, Ber. Dtschn. Chem. Ges.;1883; 16; 1465.

4. Grimmet, R. M. Imidazole and Benzimidazole Synthesis. *Academic Press,* San Diego, **1997**.

5. Brown, E. G. Ring Nitrogen and Key Biomolecules. *Kluwer Academic Press,* Dortrecht, **1998.**

6. Pozharskii, A. F. Heterocycles in Life and Society. *John Wiley & Sons*. **1997**.

7. Gilchrist, T. L. Heterocyclic Chemistry. *The Bath Press,* Oxford, **1985**.

8. Congiu, U.; Cocco, M. T.; Onnis, V. Design, synthesis, and in vitro antitumor activity of new 1,4-diarylimidazole-2-ones and their 2-thione analogues. *Bioorg. Med. Chem. Lett*. **2008**, *18*, 989-993.

9. Venkatesan, A. M.; Agarwal, A.; Abe, T.; Ushirogochi, H. O.; Santos, D.; Li Z.; Francisco, G.; Lin, Y. I.; Peterson, P. J.; Yang, Y.; Weiss, W. J.; Shales, D. M.; Mansour, T. S. 5,5,6-Fused tricycles bearing imidazole and pyrazole 6-methylidene penems as broad-spectrum inhibitors of β-lactamases. *Bioorg. Med. Chem*. **2008**, *16,* 1890-1902.

10. Nakamura, T.; Kakinuma, H.; Umemiya, H.; Amada, H.; Miyata, N.; Taniguchi, K.; Bando, K.; Sato, M. Imidazole derivatives as new potent and selective 20-HETE synthase inhibitors. *Bioorg. Med. Chem. Lett*. **2004**, *14,* 33-336.

11. Su Han, M.; Kim, D. H. Effect of zinc ion on the inhibition of carboxypeptidase A by imidazole-bearing substrate analogues. *Bioorg. Med. Chem. Lett*. **2001**, *11*, 1425-1427.

12. Roman, G.; Riley, J. G.; Vlahakis, J. Z.; Kinobe, R. T.; Brien, J. F.; Nakatsu, K.; Szarek, W. A. Heme oxygenase inhibition by 2-oxy-substituted 1-(1*H*-imidazol-1-yl)-4-phenylbutanes: effect of halogen substitution in the phenyl ring. *Bioorg. Med. Chem*. **2007**, *15*, 3225-3234.

13. Bbizhayev, M. A. Biological activities of the natural imidazole-containing peptidomimetics

n-acetylcarnosine, carcinine and L-carnosine in ophthalmic and skin care products. *Life Sci.* **2006**, *78*, 2343-3234.

14. Nantermet, P. G.; Barrow, J. C.; Lindsey, S. R.; Young, M.; Mao, S.; Carroll, S.; Bailey, C.; Bosserman, M.; Colussi, D.; McMasters, D. R.; Vacca, J. P.; Selnick, H. G. Imidazole acetic acid TAFIa inhibitors: SAR studies centered around the basic P(1)(') group. *Bioorg. Med. Chem. Lett.* **2004**, *14*, 2141-2145.

15. Adams, J. L.; Boehm, J. C.; Gallagher, T. F.; Kassis, S.; Webb, E. F.; Hall, R.; Sorenson M.; Garigipati, R.; Griswold, D. E.; Lee, J. C. Pyridinylimidazole inhibitors of p38: cyclic N-1 imidazole substituent enhance p38 kinase inhibition and oral activity *Bioorg. Med. Chem. Lett.* **2001**, *11*, 2867-2870.

16. Bhandari, K.; Srinivas, N.; Keshava, G. B. S.; Shukla, P. K. Tetrahydronaphthyl azole oxime ethers: the conformationally rigid analogues of oxiconazole as antibacterials. *Eur. J. Med. Chem.* **2009**, *44*, 437-447.

17. Ali, R.; Siddiqui, N. Biological aspects of emerging benzothiazole: A short review. *J. Chem.* **2013**, *2013,* 1-12.

18. Yurttas, L.; Duran, M.; Demirayak, S.; Gencer, H. K.; Tunalı, Y. Synthesis and initial biological evaluation of substituted 1-phenylamino-2-thio-4,5-dimethyl-1H-imidazole derivatives. *Bioorg. Med. Chem. Lett.* **2013**, *23*, 6764-6768.

19. Wang, X.Q.; Liu, L.X.; Li, Y.; Sun, C.J.; Chen, W.; Li, L.; Zhang, H.B.; Yang, X.D. Design, synthesis and biological evaluation of novel hybrid compounds of imidazole scaffold-based 2-benzylbenzofuran as potent anticancer agents. *Eur. J. Med. Chem.* **2013**, *62*, 111-121.

20. Mossman, T. Rapid Colorimetric Assay for Cellular Growth and Survival: Application to proliferation and cytotoxicity assays. *J. Immunol. Methods*, **1983**, *16*, 55-63.

21. Keiser, K.; Johnson, C.C.; Tipton, D.A. Cytotoxicity of mineral trioxide aggregate using human periodontal ligament fibroblasts. *J. Endod.,* **2000**, *26*, 288-291.

22. Yurttas, L.; Demirayak, S.; Akalın Ciftci, G. Cytotoxic, antiproliferative and apoptotic effects of new benzimidazole derivatives on A549 lung carcinoma and C6 glioma cell lines. *Anticancer Agents Med. Chem.* **2015**, *15*, 1174-1184.

(Received 23 September 2016; accepted 18 October 2016)

Acta Pharm. Sci. Vol 55 No: 1. 2017
DOI: 10.23893/1307-2080.APS.0554

Synthesis and Antimycobacterial Activity Evaluation of Isatin-derived 3-[(4-aryl-2-thiazolyl])hydrazone]-1H-indol-2,3-diones

Leyla Yurttaş[1,*], Merve Ertaş[2], Meral Yılmaz Cankılıç[3], Şeref Demirayak[2]

[1] Anadolu University, Faculty of Pharmacy, Department of Pharmaceutical Chemistry, 26470, Eskişehir, Turkey
[2] Medipol University, School of Pharmacy, Department of Pharmaceutical Chemistry, 34810, İstanbul, Turkey
[3] Anadolu University, Faculty of Science, Department of Biology, 26470, Eskişehir, Turkey

ABSTRACT

A series of 3-[(4-aryl-2-thiazolyl)hydrazone]-1*H*-indol-2,3-dione derivatives (**2a-f**) were designed and synthesized using isatin as starting material. The obtained thiazole compounds were screened to investigate their antituberculosis activity against *Mycobacterum tuberculosis* H37RV (ATCC 27294). Among them, two compounds **2c** and **2d** were displayed antitubercular potential two-fold greater than standard drugs.

Keywords: Isatin, Indole, Thiazole, Antimycobacterial activity

INTRODUCTION

Tuberculosis (TB) is an airborne infectious disease persisting with high mortality which is caused by mycobacterium, *Mycobacterium tuberculosis*. Each year, over 12 million peple suffer from the disease accompanied with 1.4 million death circumstances. Emergence of multidrug resistance against existing chemotherapeutic applications has led to find out a solution to this alarming increase of TB infections. Accordingly, Therefore, there is an intensive study to develop new, more effective antituberculotic agents[1-5].

Indoles, especially 1*H*-indole-2,3-dione (isatin) are the most prevalent heterocyclic scaffolds which have a broad spectra of medical applications such as anti-HIV, antiviral, anti-tumor, antifungal, antiangiogenic, anti-convulsant, and antiparkinsonian activity[6-8]. In particular, antituberculotic activity of various indole derivatives[9-14] and isatin derivatives[15-22] have attracted attention. The syn-

*Corresponding author: Leyla Yurttaş
E-mail address: lyurttas@anadolu.edu.tr

thetic feasibility and extensive use of this scaffold have led to medicinal chemists to this ring which has also stemmed from the interest in the biological and pharmacological properties[23,24].

In the other hand, thiazole ring is another important structure which have enhanced lipid solubility which is easily metabolized by routine biochemical reactions. Thiazole derivatives have well established with antituberculosis effects in many studies[25-30]. Studies combined these two rings, thiazole and isatin have also been reported[31,32].

In this work, based on isatin structure we have designed and synthesized new 3-[(4-aryl-2-thiazolyl)hydrazone]-1*H*-indol-2,3-dione derivatives. Six final compounds were screened for their antituberculotic activity, against *M. tuberculosis*. Log *P* values for the compounds were calculated, virtually and the biological results have been evaluated compared to standard drugs, isoniazid and rifampicin.

METHODOLOGY

Chemistry

Melting points were determined using a MP90 digital melting point apparatus (Mettler Toledo, OH) and were uncorrected. Spectroscopic data were recorded on the following instruments: a Bruker Tensor 27 IR spectrophotometer; a ^{1}H NMR (nuclear magnetic resonance) Bruker DPX- 300 FT-NMR spectrometer, ^{13}C NMR, Bruker DPX 75 MHz spectrometer (Bruker Bioscience, Billerica, MA, USA); M+1 peaks were determined by Shimadzu LC/MS ITTOF system (Shimadzu, Tokyo, Japan).

Synthesis of 1H-Indole-2,3-dione-3-thiosemicarbazone (1)

0.02 mol of isatin, 0.02 mol of thiosemicarbazide and catalytic amount of acetic acid were refluxed in ethanol for 6 hours. After the end of the reaction was controlled by TLC, the reaction mixture was allowed to cool to room temprature and obtained precipitate was filtrated. The raw product was crystallised from ethanol.

Synthesis of 3-[(4-aryl-2-thiazolyl)hydrazone]-1H-indol-2,3-dione derivatives (2a-f)

3 mmol of gained intermediate (**1**) and appropriate α-bromoarylethanone derivative (3 mmol) were stirred in ethanol at room temprature. After the reaction was ended, the mixture was filtrated with excess ethanol and recrystallised from ethanol.

3-[[4-(2-Hydroxyphenyl)-2-thiazolyl]hydrazone]-1H-indol-2,3-dione (2a)

68 % yield; mp 310 °C. IR ν_{max} (cm^{-1}): 3250 (NH), 3136 (OH), 1691 (C=O), 1616-1454 (C=C, C=N), 1386-981 (C-O, C-N). ^{1}H-NMR (300 MHz, DMSO-d_6, ppm) δ 6.84-6.97 (m, 3H, Ar-H), 7.09 (t, J=7.38 Hz, 1H, Ar-H), 7.17 (t, J=7.35 Hz,

1H, Ar-H), 7.34 (t, J=7.99 Hz, 1H, Ar-H), 7.53 (d, J=7.67 Hz, 1H, Ar-H), 7.68 (s, 1H, thiazole C_5-H), 7.92 (d, J=8.30 Hz, 1H, Ar-H), 10.54 (s, 1H, OH), 11.23 (s, 1H, NH), 13.53 (s, 1H, NH). ^{13}C-NMR (75 MHz, DMSO-d_6, ppm) δ 109.00, 111.48, 116.95, 119.61, 119.95, 120.31, 121.78, 122.84, 128.51, 129.41, 130.95, 132.57, 141.79, 148.52, 155.48, 163.42, 165.68. HRMS (*m/z*): $[M+H]^+$ calcd for $C_{17}H_{12}N_4O_2S$ 337.37; found 337.08.

3-[[4-(3-Hydroxyphenyl)-2-thiazolyl]hydrazone]-1H-indol-2,3-dione (2b)

72 % yield; mp 316 °C. IR ν_{max} (cm^{-1}): 3161 (OH, NH), 1695 (C=O), 1616-1431 (C=C, C=N), 1346-987 (C-O, C-N). ^{1}H-NMR (300 MHz, DMSO-d_6, ppm) δ 6.71-6.74 (m, 1H, Ar-H), 6.97 (d, J=7.76 Hz, 1H, Ar-H), 7.09 (t, J=7.47 Hz, 1H, Ar-H), 7.21 (t, J=8.05 Hz, 2H, Ar-H), 7.31-7.37 (m, 2H, Ar-H), 7.53-7.54 (m, 2H, Ar-H and thiazole C_5-H), 9.48 (s, 1H, OH), 11.25 (s, 1H, NH), 13.35 (s, 1H, NH). ^{13}C-NMR (75 MHz, DMSO-d_6, ppm) δ 107.13, 111.53, 113.09, 115.47, 116.96, 120.21, 120.32, 122.88, 130.16, 130.94, 132.48, 135.68, 141.74, 151.61, 158.11, 163.68, 166.25. HRMS (*m/z*): $[M+H]^+$ calcd for $C_{17}H_{12}N_4O_2S$ 337.37; found 337.07.

3-[[4-(4-Hydroxyphenyl)-2-thiazolyl]hydrazone]-1H-indol-2,3-dione (2c)

69 % yield; mp 285 °C. IR ν_{max} (cm^{-1}): 3165 (OH, NH), 1691 (C=O), 1612-1463 (C=C, C=N), 1327-987 (C-O, C-N). ^{1}H-NMR (300 MHz, DMSO-d_6, ppm) δ 6.79-6.86 (m, 3H, Ar-H), 6.96 (d, J=8.00 Hz, 1H, Ar-H), 7.08 (t, J=7.62 Hz, 1H, Ar-H), 7.34 (s, 1H, thiazole C_5-H), 7.53 (d, J=7.62 Hz, 1H, Ar-H), 7.71 (d, J=8.20 Hz, 2H, Ar-H), 9.60 (s, 1H, OH), 11.24 (s, 1H, NH), 13.32 (s, 1H, NH). ^{13}C-NMR (75 MHz, DMSO-d_6, ppm) δ 104.21, 110.15, 111.51, 115.85, 116.02, 120.25, 121.73, 122.85, 125.81, 127.62, 130.85, 132.28, 141.68, 151.85, 157.87, 163.67, 166.19. HRMS (*m/z*): $[M+H]^+$ calcd for $C_{17}H_{12}N_4O_2S$ 337.37; found 337.07.

3-[[4-(2-Pyridyl)-2-thiazolyl]hydrazone]-1H-indol-2,3-dione (2d)

65 % yield; mp 298 °C. IR ν_{max} (cm^{-1}): 3124 (NH), 1683 (C=O), 1616-1464 (C=C, C=N), 1344-987 (C-O, C-N). ^{1}H-NMR (300 MHz, DMSO-d_6, ppm) δ 6.97 (d, J=8.80 Hz, 1H, Ar-H), 7.09 (t, J=7.54 Hz, 1H, Ar-H), 7.32-7.37 (m, 2H, Ar-H), 7.55 (d, J=7.96 Hz, 1H, Ar-H), 7.81 (s, 1H, thiazole C_5-H), 7.88 (t, J=7.96 Hz, 1H, Ar-H), 7.95-7.98 (m, 1H, Ar-H), 8.60 (d, J=4.28 Hz, 1H, Ar-H), 11.26 (s, 1H, NH), 13.36 (s, 1H, NH). ^{13}C-NMR (75 MHz, DMSO-d_6, ppm) δ 111.02, 111.55, 120.17, 120.39, 120.54, 120.77, 122.91, 123.50, 131.04, 137.85, 141.82, 149.93, 152.10, 163.66, 166.90. HRMS (*m/z*): $[M+H]^+$ calcd for $C_{16}H_{11}N_5OS$ 322.36; found 322.07.

3-[[4-(3-Pyridyl)-2-thiazolyl]hydrazone]-1H-indol-2,3-dione (2e)

69 % yield; mp 318 °C. IR ν_{max} (cm^{-1}): 3298 (NH), 1666 (C=O), 1616-1462 (C=C, C=N), 1357-988 (C-O, C-N). ^{1}H-NMR (300 MHz, DMSO-d_6, ppm) δ 6.91 (d,

J=8.86 Hz, 1H, Ar-H), 7.06 (t, J=8.23 Hz, 1H, Ar-H), 7.31 (t, J=8.23 Hz, 1H, Ar-H), 7.48 (d, J=7.32 Hz, 1H, Ar-H), 7.90-7.95 (m, 1H, Ar-H), 8.04 (s, 1H, thiazole C_5-H), 8.75-8.79 (m, 2H, Ar-H), 9.25-9.26 (m, 1H, Ar-H), 11.25 (s, 1H, NH), 13.34 (s, 1H, NH). ^{13}C-NMR (75 MHz, DMSO-d_6, ppm) δ 110.62, 111.56, 111.93, 119.97, 120.42, 120.25, 121.94, 122.89, 126.43, 126.86, 131.18, 132.44, 133.25, 139.82, 141.49, 141.91, 143.16, 143.31, 146.04, 163.57, 167.50. HRMS (*m/z*): $[M+H]^+$ calcd for $C_{16}H_{11}N_5OS$ 322.36; found 322.07.

3-[[4-(4-Pyridyl)-2-thiazolyl]hydrazone]-1H-indol-2,3-dione (2f)

67 % yield; mp 297 °C. IR ν_{max} (cm^{-1}): 3156 (NH), 1684 (C=O), 1620-1466 (C=C, C=N), 1346-985 (C-O, C-N). ^{1}H-NMR (300 MHz, DMSO-d_6, ppm) δ 6.91 (d, J=7.64 Hz, 1H, Ar-H), 7.05 (t, J=7.64 Hz, 1H, Ar-H), 7.30 (t, J=7.64 Hz, 1H, Ar-H), 7.48 (d, J=8.06 Hz, 1H, Ar-H), 7.76-7.80 (m, 2H, Ar-H), 7.92 (s, 1H, thiazole C_5-H), 8.58 (d, J=5.82 Hz, 2H, Ar-H), 11.23 (s, 1H, NH), 13.31 (s, 1H, NH). ^{13}C-NMR (75 MHz, DMSO-d_6, ppm) δ 110.07, 110.40, 111.50, 111.57, 120.08, 120.15, 120.38, 121.81, 122.82, 126.36, 131.02, 131.26, 132.88, 141.07, 149.05, 150.55, 163.59, 166.99. HRMS (*m/z*): $[M+H]^+$ calcd for $C_{16}H_{11}N_5OS$ 322.36; found 322.07.

Microplate Alamar Blue Assay (MABA)

M. tuberculosis H37RV (ATCC 27294), was obtained from the American Type Culture Collection (ATCC). The microorganism was cultured at ATCC® Medium 1395: Middlebrook 7H9 broth with ADC enrichment at a temperature of 37°C for 10 day. The turbidity of the cultures was adjusted to McFarland standard no. 1. Rifampicin and isoniazid were used as standard drugs. Plates (Corning) were incubated at 37°C in 5% CO_2 for 7 days which were added freshly prepared 1:1 mixture of Alamar Blue reagent (1:10 dilution, Invitrogen, 156703SA)) and 10% Tween 80 and then plates were reincubated at 37°C for 24h. After color change from blue to pink the reagent mixture was added to all the wells of the microplate. The results were expressed as MIC (at which all bacteria were inhibited)[33].

RESULTS AND DISCUSSION

Chemistry

Novel 3-[(4-aryl-2-thiazolyl])hydrazone]-1*H*-indol-2,3-dione derivatives (**2a-f**) were synthesized in this study. Six compounds were obtained starting from isatin by nucleophilic addition and cyclization reactions in order, as can be seen **Scheme 1**. 1*H*-Indole-2,3-dione-3-thiosemicarbazone (**1**), the intermediate product was previously obtained molecule which was reported with a melting point of 240-241 °C in literature[34]. The structures of the final compounds were elucidated with spectroscopic techniques. In the IR spectra of the compounds, characteristic bands at 3124-3298 cm^{-1} and 1666-1695 cm^{-1} were observed belong to N-H and C=O bonds, respectively. In the ^{1}H NMR spectra, thiazole C_5-H proton was detected at 7.34-8.04 ppm whereas cyclic amide (lactam) proton

of indole ring was determined at 11.23-11.26 ppm. All other peaks were seen at aromatic region and between ppm 6.71-9.26 ppm. In ^{13}C NMR spectra of the compounds, carbonyl carbon was resonated at about 165.68-167.50 ppm and other carbons were observed at 104.21-163.68 ppm. MS data was also confirmed molecular weights of the compounds.

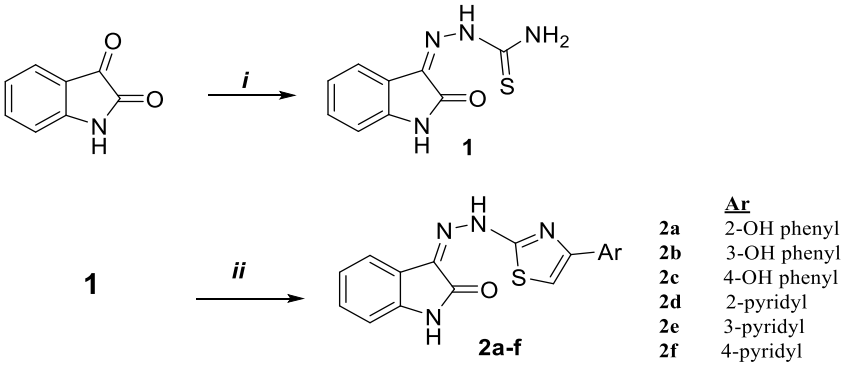

Scheme 1: Synthesis of the compounds (**2a-f**). Reagents: (i) thiosemicarbazide, catalytic amount of acetic acid, ethanol, reflux, 6h; (ii) α-bromoarylethanone, ethanol, rt.

Antitubercular activity

The antimycobacterial activity of six final compounds (**2a-f**) were investigated against *Mycobacterum tuberculosis* H37RV (ATCC 27294) compared with standard drugs isoniazid and rifampin. Minumum inhibitor concentrations (MIC) of tested compounds were found in between 15.63-500 μg/mL whereas MIC was calculated as 31.25 μg/mL for standard drugs. Compounds **2c** with 4-hydroxyphenyl moiety and **2d** with 2-pyridyl moiety displayed significant activity which were determined as the most active compounds (MIC=15.63 μg/mL) even if higher than positive controls. Besides, compound **2e** showed half potential to standard drugs with MIC=62.50 μg/mL. The rest of the compounds did not exhibit remarkable antitubercular activity.

Mycobacterium tuberculosis is known with lipid wrapped cell wall which most of the antibiotics unable to penetrate[35]. It is reported that the lipophilicity is closely associated with antimycobacterial potential of molecules[36]. Log *P* values of the synthesized compounds were predicted using Molinspiration-Calculation of Molecular Properties and Bioactivity Score toolkit[37] and compared with activity results. When MIC values and lipophilic character of the compounds (calculated log *P*) were compared, there is no distinct relationship; however, molecules **2c** and **2d** possess the lowest MIC values with average log *P* values. Accordingly, it could be declared that 3-[(4-aryl-2-thiazolyl)hydrazone]-1*H*-indol-2,3-dione derivatives (**2a-f**) did not show correlative values between log *P* and antituberculotic effects of the compounds.

Table 1: Antitubercular activities against *M. tuberculosis* H37RV (ATCC 27294) and log P predictions of compounds **2a-f**

Compounds	MIC (μg/mL)	Log P[a]
2a	250	2.89
2b	125	2.89
2c	15.63	2.92
2d	15.63	2.94
2e	62.50	3.52
2f	500	3.54
Isoniazid	31.25	-
Rifampin	31.25	-

[a]Calculated by http://www.molinspiration.com/.

REFERENCES

1. Shiradkar, M. R.; Kumar Murahari, K.; Gangadasu, H. R.; Suresh, T.; Kalyan, C. A.; Panchal, Kaur, D. R.; Burange, P.; Ghogare, J.; Mokale, V.; Raut, M. Synthesis of New S-derivatives of Clubbed Triazolyl Thiazole As Anti-*Mycobacterium tuberculosis* Agents. *Bioorg. Med. Chem.* **2007**, *15*, 3997-4008.

2. Mjambili, F.; Njoroge, M.; Naran, K.; De Kock, C.; Smith, P. J.; Mizrahi, V.; Warner, D.; Chibale, K. Synthesis and Biological Evaluation of 2-Aminothiazole Derivatives as Antimycobacterial and Antiplasmodial Agents. *Bioorg. Med. Chem. Lett.* **2014**, *24*, 560-564.

3. Velezheva, V.; Brennan, P.; Ivanov, P.; Kornienko, A.; Lyubimov, S.; Kazarian, K.; Nikonenko, B.; Majorov, K.; Apt., A. Synthesis and Antituberculosis Activity of Indole–pyridine Derived Hydrazides, Hydrazide–hydrazones, and Thiosemicarbazones. *Bioorg. Med. Chem. Lett.* **2016**, *26*, 978-985.

4. Shiradkar, M.; Bhandari, S. V.; Kale, R.; Laghate, A.; Rathi, A. Synthesis and Antimycobacterial Activity of Thiazole Derivatives. *Asian J. Chem.* **2006**, *18*, 2700-2704.

5. Makam, P.; Kannan, T. 2-Aminothiazole Derivatives As Antimycobacterial Agents: Synthesis, Characterization, In Vitro and In Silico Studies. *Eur. J. Med. Chem.* **2014**, *87*, 643-656.

6. Raj, R.; Gut, J.; Rosenthal, P. J.; Kumar, V. 1*H*-1,2,3-Triazole-tethered Isatin-7-chloroquinoline and 3-Hydroxy-indole-7-chloroquinoline Conjugates: Synthesis and Antimalarial Evaluation. *Biorg. Med. Chem.* **2014**, *24*, 756-759.

7. Raja, S.; Prakash, C. R. Novel 1-(4-Substituted Benzylidene)-4-(1-(substituted methyl)-2,3-dioxoindolin-5-yl)semicarbazide Derivatives for Use Against *Mycobacterium tuberculosis* H37Rv (ATCC 27294) and MDR-TB Strain. *Arch. Pharm. Res.* **2013**, *36*, 411-422.

8. Haj Mohammad, K.; Tehrani, E.; Hashemi, M.; Hassan, M.; Kobarfard, F.; Mohebbi, S. Synthesis and Antibacterial Activity of Schiff Bases of 5-Substituted Isatins. *Chinese. Chem. Lett.* **2016**, *27*, 221-225.

9. Zampieri, D.; Mamolo, M. G.; Laurini, E.; Scialino, G.; Banfi, E.; Vio, L. 2-Aryl-3-(1*H*-Azol-1-yl)-

1*H*-Indole Derivatives: A New Class of Antimycobacterial Compounds – Conventional Heating in Comparison with MW-Assisted Synthesis. *Arch. Pharm. Chem. Life Sci.* **2009**, *342*, 716–722.

10. Karthikeyan, S. V.; Perumal, S.; Shetty, K. A.; Yogeeswari, P.; Sriram, D. A. Microwave-Assisted Facile Regioselective Fischer Indole Synthesis and Antitubercular Evaluation of Novel 2-Aryl-3,4-dihydro-2*H*-thieno[3,2-*b*]indoles. *Bioorg. Med. Chem. Lett.* **2009**, *19*, 3006-3009.

11. Cihan-Üstündağ, G.; Çapan, G. Synthesis and Evaluation of Functionalized Indoles As Antimycobacterial and Anticancer Agents. *Mol. Divers.* **2012**, *16*, 525-539.

12. Karki, S. S.; Hazare, R.; Kumar, S.; Saxena, A.; Katiyar, A. Synthesis and Antimicrobial Activity of Some 3-Substituted-2-Oxindole Derivatives. *Turk. J. Pharm. Sci.* **2011**, *8*, 169-178.

13. Haj Mohammad, K.; Tehrani, E.; Mashayekhi, V.; Azerang, P.; Sardari, S.; Kobarfard, F.; Rostamizadeh, K. Synthesis and Antimycobacterial Activity of Novel Thiadiazolylhydrazones of 1-Substituted Indole-3-Carboxaldehydes. *Chem. Biol. Drug Des.* **2014**, *83*, 224-236.

14. Mashayekhi, V.; Haj Mohammad, K.; Tehrani, E.; Azerang, P.; Sardari, S.; Kobarfard, F. Synthesis, Antimycobacterial and Anticancer Activity of Novel Indole-Based Thiosemicarbazones. *Arch. Pharm. Res.* [Online early access]. DOI: 10.1007/s12272-013-0242-z. Published Online: September 24, **2013.**

15. Saundane, A. R.; Walmik, P. Synthesis, Antioxidant, Antimicrobial, Antimycobacterial, and Cytotoxic Activities of Azetidinone and Thiazolidinone Moieties Linked to Indole Nucleus. *J. Chem.* **2013**, 1-9.

16. Sriram, D.; Alexandra Aubry,b Perumal Yogeeswaria and L. M. Fisher Gatifloxacin derivatives: Synthesis, antimycobacterial activities, and inhibition of Mycobacterium tuberculosis DNA gyrase. *Bioorg. Med. Chem. Lett.* **2006**, *16*, 2982-2985.

17. Feng, L. S.; Liu, M. L.; Shuo, W.; Yun, C.; Hao, X. Q.; Meng, S.; Guo, H. Y. Synthesis and In Vitro Antimycobacterial Activity of Balofloxacin Ethylene Isatin Derivatives. *Eur. J. Med. Chem.* **2010**, *45*, 3407-3412.

18. Feng, L. S.; Liu, M. L.; Shuo, W.; Yun, C.; Su-jie, L.; Hui-yuan, G. Synthesis and In Vitro Antimycobacterial Activity of Moxifloxacin Methylene and Ethylene Isatin Derivatives. *Chem. Res. Chinese U.* **2012**, *28*, 61-66.

19. Feng, L. S.; Liu, M. L.; Zhang, S.; Chai, Y.; Wang, B.; Zhang, Y. B.; Lv, K.; Guan, Y.; Guo, H. Y.; Xiao, C. L. Synthesis and In Vitro Antimycobacterial Activity of 8-OCH_3 Ciprofloxacin Methylene and Ethylene Isatin Derivatives. *Eur. J. Med. Chem.* **2011**, *46*, 341-348.

20. Pandeya, S. N.; Smitha, S.; Jyoti, M.; Sridhar, S. K. Biological Activities of Isatin and Its Derivatives. *Acta Pharm.* **2005**, *55*, 27-46.

21. Aboul-Fadl, T.; Bin-Jubair, F. A. S. Anti-Tubercular Activity of Isatin Derivatives. *Int. J. Res. Pharm. Sci.* **2010**, *1*, 113-126.

22. Jeankumar, V. U.; Alokam, R.; Sridevi, J. P.; Suryadevara, P.; Matikonda, S. S.; Peddi, S.; Sahithi, S.; Alvala, M.; Yogeeswari, P.; Sriram, D. Discovery and Structure Optimization of a Series of Isatin Derivatives as *Mycobacterium tuberculosis* Chorismate Mutase Inhibitors. *Chem. Biol. Drug Des.* **2014**, *83*, 498-506.

23. Kumar, R. S.; Rajesh, S. M.; Perumal, S.; Banerjee, D.; Yogeeswari, P.; Sriram, D. Novel Three-component Domino Reactions of Ketones, Isatin and Amino acids: Synthesis and Discovery of Antimycobacterial Activity of Highly Functionalized Novel Dispiropyrrolidines. *Eur. J. Med. Chem.* **2010**, *45*, 411-422.

24. Meenakshi, K.; Gopal, N.; Sarangapani, M. Synthesis, Characterization and Antimicrobial Activity of Some Novel Schiff and Mannich Bases of Isatin. *Int. J. Pharm. Pharmaceut. Sci.* **2014**, *6*, 318-322.

25. Rangaraju, A.; Pannerselvam, P.; Murali, K. Synthesis of Novel 1*H*-Indole-2,3-dione Derivatives as Potent Antimycobacterial Agents. *Int. J. Adv. Pharm. Biol.Chem.* **2013**, *2*, 616-622.

26. Mundhe, D.; Chandewar, A. V.; Shiradkar, M. R. Design and Synthesis of Substituted Clubbed Triazolyl thiazole as XDR & MDR Antituberculosis Agents Part-II. *Pharm. Chem.* **2011**, *3*, 89-102.

27. Nagesh, H. N.; Suresh, A.; Sri Sairam, S. D. S.; Sriram, D.; Yogeeswari, P.; Chandra Sekhar, K. W. S. Design, Synthesis and Antimycobacterial Evaluation of 1-(4-(2-Substitutedthiazol-4-yl)phenethyl)-4-(3-(4-substitutedpiperazin-1-yl)alkyl)piperazine Hybrid Analogues. *Eur. J. Med. Chem.* **2014**, *84*, 605-613.

28. Mamolo, M. G.; Falagiani, V.; Zampieri, D.; Vio, L.; Banfi, E.; Scialino, G. Synthesis and Antimycobacterial Activity of (3,4-Diaryl-3*H*-thiazol-2-ylidene)-hydrazide Derivatives. *Il Farmaco* **2003**, *58*, 631-637.

29. Aridoss, G.; Amirthaganesan, S.; Kim, M. S.; Kim, J. T.; Jeong, Y. T. Synthesis, Spectral and Biological Evaluation of Some New Thiazolidinones and Thiazoles Based on t-3-Alkyl-r-2,c-6-Diarylpiperidin-4-ones. *Eur. J. Med. Chem.* **2009**, *44*, 4199-4210.

30. Makam, P.; Kankanala, R.; Prakash, A.; Kannan, T. 2-(2-Hydrazinyl)thiazole derivatives: Design, Synthesis and In Vitro Antimycobacterial studies. *Eur. J. Med. Chem.* **2013**, *69*, 564-576.

31. Ramshid, P. K.; Jagadeeshan, S.; Krishnan, A.; Mathew, M.; Nair, S. A.; Pillai, M. R. Synthesis and In Vitro Evaluation of Some Isatin-Thiazolidinone Hybrid Analogues as Anti-Proliferative Agents. *Med. Chem.* **2010**, *6*, 306-312.

32. Meleddu, R.; Distinto, S.; Corona, A.; Bianco, G.; Cannas, V.; Esposito, F.; Artese, A.; Alcaro, S.; Matyus, P.; Bogdan, D.; Cottiglia, F.; Tramontano, E.; Maccioni, E. (3*Z*)-3-(2-[4-(aryl)-1,3-Thiazol-2-yl]hydrazin-1-ylidene)-2,3-dihydro-1H-indol-2-one Derivatives As Dual Inhibitors of HIV-1 Reverse Transcriptase. *Eur. J. Med. Chem.* **2015**, *93*, 452-460.

33. Kumar, M.; Khan, I. A.; Verma, V.; Qazi, G. N. Microplate Nitrate Reductase Assay Versus Alamar Blue Assay For MIC Determination of *Mycobacterium tuberculosis*. *Int. J. Tuberc. Lung Dis.* **2005**, *9*, 939-941.

34. Singh, A. S.; Shukla, S. K.; Ahamad, I.; Quraishi, M. A. Solvent-Free Microwave-Assisted Synthesis of 1*H*-Indole-2,3-dione Derivatives. *J. Heterocyclic Chem.* **2009**, *46*, 571-574.

35. Brennan, P. J.; Nikaido, H. The Envelope of Mycobacteria. *Ann. Rev. Biochem.* **1995**, *64*, 29-63.

36. Krátký, M.; Vinsová, J.; Novotná, E.; Mandíková, J.; Wsól, V.; Trejtnar, F.; Ulmannd, V.; Stolaríková, J.; Fernandes, S.; Bhat, S.; Liu, J. O. Salicylanilide Derivatives Block *Mycobacterium tuberculosis* is Through Inhibition of Isocitrate Lyase and Methionine Aminopeptidase. *Tuberculosis*, **2012**, *92*, 434-439.

37. http://www.molinspiration.com/cgi-bin/properties. (Last Accessed: 26.08.20106).

(Received 25 August 2016; accepted 15 November 2016)

Acta Pharm. Sci. Vol 55 No: 1. 2017
DOI: 10.23893/1307-2080.APS.0555

Diabetes Mellitus: A Review on Pathophysiology, Current Status of Oral Medications and Future Perspectives

Mehmet Evren Okur*[1,2], Ioannis D. Karantas[3], Panoraia I. Siafaka[4]

[1] Department of Pharmacology, Faculty of Pharmacy, University of Anadolu, 26470, Tepebaşı, Eskişehir, Turkey
[2] Eskişehir State Hospital, Odunpazarı, Eskişehir, Turkey
[3] Ippokratio General Hospital, B Clinic of Internal Medicine, Thessaloniki, 541 24, Greece
[4] Laboratory of Polymer Chemistry and Technology, Department of Chemistry, Aristotle University of Thessaloniki, 54 124, Thessaloniki, Greece

ABSTRACT

Diabetes mellitus (DM), belongs to the class of metabolic diseases which the main symptom associated with this disease is the high sugar levels in blood for a long period. It can be categorized to the world's major diseases considering that affects high population in earth and presents two main types I and II. Diabetes complications include possible blindness, amputation of lower limb, renal failure, and cardiac arrest or stroke. This review summarizes the pathophysiology for both types of DM, the variety of antidiabetic medications as well as future perspectives. Until now injectable medications are more frequently used in order to achieve the desirable treatment. Patients prefer oral antidiabetic medications since are easier to be administered and for this reason researchers focus their studies at this direction. This work also aimed to present and evaluate possible oral formulations against DM type II.

Keywords: Diabetes mellitus, Epidemiology, Medications, Current status

INTRODUCTION

Diabetes, epidemiology and pathophysiology

Recently, it was recorded that only in 2012 at least 1.5 million deaths induced from diabetes[1]. The terms "Diabetes" and "Mellitus" are derived from Greek language. "Diabetes" denotes "a passer through, a siphon" whereas the "Mellitus" means "sweet". It is believed that Greeks entitled it such way, due to the exaggerated urine proportions produced by diabetic patients which attracted flies and

*Corresponding author: Mehmet Evren Okur
E-mail address: evrenokurecz@gmail.com

bees[2,3]. From the very first described case of DM 3000 years ago by the ancient Egyptians and Araetus of Cappadocia (81-133AD) to 1675 when British Thomas Willis rediscover the sweetness of urine and blood of patients[4,5], since now huge improvement in the knowledge for DM has been achieved. Some theories support that economic[6] and insurance[7] status would play a major role on the express of DM (type II). Moreover a recent study showed that race would also have an important factor on DM prevalence (type I and II)[8].

DM is a serious, chronic and complex illness characterized by hyperglycemia that resulted from the pancreaticβ-cells generate deficient insulin (a hormone that adjusts blood glucose) when the body cannot efficiently custom the insulin or both of them[1,9,10].World health organization has categorized DM as the 7th leading cause in USA while it was estimated that 422 million adults present diabetes in 2014, 4 times higher than the recorded cases in 1980[1]. Clinicians also believe that DM may be occurred by the carbohydrates and fat existence in daily diet given that starch digestion in mammals is accomplished by a-amylase and a-glucosidase. Inhibition of starch digestive enzymes or glucose transporters can reduce glucose release and absorption in the small intestine. This decrement could help to manage DM[11,12].

Although, DM is one of the highest health crisis of the 21st century the majority of ministries and public health authorities keep being oblivious for the current impact of this disease and its complications. Table 1 summarizes the estimation diabetic patients at 2015 and 2040. In developed countries, approximately 87% to 91% of the diagnosed diabetic people are estimated to have type II diabetes, 7% to 12% present type 1 diabetes while 1% to 3% to have other types of diabetes. In under developed and developing countries the relative cases of type I and type II diabetes have not been studied in great detail. Nonetheless, it seems that type I diabetes is less frequent than type II diabetes, as well as it is increasing by almost 3% each year globally. It has been correlated that in most developed countries, the greater part of DM cases in toddlers and juveniles are associated with type I diabetes whereas type II diabetes is reported as a more common condition. Mostly, type II diabetes presence has been elevated alongside accelerated sociocultural alterations: ageing populations, increasing people living in urban areas, low physical activity, increased sugar consumption as well as low fruit and vegetable intake[1,13].

The exact cause of DM is uncertain until now. Nevertheless, scientists believe that genes, environmental factors and other pathological conditions such as autoimmune eradication of the pancreatic β-cells which provoke insulin deficiency and other abnormalities which cause resistance to insulin action seems to involve in the development of the disease[9,10,14].

Table 1: IDF Diabetes Atlas global estimates, 2015 and 2040[1]

	2015	2040
Total word population	7.3 billion	9.0 billion
Adult population (20-79 years old)	4.72 billion	6.16 billion
Child population (0-14 years old	1.92 billion	-
Diabetes (20-79 years)	2015	2040
Global prevalence	8.8% (7.2-11.4%)	10.4% (8.5-13.5%)
Number of people with diabetes	415 million (340-536 million)	642 million (521-829 million)
Number of deaths due to diabetes	5.0 million	-
Health expenditure due to diabetes (20-79 years)	2015	2040
Total health expenditure, R=2* 2015 USD	673 billion	802 billion
Hyperglycaemia in pregnancy (20-49 years)	2015	2040
Proportion of live births affected	16.2%	-
Number of live births affected	20.9 million	-
Impaired glucose tolerance (20-79 years)	2015	2040
Global prevalence	6.7% (4.5-12.1%)	7.8% (5.2-13.9%)
Number of people with impaired glucose tolerance	318 million (212.2-571.6 million)	481 million (317.1-855.7 million)
Type I diabetes (0-14 years)	2015	2040
Number of children with type 1 diabetes	542,000	-
Number of newly diagnosed cases each year	86,000	-

The main symptoms of DM marked hyperglycemia combined with polyuria, polydipsia, polyphagia also known as the 3 P's signs. The presence of the 3 P's could indicate that the blood sugar level is high. In type I, 3 P's can be observed in higher rate while they can be developed quickly. In type the 3 signs are nearly undetectable and develop more gradually. Not so often, weight loss, blurred vision as well as susceptibility to infections could also be aroused by chronic hyperglycemia. The most acute complication of uncontrolled DM which could be

threatening to the life is the hyperglycemia accompanied with ketoacidosis or the nonketotic hyperosmolar syndrome. Diabetic patients may also have high blood pressure and anomaly of lipoprotein metabolism. Among other long-term symptoms, retinopathy with possible vision loss, nephropathy inducing kidney failure, peripheral neuropathy related with the presence of foot lesions, amputations, and Charcot joints. Furthermore autonomic neuropathy generating gastrointestinal, genitourinary, and cardiovascular signs and sexual dysfunction can coexist to diabetic patients. Finally, people diagnosed with DM appear usually atherosclerotic cardiovascular, peripheral arterial, and cerebrovascular diseases[9,10,14].

Classification and diagnosis of diabetes

Three main types of DM are known type **I** associated with full insulin deficiency, type **II**-progressive insulin deficiency[15] and gestational DM which is diagnosed in 2nd or 3rd semester of pregnancy. Currently, although type I cannot be prevented, type II is preventable with good health, exercising and healthy diet. Early diagnosis is the key in diabetes management. Nevertheless, type II have affected high population and lead to complications in several body parts, heart, nerves, eyes, kidney and so on[16]. Diabetes falls into three below general categories:

1. Type I diabetes is as a result of β-cell destruction which customarily provoke complete insulin insufficiency. It was formerly known as insulin-dependent, juvenile or childhood-onset diabetes and it is occasioned by an autoimmune reaction, in which the immune system invaded against the insulin-producing pancreatic beta cells. Type I diabetes is distinguished by deficient insulin production in the body. In such type of DM the patients require daily administration of insulin so as to normalize the glucose level in the blood. Have not taken the insulin, their life is being threatened and can be fatal. The reason of type IDM is not identified yet being presently not preventable. Albeit, the reasons for type I diabetes are still unclear, changes in environmental risk factors and/or viral infections may have an impact on the appearance of DM. Extreme urination and thirst, continuous hunger, weight loss, vision changes and fatigue are the main symptoms of this type of DM. More often than not, the number of people who diagnosed with type I diabetes is escalated.

2. Type II diabetes which earlier termed non-insulin-dependent or adult-onset diabetes, assumed to be a result from a continuous insulin secretory defect on the background of insulin resistance on account of the body's inefficient use of insulin. Type II diabetes is the most typical DM. In this type, the body is capable of producing insulin but becomes so resistant that the insulin is ineffective. By the time, insulin levels could subsequently turned out insufficient. The cause of

high blood glucose levels are both the insulin resistance and deficiency. Given that the symptoms (coincidental to type I diabetes symptoms) are generally less noticeable or absent, the illness could be dismissed and be undiagnosed for numerous years, and not until complications have already ascended. For various years, type IIDM was observed only in adults, nowadays it has started to be seen also in children. Until present the exact causes for the development of type II diabetes are unknown, some significant risk factors being pointed out. The most significant ones include: excess body weight, physical inactivity and poor nutrition. Other factors which impacted are ethnicity, family history of DM, past history of gestational diabetes and advancing age[1,13,17–19].

3. Gestational diabetes mellitus (GDM) is a type of DM determined in the second or third trimester of pregnancy that is not clearly overt diabetes. GDM is a provisional disorder that happens in pregnancy and brings enduring danger of type II diabetes[2,18].Women with slightly elevated blood glucose levels are diagnosed as having gestational diabetes, whilst women with substantially elevated blood glucose levels are classified as having diabetes mellitus in pregnancy. GDM tends to arise from the 24th week of pregnancy. Screening by means of an oral glucose tolerance test is therefore recommended and must be conducted early in pregnancy for high risk women, and between the 24th and 28th week of pregnancy in all other women. Women with hyperglycemia diagnosed during pregnancy are at greater risk of adverse pregnancy outcomes such as: very high blood pressure and foetal macrosomia, with the vaginal birth being difficult and risky. In some cases, clinicians prescribe insulin or oral medication in order to control the blood glucose levels. Notwithstanding, gestational diabetes normally disappears after delivery but women who have been previously diagnosed are in danger of presenting GDM in subsequent pregnancies and type IIDM later in their life. In addition, infants beared by mothers with GDM also have a higher risk of developing type II diabetes during adolescence or early adulthood[1,13,18,19].

Diagnostic Tests for Diabetes Mellitus

DM could be set on diagnosis mainly formed on A1C criteria or plasma glucose criteria, the fasting plasma glucose (FPG) or the 2-h plasma glucose value after a 75-g oral glucose tolerance test (OGTT). The same diagnostics are utilized to screen for and diagnose DM as well as to detect individuals with prediabetes[9,10,14,18,19]. The American Diabetes Association (ADA)/European Association for the Study of Diabetes (EASD) and the American Association of Clinical Endocrinologists (AACE) suggest an HbA1c level of b7.0% and ≤6.5%, respectively, for decreasing the risk of diabetic compromises in most patients[20–22].Table 2 shows criteria in order to diagnose prediabetes and diabetes.

Table 2: Criteria for the Diagnosis of Prediabetes and Diabetes[19]

	Normal	Prediabetes	Diabetes
A1C	≤5.6 %	5.7-6.4 %	≥6.5 %
FPG	≤99 mg/dL	100-125 mg/dL (5.6-6.9 mmol/L)	≥ 126 mg/dL (7.0 mmol/L)
OGTT	1313≤139 mg/dL	100-140-199 mg/dL (7.8-11.0 mmol/L)	≥ 200 mg/dL (11.1 mmol/L)*
RPG	RPG		≥ 200 mg/dL (11.1 mmol/L)**

*In the absence of unequivocal hyperglycemia, results should be confirmed by repeat testing.
**Only diagnostic in a patient with classic symptoms of hyperglycemia or hyperglycemic crisis.
RPG, random plasma glucose.

Complications of Diabetes mellitus

DM may induce several complications or can co-exist with other diseases. In everyday clinical management of diabetic patients, doctors battle with diabetic complications which are very common and come in broad spectrum of manifestations. The complications are divided in microvascular and macrovascular. The macrovascular, which are more severe, are coronary disease, stroke and peripheral neuropathy. The microvascular are sneakier and in long-term maylead on macrovascular complications are diabetic retinopathy, diabetic nephropathy and diabetic foot. In this part several case reports are present among the numerous found in the literature. Neonatal diabetes is a rare form of diabetes mellitus (DM) which might occurs during the first six months of infant's life. The two forms permanent and transient have been associated with alterations in the KCNJ11 and ABCC8 genes most frequently and in the GATA6 gene less frequently. These mutations coexist with gastrointestinal and heart abnormalities. Such is a report of a Caucasian male infant with a GATA6 mutation that developed DM due to pancreatic hypoplasia, ventricular and atrial septal defect, an absent gallbladder and a right inguinal hernia[23].

DM was also correlated with Friedreich's ataxia (FA). A14-year-old male adolescent had insulin-dependent DM on a FA background, while being under treatment with insulin. Studies have shown that islet pancreatic cells reduction that happen in FA is the cause of DM[24].There are cases that pancreatic neuroendocrine tumor (PNET) was connected with DM developing. Such is a case of a patient with a pancreatic somatostatin tumor[25].

ABCC8 mutation in a homozygous state was also connected with DM. The insulin-dependent DM that occurs due to this mutation can be misinterpreted with neonatal DM, although its beginning is later. In those patients sulfonylurea treatment was chosen as primary medication[26].

Despite diabetic striatopathy is a common complication on adults was only reported twice in children. In those cases along with weight loss, polyuria, and polydipsia was reported hemichorea–hemiballism that was receded after glucose control[27].

Among others taking right clinical history of a patient and not only the lean on the lab results for diabetic patients is quite important. A 37-year-old man with many diabetic complications and trouble in glucose regulation was misdiagnosed as DM type I while he was suffering from Neonatal DM as long as two weeks old. The proper taking of the family history revealed that his mother and his brother was also suffering from the same problem. This will help the patient now on his family making options[28]. In another report, a Caucasian woman, 55 years of age without medical history and not ever under any medication, presented with signs of diabetic retinopathy and high blood glucose. Patient's lab tests were found normal. The clinical history revealed recent appearance of polyuria and polydipsia. That set the diagnosis of DM type I which should always be in the front line of a medical doctor's thinking. However, in this case did not conformed with the patient's age[29]. Another category of DM complications is the infections. This category includes bone infections such as patellar osteomyelitis. Two reports of patellar osteomyelitis were revealed, both in adult diabetic women with uncontrolled blood glucose and no formerly medical history. The two patients presented with knee pain and after lab and screening tests were found that they suffered from patellar osteomyelitis. Both were treated with surgery and oral antibiotics with good prognosis. It is believed that diabetic neuropathy which causes dwindling or absence of pain is one factor of the late doctor's consultation. It remains to be found the reasons of the increased frequency of bone and other systemic infections in patients with DM[30].A rare complication that was recorded on a DM patient was Cryptococcosis[31]. This is a common fungal infection on patients that are under chronic immunosuppressant therapy. A 48-year-old man with a lung mass suspected to be cancer had that infection. Cryptococcosis can appear on immunocompetent patients only with a predisposing background and DM is one of them. Another uncommon fungal infection is mucormicosis which has been proven to present more often to DM patients. It remains to be investigated the reasons that this occurred[32].

Update Guidelines for DM treatment

The 2016 Guidelines for Diabetes treatment according to American Diabetes Association are very certain and not controversial[33]. Similar to those are the guidelines of European Association for the Study of Diabetes. The presented guidelines are in most common use and the majority of clinicians obey on them. Firstly, for DM type I the main course of treatment include only insulin in vari-

ous forms: the fast acting involve Lispro, Aspart, Glulisine, the long acting Detemir, Glargine, Degludec and finally the intermediate acting insulin.

For the DM type II the guidelines contain 4 stages which are not meant to be used on the same patient. At the first stage metformin is the cornestone of the treatment. If the target of HbA1c level is not reached in 3 months clinician should add a second drug from the following categories DPP-4 inhibitors, Thiazolidinediones, Sulfonylureas, SGLT2 inhibitors, GLP-1 receptor agonist and basal insulin (stage 2). On third stage (also three months later) and only if the HbA1c level target is not yet reached, a third drug should be used from a different category. Eventually, on the fourth stage (after three months of stage 3) and the HbA1c is above the treatment level the course of treatment consists of metformin, basal insulin and mealtime insulin or GLP-1 receptor agonist.

In fact, there are two major reasons for a clinical doctor to deviate from the guidelines above. The first one is when the patient reveals an allergic reaction to one of medication. In this case they should consider to alter the drug category or moving to the next stage. The second case is when the patient suffers from another condition (which is very common among diabetic patients) and cannot receive a medication from a certain category because it has a contraindication for that condition. The most important part among treatment is the patient to discipline as in drug reception as in the diet.

Current Status on Medications for Type I and II Diabetes mellitus

Howbeit, there is a variety of pharmacological agents for the type II diabetic patients to choose, for type I patients the list is too short. The most significant limitation on antidiabetic treatment is the type of drug administration. Whether insulin formulation was oral then many patients could have a better quality of life. In most cases insulin is the only proposed way in order to reduce the glucose levels. Many researchers now mainly focused on improving the quality of these patients by using novel pharmacological agents. Every patient diagnosed with type I requires lifelong insulin therapy which three main categories are the rapid-acting insulin, long-acting insulin and intermediate options to be chosen. It was 10 years ago when FDA approved an injectable medication known as pramlintide, for people diagnosed with type I diabetes and insulin-treated patientswith type II. Amylin is a natural hormone derived from the pancreatic beta cells and is the hormone which synthetic pramlintide was based on. Pramlintide act as follows: "It is administrated after the meal holding it longer in the stomach, promoting weight loss which keeps the blood glucose level low while also suppress the glucagon production". Until today the main approved treatments for type I DM is insulin and Pramnlitide. However some researchers believe that Metformin

and Sodium Glucose Co-Transporter 2 Inhibitors approved for type II DM could also be involved for type I DM[34,35]. Medications of type II DM include several active ingredients and not only insulin. As it was already referred diabetes type II could complicate the health of the patients and affect a huge adult population. The majority of diabetic people are treated with glucose-lowering medication in order to decrease the long-term compromises.

The main classes of diabetes therapeutics are seven with the main differentiations of such medications include safety, glucose-lowering, type of delivery (oral or injectable) and so on. The history of type II diabetic formulations is long since the first use of synthetic guanidine to take place on 1918[5]. After almost one century, new drugs against type II diabetes based on peptides have been approved from FDA. A brief history of diabetes type II medications is presented in Table 3.

It is widely known between clinicians and patients that insulin is the primary choice for the treatment of type I diabetes. Nonetheless, insulin use is not only limited for type I but can also be applied for type 2 diabetic patients. This is fact when the other antidiabetic formulation does not fulfill the criteria to low blood glucose. The main categories as already reported in literature are also demonstrated in Table 3. Moreover, what researchers should evaluate is the limitation on oral medications and this is why many pharmaceutical technologists and companies target on oral administration of antidiabetic drugs.

Biguanides

Biguanides are organic compounds with the chemical formula shown in Figure 1. Their application as antidiabetic drug is historical long. Although, metformin the most significant analogue of biguanides was known for its antidiabetic properties since 1959, it was not commercially available before late 90s. Metformin mechanism involves the reduce of hepatic glucose production, improve insulin sensitivity as well as peripheral glucose utilization[5,16,36,37]. Metformin use in Type 2 DM may be associated with reduced cancer mortality rates. It lowers A1C by 1-2% and can be used in combination with most other glucose lowering agents[38].

Pharmaceutical formulations for the delivery of metformin

Metformin is aqueous soluble molecule which limited its sustained use as matrix. In current status, researchers try to avoid the burst release in order to extent the utility of the tablets. It is commonly known that sustained release is quite important for oral pharmaceutical products in order to avoid the frequent dosage.

Sustained release dosage form prepared by wet granulation method including a variety of hydrophilic macromolecules such as Hydroxyl-propyl methylcellulose (HPMC) K15M, HPMC K100M and HPMC K200M) and Polyacrylate poly-

mers, Eudragit RL100 and Eudragit RS100 were investigated as drug delivery system of Metformin controlled administration. The in vitro release studies of the above system indicated that the combination of this material may modify the dissolution rate[39]. An extended release tablet containing metformin was successfully prepared via melt granulation combining the hydrophobic stearic acid and hydrophilic poly(ethylene oxide). The matrix tablet formulation showed a controlled drug release profile[40]. Solid dispersions of metformin hydrochloride developed with methocel K100M were investigated also as alternative carrier for the antidiabetic molecule. These carriers prepared by solvent evaporation and co-grinding method revealing that the polymer ratio affected the drug release rate[41]. Similar solid dispersions were also formulated by solvent evaporation and closed melt method, using Compritol 888 ATO as the polymer. Solvent evaporation led to sustained release[42]. Gastro retentive floating tablets containing metformin were produced via wet solid dispersion methodology with cellulose derivatives such as HPMC K4M, HPMC K15M in different ratios, sodium bicarbonate and citric acid gas generating agents and other excipients. Floating tablets were prepared by wet solid dispersion method. Adjusting different parameters the release is controlled whereas the formulations are stable[43].

Table 3: Brief history of type II diabetes pharmacological agents[5]

Year	Active Ingredient	Category of medications
before 1920s	no effective drugs	-
1921	first commercially available insulin in USA	Hormones
1946	Insulin	Neutral protamine Hagedorn-
1950	Tolbutamide	Sulfonylureas
1959	Metformin	Biguanides
1996	Troglitazone	Thiazolidinediones
1997	Repaglinide	Meglitinides
1995	Acarbose	α-Glucosidase Inhibitors
2005	Pramlintide	Amylin Agonists
2008	Colesevelam	Bile acid sequestrants
2009	Bromocriptine	Dopamine agonist
2013	Canagliflozin	Sodium GlucoseCo-Transporter 2 Inhibitors
2014	Dapagliflozin	Sodium Glucose Co-Transporter 2 Inhibitors
2016	Lixisenatide	Peptide

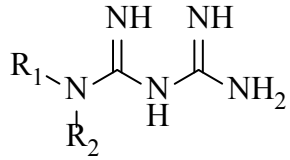

Figure 1: Chemical formula of biguanides

Among the antidiabetic properties metformin also applied as anticancer agent against liver cancer. Gold nanoparticles (AuNPs) were conjugated with hyaluronic acid (HA) and loaded with Metformin on HA capped AuNPs (H-AuNPs). These nanoparticles have an affinity to easily bind on the surface of the liver cancer cells, exhibiting promising results[44].

Sulfonylureas

Sulfonylureas (SU) appearance was found in 1937 when some doctors observe their properties as hypoglycemic agents. Its chemical formula can be seen in Figure 2. Their mechanism of action is to trigger insulin release from pancreatic b-cells[45] In addition can decrease the hepatic glucose production and the uptake of hepatic insulin while can increase the glucagon secretion by pancreatic α-cells[5] The main drawback of SU is that can induce hypoglycemia due to the excess of insulin production and release. First generation drugs include acetohexamide, carbutamide, chlorpropamide, glycyclamide (tolhexamide), metahexamide, tolazamide and tolbutamide while as second generation drugs classified glibenclamide (glyburide), glibornuride, gliclazide, glipizide, gliquidone, glisoxepide and glyclopyramide. Glimepiride may be considered as third generation drug[46].

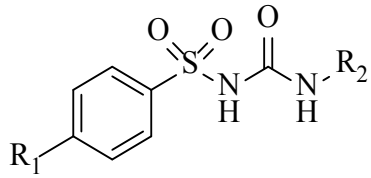

Figure 2: Chemical formula of sulfonylurea

2.2.1 Pharmaceutical formulations for the delivery of sulfonylureas

In most case sulfonylurea agents are lipophilic molecules which their low solubility decrease their bioavailability and therapeutic efficacy. Pharmaceutical technology purposed to improve their water solubility by the preparation of solid dispersions and other pharmaceutical formulations. More specifically, solid dispersions of the glibenclamide were developed by solvent evaporation utilizing hydrophilic polymers as PEG 6000, PVP K30, sorbitol, mannitol, man-

nitol, citric acid and urea in various concentrations. The results depicted that the amorphous formulation present high dissolution rates [47]. Solid dispersion via solvent evaporation and micronized techniques were applied so as to improve oral absorption of the poorly soluble, glimepiride. The release studies illustrated that the two methods were able to enhance and extend the release rate while the formulations were bioequivalent with a marketed product[48].

Furthermore, controlled release matrices of glipizide were synthesized from ethyl cellulose via the direct compression method. Various co-excipients such as HPMC K100M, starch and CMC, were also studied. It was investigated that the release was enhanced[49]Atenolol and Glyburide were both encapsulated in hard gelatin capsule by direct compression method using Avicel, Lactose DC, Crospovidone and Magnesium Stearate in various ratios. Some formulations showed that can improve patient compliance by improving the ease of two drugs administration together [50] An enhancement on the solubility of glipizide was aroused after being dispersed with the help of the hydrophilic poloxamer, cyclodextrin, and povidone. The optimized candidate was further entrapped into non-effervescent floating tablets (NEFT) with the use of crospovidone and release retarding agents like HPMC and PEO. In-vitro buoyancy and release studies demonstrated that non-effervescent floating drug carriers can be a promising method so as to extent the gastric retention time and enhance bioavailability of glipizide[51] Several systems incorporated Glibenclamide based on spray congealing were formulated with the use of sufficient excipients, solid at room temperature, as Myverol, Myvatex, Gelucire. Cremophor EL and Poloxamer 188 were selected as surfactants and PEG 4000 as co-solvent. Researchers believe that the spray congealing is an auspicious novel manufacturing technique of solid self-emulsifying systems[52].

Microcapsules of gliclazide-deoxycholicacid using sodium alginate were studied for their efficiency and size, release kinetics, stability and swelling studies at various pH and temperatures. The micro-carrier displayed colon-targeted delivery and the addition of deoxycholic acid prolonged gliclazide release suggesting its suitability for the sustained and targeted delivery of both molecules to the lower intestine[53].

Meglitinides

Meglitinide (Figure 3) have a similar mechanism action to reduce glucose production as sulfonylureas but they did not present similar chemical formula. They have a weaker binding affinity and faster dissociation from the sulfonylureas binding site[54]. The main analogues of Meglitinides are repaglinide, nateglinide and mitiglinide.

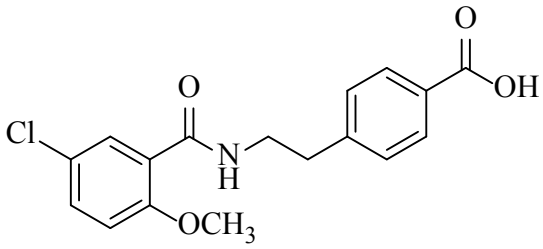

Figure 3: Chemical formula of Meglitinide

Pharmaceutical formulations for the delivery of Meglitinides

Repaglinide present very short half time limited such way its use. Consequently, preparing a controlled release formulation seems important issue. Sustained release pellets of Repaglinide comprised from Avicel, lactose and different polymers were synthesized via extrusion-spheronisation method. The optimized pellet was orally administrated to normal and diabetic rats, decreasing the blood glucose in both normal and diabetic rats throughout 8-12 h[55]**.** Nanoemulsion of repaglinide was characterized as a hopeful carrier for RPG for persistent hypoglycemic effect since showed better hypoglycemic effect in comparison to tablet formulation in experimental diabetic rats [56] Moreover, repaglinide encapsulated floating microspheres were investigated as safe, economical and improved bioavailable formulation showing important ($p < 0.01$) reduce in blood glucose in contrast to pure drug treated group [57].Repaglinide-loaded solid lipid nanoparticles (SLNs) were manufactured with a variety of surfactants (Stearic acid and glyceryl mono stearate, phosphatidylcholin, Tween80, Pluronic F127, poly(vinyl alcohol) and poly(vinyl pyrrolidone) and characterized *in vitro*. It was resulted that the phosphatidylcholin-based SLNs reveal extended drug release time and the highest loading capacity. The drug dissolution rate was slow from all formulations[58]. Nano-crystal formulations of repaglinide were manufactured using soluplus as a stabilizer and KolliphorE-TPGS as an oral absorption enhancer. Nano-crystal formulations revealed significant ($p < 0.001$) hypoglycemic activity with faster onset (less than 30 min) and prolonged duration (up to 8 h) compared to neat repaglinide[59].

Thiazolidinediones

Thiazolidinediones (TZD) or glitazones, belong to the medications of type II diabetes. Their chemical structure consists of thiazolidine groups (Figure 4) which produce the main action of these active ingredients. Their mechanism of action involve activation of peroxisome proliferator-activated receptor (PPAR gamma), a nuclear receptor. This action change the transcription of several genes play a role in glucose and lipid metabolism and energy balance[60]. The main derivatives of TZDs are Pioglitazone, Rosiglitazone and Lobeglitazone.

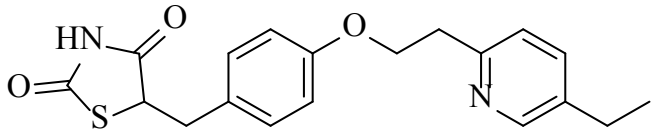

Figure 4: Chemical formula of pioglitazone

Pharmaceutical formulations for the delivery of Thiazolidinediones

Pioglitazone use for more than one year may have an increased danger to provide bladder cancer as FDA warned. However, some formulations are still under experimental design especially to prolong the release.

N-Acyloxymethyl derivatives of pioglitazone were applied as extended-release injectable system. It was found that but acyroyloxymethyl derivative was efficiently converted to pioglitazone as it was established from in vitro rat plasma with a half-life of less than 2 min at 37°C, whereas the level of enzymatic cleavage in rat plasma declined as the ester chain length improves for the longer acyloxymethyl derivatives. The researchers suggested that palmitoyloxymethyl derivative of pioglitazone can be potentially applied as injectable medication in order to treat diabetes[61]. Cyclodextrine complexes of glimepiride) and pioglitazone were studied in order to enhance drug release properties as it was finally proved right[62]. Further, an in-situ injectable and biodegradable triple-interpenetrating network (3XN) hydrogel, was developed in order to deliver rosiglitazone which was comprised from dextran, teleostean and N-carboxyethyl chitosan. The dissolution ability was reported as sustained for the model drug[63].

Glucosidase Inhibitors

Alpha-glucosidase inhibitors are mainly delivered to the patients via oral route so as to decrease blood glucose. Alpha-Glucosidase Inhibitors inhibit alpha- glucosidases that convert polysaccharide carbohydrates into monosaccharides in upper GI system. These drugs slow the absorption of glucose. Acarbose, was the first medication approved by FDA in 1995 and miglitol was following in 1996. Their use is quite limited because they must administer in multiple daily doses while some gastrointestinal (GI) side effects have been recorded.

Pharmaceutical formulations for the delivery of a-Glucosidase Inhibitors

Researchers synthesized microspheres rosiglitazone maleate with desirable yields between 69 and 75%, high entrapment, precarious size distribution, and seductive target release as promising carrier for diabetes management[64]. Among others a-Glucosidase Inhibitors can be found in several plant extract. Literature findings indicate this opinion. Nineteen plants derived from Fabaceae family,

which were applied in Thai traditional medicine for DM management, showed α-glucosidase inhibitory activity via enzymatic reaction[65]. A commonly popular medicinal herb which exhibit α-glucosidase inhibitory activity is Radix Astragali[66]. Pistagremic acid was isolated from the dried galls extract of P. integerrima showing which is the molecule for the antidiabetic property[67].

Sodium-glucose transporter-2 inhibitors

The sodium-glucose transporter-2 (SGLT-2) inhibitors (SGLT-2i) have been newly categorized as antidiabetic agents. SGLT2 is a human protein in humans which inhibit the glucose reabsorption in the kidney, enhancing glucose excretion, and finally decrease blood glucose levels. Canagliflozin (2013), dapagliflozin (2014) and empagliflozin (2014) have taken approval from FDA and EMA for type II diabetes. Diabetic patients could control the glucose levels along with exercise and a healthy diet[5,68–70]. Furthermore, SGLT inhibitors could offer additional options for the achievement of DM management. However, due to their new existence pharmaceutical technologists have not yet evaluated any formulations related with such proteins.

Incretin based-therapies

Incretins consist a group of hormones (the two main are GLP-1 and glucose-dependent insulinotropic peptide) produced by GI that raise insulin secretion in a glucose-dependent manner. Incretin-based therapies focused on GLP-1 consider that native GLP-1 does not present high pharmacological value. This is because of the low half-time of GLP due to its degradation by the peptidase enzyme DPP-4. Two significant strategies have been proposed to control GLP-1-mediated effects: the inhibition of DPP-4, improving the half-life of GLP-1 (DPP-4 inhibitors) and use of glucagon-like peptide-1 receptor agonists (GLP-1 agonists) which can provide supra physiological stimulation of the GLP-1R.Incretin based strategies can enhance the glycemic control with low incidence of hypoglycemia and without fatten. According to some researchers DPP-4 and GLP-1 therapies are more advantageous than metformin[71]. Until now, formulations of incretin-based therapies have not been found in the literature.

Dipeptidyl peptidase -4 Inhibitors

DPP-4 Inhibitors are oral hypoglycemic agents inhibit in DPP-4 enzyme and are not considered as the initial therapy for type II DM. Their applications and formulations are quite new, almost one decade. The first FDA approved drug was sitagliptin with the newest candidate of this class Omarigliptin being commercially available in 2015. DPP-4I mechanism of action involve increment of incretin levels which hinder glucagon release, followed by insulin secretion, re-

duced gastric emptying and decrement of blood glucose levels[72,73]. A recent study showed that patients with severe renal impairment may be improved after DPP-4I administration[74]. Among other recorded side-effects such as pancreatitis, angioedeama, anaphylaxis[75]at 2015 FDA warned that some patients could present sever joint pain. Consequently, safety of DPP-4 use is still under investigation although their numerous advantages.

Glucagon-like peptide-1 receptor agonists

These injectable analogues are also known as GLP-1 receptor agonists or incretin mimetics. Their mechanism of action is to agonists the GLP-1 receptor. Nowadays, the approved agonists are: exenatide, liraglutide, lixisenatide (2016), abliglutide (2014) and dulaglutide. The main advantage of GLP over sulfonylureas or meglitinides is that hypoglycemia can be avoided. On the contrary, these medications may affect the pancreas as DPP-4I drugs[76,77].Up to date, two more agonists are under investigation taspoglutaide and semaglutide. Nonetheless, some undesirable adverse effects of GLP-1 receptor agonists include diarrhea, nausea, and vomiting. Additionally, hypoglycemia occurred in several cases during clinical trials and it was related with concomitant insulin or insulin secretagogues. Nowadays, all guidelines suggest GLP-1 receptor agonists as potential add-on therapy to metformin for patients with uncontrolled type II diabetes. It can be concluded that long-term safety of these drugs is unspecified given their limited time on the market[78].

Future Perspectives

A number of potential therapies for DM are recently being investigated. The current insulin therapy includes subcutaneous injection, which regularly fails to emulate the glucose homeostasis that normal individuals eventuate. This fact generates numerous experiments in order to develop a safer and more effective non-invasive route for insulin delivery. It is widely reported that oral delivery is the most convenient administration route. However, insulin cannot be well absorbed orally because can be rapidly degrade via enzymatic cleavage in the gastrointestinal tract. Nanotechnology plays a key role in future marketed products. Several polymeric nanoparticles and nanocarriers such as liposomes, dendrimers and micelles have been studied in order to safely develop new medications[79–81]. The main properties of such nanoparticles are to present stability in gastrointestinal tract, be nontoxic and biocompatible as well as to be easily developed on a large scale. Moieties conjugation in order to prepare permeation-enhanced properties and high bioavailability revealed promising results indicating that nanoparticle based systems for insulin delivery could be advantageous for DM managements. Among others, herbal plants possess therapeutic values

against DM. In fact, some ingredients of folklore medicinal plants seem to reveal hypoglycemic activity, antioxidant action and antidiabetic activity with desirable properties[82–84].

CONCLUSION

Diabetes mellitus a metabolic disease and its management have aware the clinicians in all over the countries. In current status, a high number of populations have this disease which is related with the modern life style, unhealthy diet and sedentary life. The management of Diabetes Mellitus for Type I, is usually injectable insulin delivery in contrast to Type II which the majority of drugs are orally administered. Currently, the management of Type II diabetes focuses on glucose control via lowering of fasting and postprandial blood glucose and hemoglobin A(1c). In the foreseeable future, researchers believe that the replacement of subcutaneous injections of insulin with nanocarriers could improve the quality of diabetic patients. Furthermore, reducing of blood sugar levels with active ingredients of plants either as primary treatment or as adjunct therapy to conventional medications is a hopeful therapy.

REFERENCES

1. World Health Organization. Global Report on Diabetes. **2016**, 88.

2. Piero, M. N. Diabetes Mellitus – a Devastating Metabolic Disorder. *Asian J. Biomed. Pharm. Sci.* **2015**, *4* (40), 1–7.

3. Patlak, M. New Weapons to Combat an Ancient Disease: Treating Diabetes. *FASEB J.* **2002**, *16* (14), 1853.

4. Ahmed, A. M. History of Diabetes Mellitus. *Saudi Med. J.* **2002**, *23* (4), 373–378.

5. White Jr. J.R. A Brief History of the Development of Diabetes Medications. *Diabetes Spectr.* **2014**, *27* (2), 82–86.

6. Link, C. L.and McKinlay, J. B. Disparities in the Prevalence of Diabetes: Is It Race/ethnicity or Socioeconomic Status? Results from the Boston Area Community Health (BACH) Survey. *Ethn. Dis.* **2009**, *19* (3), 288–292.

7. Miller, S. T.; Schlundt, D. G.; Larson, C.; Reid, R.; Pichert, J. W.; Hargreaves, M.; Brown, A.; McClellan, L.; Marrs, M. Exploring Ethnic Disparities in Diabetes, Diabetes Care, and Lifestyle Behaviors: The Nashville REACH 2010 Community Baseline Survey. *Ethn. Dis.* **2004**, *14* (3 Suppl 1), S38-45.

8. Heidemann, D. L.; Joseph, N. A.; Kuchipudi, A.; Perkins, D. W.; Drake, S. Racial and Economic Disparities in Diabetes in a Large Primary Care Patient Population. *Ethn. Dis.* **2016**, *26* (1), 85–90.

9. Diagnosis and Classification of Diabetes Mellitus. *Diabetes Care* **2010**, *33* (Supplement_1), S62–S69.

10. Diagnosis and Classification of Diabetes Mellitus. *Diabetes Care* **2013**, *36* (Supplement_1), S67–S74.

11. Tan, Y.; Chang, S. K. C.and Zhang, Y. Comparison of α-Amylase, α-Glucosidase and Lipase Inhibitory Activity of the Phenolic Substances in Two Black Legumes of Different Genera. *Food Chem.* **2017**, *214*, 259–268.

12. Rossi, E. J.; Sim, L.; Kuntz, D. A.; Hahn, D.; Johnston, B. D.; Ghavami, A.; Szczepina, M. G.; Kumar, N. S.; Sterchi, E. E.; Nichols, B. L.; Pinto, B. M.; Rose, D. R. Inhibition of Recombinant Human Maltase Glucoamylase by Salacinol and Derivatives. *FEBS J.* **2006**, *273* (12), 2673–2683.

13. http://www.diabetesatlas.org/resources/2015-atlas.html

14. Diagnosis and Classification of Diabetes Mellitus. *Diabetes Care* **2014**, *37*(Supplement_1), S81–S90.

15. Gale, E. The Discovery of Type 1 Diabetes. *Diabetes* **2001**, *50*, 217–226.

16. Wu, H.; Walker, J.; Damhuis, R. A.; Brewster, D. H.; Wild, S. H. Metformin and Survival of People with Type 2 Diabetes and Pleural Mesothelioma: A Population-Based Retrospective Cohort Study. *Lung Cancer* **2016**, *99*, 194–199.

17. Olokoba, A. B.; Obateru, O. A.and Olokoba, L. B. Type 2 Diabetes Mellitus: A Review of Current Trends. *Oman Med. J.* **2012**, *27* (4), 269–273.

18. Standards of Medical Care in Diabetes--2014. *Diabetes Care* **2014**, *37* (Supplement_1), S14–S80.

19. Standards of Medical Care in Diabetes—2015 Abridged for Primary Care Providers. *Clin. Diabetes* **2015**, *33* (2), 97–111.

20. Milligan, S. Combination Therapy for the Improvement of Long-Term Macrovascular and Microvascular Outcomes in Type 2 Diabetes: Rationale and Evidence for Early Initiation. *J. Diabetes Complications* **2016**, *30* (6), 1177–1185.

21. Inzucchi, S. E.; Bergenstal, R. M.; Buse, J. B.; Diamant, M.; Ferrannini, E.; Nauck, M.; Peters, A. L.; Tsapas, A.; Wender, R.; Matthews, D. R. Management of Hyperglycemia in Type 2 Diabetes, 2015: A Patient-Centered Approach: Update to a Position Statement of the American Diabetes Association and the European Association for the Study of Diabetes. *Diabetes Care* **2015**, *38* (1), 140–149.

22. Garber, A. J.; Abrahamson, M. J.; Barzilay, J. I.; Blonde, L.; Bloomgarden, Z. T.; Bush, M. A.; Dagogo-Jack, S.; DeFronzo, R. A.; Einhorn, D.; Fonseca, V. A.; Garber, J. R.; Garvey, W. T.; Grunberger, G.; Handelsman, Y.; Henry, R. R.; Hirsch, I. B.; Jellinger, P. S.; McGill, J. B.; Mechanick, J. I.; Rosenblit, P. D.; Umpierrez, G. E. Consensus statement by the AmericN Association of clinical endocrinologists and American College of Endocrinology on the comprehensive type2 diabetes management algorithm-2016 executive summary. *Endocr. Pract.* **2016**, *22* (1), 84–113.

23. McMillan, T.; Girgis, R.and Sellers, E. A. C. Neonatal Diabetes and Protein Losing Enteropathy: A Case Report. *BMC Med. Genet.* **2016**, *17* (1), 32.

24. Chakraborty, P. P.; Ray, S.; Bhattacharjee, R.; Ghosh, S.; Mukhopadhyay, P.; Mukhopadhyay, S.; Chowdhury, S. First Presentation of Diabetes as Diabetic Ketoacidosis in a Case of Friedreich's Ataxia. *Clin. Diabetes* **2015**, *33* (2), 84–86.

25. Han, B.; Zhai, H.; Yu, J.; Xia, F.; Lu, Y. Diabetes Mellitus Associated with Pancreatic Somatostatin Tumor: A Case Report. *J. Clin. Transl. Endocrinol. Case Reports* **2016**, *2*, 20–22.

26. Shaikh, S. T.; Jadhav, S. S.; Shivane, V. K.; Lila, A. R.; Bandgar, T. R.; Shah, N. S. Childhood

Onset of Sulfonylurea Responsive Neonatal Diabetes Due to a Novel Homozygous Autosomal Recessive Mutation in the ABCC8 Gene Which Was Presumed to Be Type 1B Diabetes Before Genetic Analysis. *AACE Clin. Case Reports* **2016**, *2* (2), e117–e121.

27. Faundez, T.; Klee, P.; Hanquinet, S.; Schwitzgebel, V.; Burkhard, P. R.; Korff, C. M. Diabetic Striatopathy in Childhood: A Case Report. *Pediatrics* **2016**, *137* (4).

28. Arce, K. M.and Pantalone, K. M. Not All Diabetes in Infants Is Type 1: A Case Report. *Diabetes Ther.* **2016**, *7* (2), 369–375.

29. Saleh, A. Diagnosis of Type 1 Diabetes Mellitus in Adulthood – a Case Report. **2015**, *44* (4), 233–235.

30. Kumar, R. S.; Singhi, P. K.and Kakkandki, K. Case Report of Two Cases of Patella Subacute Osteomyelitis in Diabetic Women A Rare Entity. *J. Orthop. Case Reports* **2016**, *6* (2), 13–15.

31. Prasad, K. T.; Sehgal, I. S.; Shivaprakash, M. R.; Dhooria, S. Uncommon Mycosis in a Patient with Diabetes. *BMJ Case Rep.* **2016**, bcr2016214453.

32. Saul, S. R.; Aleksic, S.and Magnotti, M. A Patient with Newly Diagnosed Diabetes Presenting with Sino-Orbital Mucormycosis. *AACE Clin. Case Reports* **2016**, *2* (1), e41–e45.

33. Standards of Medical Care in Diabetes - 2016. *Diabetes Care* **2016**, *39* (1), S1–S112.

34. Perkins, B. A.; Cherney, D. Z. I.; Partridge, H.; Soleymanlou, N.; Tschirhart, H.; Zinman, B.; Fagan, N. M.; Kaspers, S.; Woerle, H.-J.; Broedl, U. C.; Johansen, O.-E. Sodium-Glucose Cotransporter 2 Inhibition and Glycemic Control in Type 1 Diabetes: Results of an 8-Week Open-Label Proof-of-Concept Trial. *Diabetes Care* **2014**, *37* (5), 1480–1483.

35. Liu, W.and Yang, X.-J. The Effect of Metformin on Adolescents with Type 1 Diabetes: A Systematic Review and Meta-Analysis of Randomized Controlled Trials. *Int. J. Endocrinol.* **2016**, *2016*, 1–12.

36. Inzucchi, S. E.; Bergenstal, R. M.; Buse, J. B.; Diamant, M.; Ferrannini, E.; Nauck, M.; Peters, A. L.; Tsapas, A.; Wender, R.; Matthews, D. R.; American Diabetes Association (ADA); European Association for the Study of Diabetes (EASD). Management of Hyperglycemia in Type 2 Diabetes: A Patient-Centered Approach: Position Statement of the American Diabetes Association (ADA) and the European Association for the Study of Diabetes (EASD). *Diabetes Care* **2012**, *35* (6), 1364–1379.

37. Maruthur, N. M.; Tseng, E.; Hutfless, S.; Wilson, L. M.; Suarez-Cuervo, C.; Berger, Z.; Chu, Y.; Iyoha, E.; Segal, J. B.; Bolen, S. Diabetes Medications as Monotherapy or Metformin-Based Combination Therapy for Type 2 Diabetes. *Ann. Intern. Med.* **2016**, *164* (11), 1–20.

38. El-Kaissi, S.and Sherbeeni, S. Pharmacological Management of Type 2 Diabetes Mellitus: An Update. *Curr. Diabetes Rev.* **2011**, *7* (6), 392–405.

39. Roy, H.; Brahma, C. K.; Nandi, S.; Parida, K. R. Formulation and Design of Sustained Release Matrix Tablets of Metformin Hydrochloride: Influence of Hypromellose and Polyacrylate Polymers. *Int. J. Appl. basic Med. Res.* **2013**, *3* (1), 55–63.

40. Nanjwade, B. K.; Mhase, S. R.and Manvi, F. V. Formulation of Extended-Release Metformin Hydrochloride Matrix Tablets. *Trop. J. Pharm. Res.* **2011**, *10* (4), 375–383.

41. Patil, S. A.; Kuchekar, B. S.; Chabukswar, A. R.; Jagdale, S. C. Formulation Evaluation of Extended-Release Solid Dispersion of Metformin Hydrochloride. *J. Young Pharm.* **2010**, *2* (2), 121–129.

42. Jagdale, S.; Patil, S.; Kuchekar, B.; Chabukswar, A. Preparation and Characterization of Metformin Hydrochloride – Compritol 888 ATO Solid Dispersion. *J. Young Pharm.* **2011**, *3* (3), 197–204.

43. Parveen, R.; Singh, A. P.; Kumar Bhargav, R.; Verma, A.; Priyanka, S. Formulation and evaluation of floating tablet of Metformin HCL. *World J. Pharm. Pharm. Sci.* **2016**, *5* (7), 1317–1326.

44. Kumar, C. S.; Raja, M. D.; Sundar, D. S.; Gover Antoniraj, M.; Ruckmani, K. Hyaluronic Acid Co-Functionalized Gold Nanoparticle Complex for the Targeted Delivery of Metformin in the Treatment of Liver Cancer (HepG2 Cells). *Carbohydr. Polym.* **2015**, *128*, 63–74.

45. Seino, S. Cell Signalling in Insulin Secretion: The Molecular Targets of ATP, cAMP and Sulfonylurea. *Diabetologia* **2012**, *55* (8), 2096–2108.

46. Davidson, J. *Clinical Diabetes Mellitus: A Problem-Oriented Approach Diabetes Mellitus*; Thieme Medical Publishers, **2000**.

47. Mudgal, S.and Pancholi, S. Formulation of Glibenclamide Solid Dispersions by Solvent Evaporation Technique. *J. Chem. Pharm. Res.* **2012**, *4* (1), 353–359.

48. Ning, X.; Sun, J.; Han, X.; Wu, Y.; Yan, Z.; Han, J.; He, Z. Strategies to Improve Dissolution and Oral Absorption of Glimepiride Tablets: Solid Dispersion versus Micronization Techniques. *Drug Dev. Ind. Pharm.* **2011**, *37* (6), 727–736.

49. Mehsud, S. U.; Khan, G. M.; Hussain, A.; Akram, M.; Akhlaq, M.; Khan, K. A.; Shakoor, A. Controlled Release Matrix Tablets of Glipizide: Influence of Different Grades of Ethocel and Co-Excipient on Drug Release. *Pak. J. Pharm. Sci.* **2016**, *29* (3), 779–787.

50. Maboos, M.; Yousuf, R. I.and Shoaib, M. H. Formulation Development and Optimization: Encapsulated System of Atenolol and Glyburide. *Pak. J. Pharm. Sci.* **2016**, *29* (2), 569–577.

51. Meka, V. S.; Pillai, S.; Dharmalingham, S. R.; Sheshala, R.; Gorajana, A. Preparation and in Vitro Characterization of a Non-Effervescent Floating Drug Delivery System for Poorly Soluble Drug, Glipizide. *Acta Pol. Pharm.* **2015**, *72* (1), 193–204.

52. Albertini, B.; Sabatino, M. Di; Melegari, C.; Passerini, N. Formulation of Spray Congealed Microparticles with Self-Emulsifying Ability for Enhanced Glibenclamide Dissolution Performance. *J. Microencapsul.* **2015**, *32* (2), 181–192.

53. Mooranian, A.; Negrulj, R.; Al-Sallami, H. S.; Fang, Z.; Mikov, M.; Golocorbin-Kon, S.; Fakhoury, M.; Arfuso, F.; Al-Salami, H. Release and Swelling Studies of an Innovative Antidiabetic-Bile Acid Microencapsulated Formulation, as a Novel Targeted Therapy for Diabetes Treatment. *J. Microencapsul.* **2015**, *32* (2), 151–156.

54. Blicklé, J. F. Meglitinide Analogues: A Review of Clinical Data Focused on Recent Trials. *Diabetes Metab.* **2006**, *32* (2), 113–120.

55. Tavakoli, N.; Minaiyan, M.; Tabbakhian, M.; Pendar, Y. Preparation and Evaluation of a Controlled Drug Release of Repaglinide through Matrix Pellets: In Vitro and in Vivo Studies. *J. Microencapsul.* **2014**, *31* (6), 529–534.

56. Akhtar, J.; Siddiqui, H. H.; Fareed, S.; Badruddeen; Khalid, M.; Aqil, M. Nanoemulsion: For Improved Oral Delivery of Repaglinide. *Drug Deliv.* **2016**, *23* (6), 2026–2034.

57. Sharma, M.; Kohli, S.and Dinda, A. In-Vitro and in-Vivo Evaluation of Repaglinide Loaded Floating Microspheres Prepared from Different Viscosity Grades of HPMC Polymer. *Saudi Pharm. J.* **2015**, *23* (6), 675–682.

58. Ebrahimi, H. A.; Javadzadeh, Y.; Hamidi, M.; Jalali, M. B. Repaglinide-Loaded Solid Lipid Nanoparticles: Effect of Using Different Surfactants/stabilizers on Physicochemical Properties of Nanoparticles. *DARU J. Pharm. Sci.* **2015**, *23* (1), 46.

59. Gadadare, R.; Mandpe, L.and Pokharkar, V. Ultra Rapidly Dissolving Repaglinide Nanosized Crystals Prepared via Bottom-Up and Top-Down Approach: Influence of Food on Pharmacokinetics Behavior. *AAPS PharmSciTech* **2015**, *16* (4), 787–799.

60. Hauner, H. The Mode of Action of Thiazolidinediones. *Diabetes. Metab. Res. Rev.18 Suppl 2*, **2002**, S10-5.

61. Sanrame, C. N.; Remenar, J. F.; Blumberg, L. C.; Waters, J.; Dean, R. L.; Dong, N.; Kriksciukaite, K.; Cao, P.; Almarsson, Ö. Prodrugs of Pioglitazone for Extended-Release (XR) Injectable Formulations. *Mol. Pharm.* **2014**, *11* (10), 3617–3623.

62. Taupitz, T.; Dressman, J. B.and Klein, S. New Formulation Approaches to Improve Solubility and Drug Release from Fixed Dose Combinations: Case Examples Pioglitazone/glimepiride and Ezetimibe/simvastatin. *Eur. J. Pharm. Biopharm.* **2013**, *84* (1), 208–218.

63. Zhang, H.; Qadeer, A.; Mynarcik, D.; Chen, W. Delivery of Rosiglitazone from an Injectable Triple Interpenetrating Network Hydrogel Composed of Naturally Derived Materials. *Biomaterials* **2011**, *32* (3), 890–898.

64. Mohan Kamila, M.; Mondal, N.; Kanta Ghosh, L.; Kumar Gupta, B. Multiunit Floating Drug Delivery System of Rosiglitazone Maleate: Development, Characterization, Statistical Optimization of Drug Release and In Vivo Evaluation. *AAPS PharmSciTech* **2009**, *10* (3), 887–899.

65. Dej-Adisai, S.and Pitakbut, T. Determination of a-Glucosidase Inhibitory Activity from Selected Fabaceae Plants. *Pak. J. Pharm. Sci.* **2015**, *28* (5), 1679–1683.

66. Zhao, H.; Zhang, Y.; Guo, Y.; Shi, S. Identification of Major α-Glucosidase Inhibitors in Radix Astragali and Its Human Microsomal Metabolites Using Ultrafiltration HPLC–DAD–MSn. *J. Pharm. Biomed. Anal.* **2015**, *104*, 31–37.

67. Uddin, G.; Rauf, A.; Al-Othman, A. M.; Collina, S.; Arfan, M.; Ali, G.; Khan, I. Pistagremic Acid, a Glucosidase Inhibitor from Pistacia Integerrima. *Fitoterapia* **2012**, *83* (8), 1648–1652.

68. Haas, B.; Eckstein, N.; Pfeifer, V.; Mayer, P.; Hass, M. D. S. Efficacy, Safety and Regulatory Status of SGLT2 Inhibitors: Focus on Canagliflozin. *Nutr. Diabetes* **2014**, *4*, e143.

69. Powell, J.; Miller, S. A.and Taylor, J. R. Sodium-Glucose Cotransporter 2 Inhibitors: The New Option for Diabetes Mellitus Management. *South. Med. J.* **2015**, *108* (2), 82–90.

70. Wu, J. H. Y.; Foote, C.; Blomster, J.; Toyama, T.; Perkovic, V.; Sundström, J.and Neal, B. Effects of Sodium-Glucose Cotransporter-2 Inhibitors on Cardiovascular Events, Death, and Major Safety Outcomes in Adults with Type 2 Diabetes: A Systematic Review and Meta-Analysis. *Lancet Diabetes Endocrinol.* **2016**, *4* (5), 411–419.

71. Brunton, S. GLP-1 Receptor Agonists vs. DPP-4 Inhibitors for Type 2 Diabetes: Is One Approach More Successful or Preferable than the Other? *Int. J. Clin. Pract.* **2014**, *68* (5), 557–567.

72. Behme, M. T.; Dupré, J.and McDonald, T. J. Glucagon-like Peptide 1 Improved Glycemic Control in Type 1 Diabetes. *BMC Endocr. Disord.* **2003**, *3* (1), 3.

73. Koliaki, C.and Doupis, J. Incretin-Based Therapy: A Powerful and Promising Weapon in the Treatment of Type 2 Diabetes Mellitus. *Diabetes Ther.* **2011**, *2* (2), 101–121.

74. Chen, M.; Liu, Y.; Jin, J.and He, Q. The Efficacy and Safety of Dipeptidyl Peptidase-4 In-

hibitors for Treatment of Type 2 Diabetes Mellitus Patients with Severe Renal Impairment: A Meta-Analysis. *Ren. Fail.* **2016**, *38* (4), 581–587.

75. Karagiannis, T.; Boura, P.and Tsapas, A. Safety of Dipeptidyl Peptidase 4 Inhibitors: A Perspective Review. *Ther. Adv. Drug Saf.* **2014**, *5* (3), 138–146.

76. Trujillo, J. M.; Nuffer, W.and Ellis, S. L. GLP-1 Receptor Agonists: A Review of Head-to-Head Clinical Studies. *Ther. Adv. Endocrinol. Metab.* **2015**, *6* (1), 19–28.

77. Kalra, S.; Baruah, M.; Sahay, R.; Unnikrishnan, A.; Uppal, S.; Adetunji, O. Glucagon-like Peptide-1 Receptor Agonists in the Treatment of Type 2 Diabetes: Past, Present, and Future. *Indian J. Endocrinol. Metab.* **2016**, *20* (2), 254.

78. Prasad-Reddy, L.and Isaacs, D. A Clinical Review of GLP-1 Receptor Agonists: Efficacy and Safety in Diabetes and beyond. *Drugs Context* **2015**, *4*, 1–19.

79. Sharma, G.; Sharma, A. R.; Nam, J.-S.; Doss, G. P. C.; Lee, S.-S.; Chakraborty, C. Nanoparticle Based Insulin Delivery System: The next Generation Efficient Therapy for Type 1 Diabetes. *J. Nanobiotechnology* **2015**, *13* (1), 74.

80. Alai, M. S.; Lin, W. J.and Pingale, S. S. Application of Polymeric Nanoparticles and Micelles in Insulin Oral Delivery. *J. Food Drug Anal.* **2015**, *23* (3), 351–358.

81. Subramani, K. and Pathak, S. Recent Trends in Diabetes Treatment Using Nanotechnology. **2012**, *7* (1), 85–95.

82. Ezuruike, U. F. and Prieto, J. M. The Use of Plants in the Traditional Management of Diabetes in Nigeria: Pharmacological and Toxicological Considerations. *J. Ethnopharmacol.* **2014**, *155* (2), 857–924.

83. Patel, D. K.; Kumar, R.; Laloo, D.; Hemalatha, S. Diabetes Mellitus: An Overview on Its Pharmacological Aspects and Reported Medicinal Plants Having Antidiabetic Activity. *Asian Pac. J. Trop. Biomed.* **2012**, *2* (5), 411–420.

84. Rahimi, M. A Review: Anti Diabetic Medicinal Plants Used for Diabetes Mellitus. *Bull. Environ. Pharmacol. Life Scienes* **2015**, *4* (2), 163–180.

(Received 29 August 2016; accepted 14 November 2016)

Acta Pharm. Sci. Vol 55 No: 1. 2017
DOI: 10.23893/1307-2080.APS.0556

Synthesis, Antimicrobial Activity Studies and Molecular Property Predictions of Schiff Bases Derived from ortho-Vanillin

Barkın Berk*[1], Merve Ertaş[1], Sevde Nur Biltekin[1]

[1] İstanbul Medipol University, School of Pharmacy, Kavacık Mah. Ekinciler Cad. No.19 Kavacık Kavşağı, TR-34810, Beykoz, İstanbul, Turkey

ABSTRACT

Schiff bases are known to possess anticancer, antibacterial, antifungal, antitubercular, anti-inflammatory, antibacterial and antimalarial properties. At the same time, in recent years, prediction of drug-likeness, molecular, absorption, distribution, metabolism, and excretion (ADME) properties using in silico techniques has become a standard procedure for the evaluation of clinical usable molecules. In this study, Schiff base structured 2-methoxy-6-{[(2-alkyl/arylethyl)imino]methyl}phenol derivatives were synthesized from 3-methoxysalicylaldehyde (*o*-vanillin). The antibacterial and antifungal activities of these compounds were determined against *Staphylococcus aureus, Escherichia coli*, *Candida albicans and Pseudomonas aeruginosa* using agar-well diffusion and broth microdilution techniques. Further analysis was conducted using the in silico technique to predict the drug-likeness, molecular and ADME properties of these molecules. Among all the compounds, 2-{[(4-fluorophenethyl)imino]methyl}-6-methoxyphenol (Compound 9) exhibited the highest activity with good minimum inhibition concentration and radius of inhibition zone values against *Candida albicans*.

Keywords: Schiff bases, Antifungal, *Candida albicans*, Molecular properties, In silico

INTRODUCTION

Schiff bases (azomethines) are compounds containing structures of R-CH=N-R' (R^1H), where R and R' can be either alkyl, aryl, cycloalkyl or heterocyclic groups [1-3]. These compounds are very well recognized and due to their unusual properties, they are used in a wide range of application areas including organic

*Corresponding author. Tel.; +90-216-6815364 Fax: +90-212-5317555.
E-mail address: bberk@medipol.edu.tr (Barkın Berk).

and bioinorganic chemistry as common non-enzymatic/enzymatic intermediates, coordination and supramolecular chemistry as common ligands as well as biomedical applications and material sciences [4-11]. They have also been reported to show antibacterial[12-17], antifungal[14-16] and antitumoral[18-19] activities.

Schiff bases can be synthesized by nucleophilic addition followed by dehydration reaction cascade between aliphatic or aromatic amines and active carbonyl compounds. Various derivatives of these compounds formed from the reaction between salicylaldehydes and amines act as cellular growth regulators for plants[20] and have antibacterial[21] and antimycotic[22] activities. A wide range of different Schiff base ligands produced from *ortho*-hydroxyl substituted aromatic aldehydes have shown important coordinating properties for specific metal ions such as Al (III), Zn (II), Ag (II), Y (III), Co (II), Pb (II), Cu (II), Ni (II), Gd (III), Hg (II)[23-28] and act as bidentate ligands for transitional metal ions[29-33]. At the same time, these compounds and/or their metal complexes have exhibited important anticancer and herbicidal properties[34-35].

Similarly, a wide range of aldehyde and phenol structured secondary metabolites of plants isolated as crude extracts or oils have been studied for their potential antibacterial and antioxidant activities[36-39]. *Ortho*-vanillin (*o*-vanillin) can be considered one of the several examples of these compounds with antibacterial and antifungal activity [37, 40-41] as well as irritant properties.

In the course of our study, we synthesized 2-methoxy-6-{[(2-alkyl/arylethyl)imino]methyl}phenol derivatives, Schiff bases of *ortho*-vanillin and 2-aryl/alkylethaneamines. The antibacterial and antifungal activities of the compounds were determined against *Staphylococcus aureus, Escherichia coli*, *Candida albicans and Pseudomonas aeruginosa* using agar-well diffusion and broth microdilution techniques. Furthermore, their absorption, distribution, metabolism, and excretion (ADME), drug-likeness and molecular properties were predicted using in silico techniques. Although Compounds 1, 3, 4, 7, 8, 13, 14 and 15 had been previously synthesized using different methods and investigated in other subjects[42-49], in this study, we resynthesized them and performed a microbiological and prediction analysis to test their antibacterial and antifungal activities.

METHODOLOGY

Chemistry

All chemicals were purchased from Aldrich Chemical Co. (Steinheim, Germany). Melting points were determined with a Mettler-Toledo FP62 capillary melting point apparatus (Columbus, OH, USA) and uncorrected. IR spectra (KBr) were recorded on a PerkinElmer Spectrum One FT-IR spectrometer (Waltham,

MA, USA) and ^{1}H-NMR spectra were obtained by Bruker DPX-400, 400 MHz High Performance Digital FT-NMR. All chemical shift values were recorded as δ (ppm). Mass spectra were recorded using an Agilent 1100 series LC/APCI/MS 1946 G spectrometer in the negative ionization mode. The purity of the compounds was checked by thin-layer chromatography on silica gel-coated aluminum sheets (Merck, 1.005554, silica gel HF254–361, Type 60, 0.25 mm; Darmstadt, Germany). The elemental analyses were performed with a Leco CHNS 932 analyzer (Leco Corp., MI, USA) and were found to be within ± 0.4 % of the theoretical values for C, H and N.

General synthesis for Schiff derivatives

Equimolar quantities (0.01 mol) of 3-methoxysalicylaldehyde and 2-aryl/alkylethaneamines were dissolved in methanol and stirred at room temperature for 10 to 120 min to obtain a clear solution using activated molecular sieves. Then, depending on the type of the substance, the solutions were either kept at room temperature or refrigerated overnight. The solutions that had precipitates were filtered, recrystallized, washed with cold methanol three times and dried in a vacuum desiccator. For the solutions that did not have any precipitates, column chromatography was performed using ethanol-ethyl acetate (1:1 v/v) as a mobile phase and the final compounds were obtained as either dark to light yellow solid crystals or yellow oils (Scheme 1).

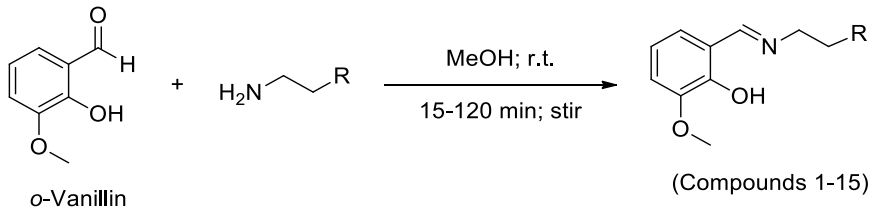

Scheme 1: Synthetic pathway followed for the preparation of 2-methoxy-6-{[(2-alkyl/arylethyl)imino]methyl}phenol derivatives (Compounds 1-15)

2-methoxy-6-({[2-(pyridin-2-yl)ethyl]imino}methyl)phenol (Compound 1)

Yield 80%, yellow oil. IR (KBr) $\bar{\upsilon}_{max}$ (cm^{-1}): 3444 (s, OH), 3000 (CH, aromatic), 2795 (CH, aliphatic), 1632 (C=N), 1254. ^{1}H-NMR (400 MHz, DMSO-*d6*, δ): 3.2 (t, J=7.10 Hz, 2H, Py-CH_2), 3.90 (s, 3H, O-CH_3), 4.1 (t, J=7.10 Hz, 2H, CH_2-N=C), 5.30 (s, 1H, OH), 6.80-7.2 (m, 3H, Ph), 7.2-7.60, (m, 3H, Py), 8.2 (s, 1H, HC=N), 8.55 (d, 1H, Py). MS 256.1 (M^+). Anal. calcd for $C_{15}H_{16}N_2O_2$: C, 70.29; H, 6.29; N, 10.93. Found: C, 70.26; H, 6.31; N, 10.90.

2-methoxy-6-({[2-(morpholin-4-yl)ethyl]imino}methyl)phenol (Compound 2)

Yield 70%, yellow crystals, mp 38-39 °C. IR (KBr) $\bar{\upsilon}_{max}$ (cm^{-1}): 3008 (CH, aromatic), 2938 (CH, aliphatic), 1633 (C=N), 1253. ^{1}H-NMR (400 MHz, DMSO-*d6*, δ): 2.37 (t, J=7.00 Hz, 4H, Mor), 3.2 (t, J=7.10 Hz, 2H, Mor-CH_2), 3.5 (t, J=7.00 Hz, 4H, Mor), 3.90 (s, 3H, O-CH_3), 4.0 (t, J=7.10 Hz, 2H, CH_2-N=C), 5.35 (s, 1H, OH), 6.90-7.1 (m, 3H, Ph), 8.25 (s, 1H, HC=N). MS 264.1 (M^+). Anal. calcd for $C_{14}H_{20}N_2O_3$: C, 63.62; H, 7.63; N, 10.60. Found: C, 63.60; H, 7.65; N, 10.59.

2-methoxy-6-({[2-(pyrrolidin-1-yl)ethyl]imino}methyl)phenol (Compound 3)

Yield 85%, yellow oil. IR (KBr) $\bar{\upsilon}_{max}$ (cm^{-1}): 3429 (s, OH), 2932 (CH, aromatic), 2794 (CH, aliphatic), 1632 (C=N), 1254. ^{1}H-NMR (400 MHz, DMSO-*d6*, δ): 1.7 (t, J=6.5 Hz, 4H, Pyr H), 2.60 (t, J=6.5 Hz, 4H, Pyr H), 2.80 (t, J=7.10 Hz, 2H, CH_2-Pyr), 3.76 (t, J=7.10 Hz, 2H, CH_2-N=C), 3.90 (s, 3H, O-CH_3), 5.30 (s, 1H, OH), 6.40-6.80 (m, ,3H, Ph), 8.1 (s, 1H, HC=N). MS 248.2 (M^+). Anal. calcd for $C_{14}H_{20}N_2O_2$: C, 67.71; H, 8.12; N, 11.28. Found: C, 67.69; H, 8.15; N, 11.24.

2-methoxy-6-({[2-(piperidin-1-yl)ethyl]imino}methyl)phenol (Compound 4)

Yield 75%, yellow oil. IR (KBr) $\bar{\upsilon}_{max}$ (cm^{-1}): 3429 (s, OH), 2932 (CH, aromatic), 2794 (CH, aliphatic), 1632 (C=N), 1254. ^{1}H-NMR (400 MHz, DMSO-*d6*, δ): 1.6- 1.8 (m, 6H, Pip H), 2.60 (t, J=7.00 Hz, 4H, Pip H), 2.80 (t, J=7.10 Hz, 2H, CH_2-Pip), 3.76 (t, J=7.10 Hz, 2H, CH_2-N=C), 3.90 (s, 3H, O-CH_3), 5.35 (s, 1H, OH), 6.40-6.80 (m, 3H, Ph), 8.1 (s, 1H, HC=N). MS 262.2 (M^+). Anal. calcd for $C_{15}H_{22}N_2O_2$: C, 68.67; H, 8.45; N, 10.68. Found: C, 68.69; H, 8.48; N, 10.72.

2-{[(2-chlorophenethyl)imino]methyl}-6-methoxyphenol (Compound 5)

Yield 82%, yellow crystals, mp 63-64 °C. IR (KBr) $\bar{\upsilon}_{max}$ (cm^{-1}): 3010-3053 (CH, aromatic), 2856-2931 (CH, aliphatic), 1632 (C=N), 1253, 735-790. ^{1}H-NMR (400 MHz, DMSO-*d6*, δ): 3.1 (t, J=7.10 Hz, 2H, CH_2-Ph), 3.80 (t, J=7.10 Hz, 2H, CH_2-N=C), 3.90 (s, 3H, O-CH_3), 5.35 (s, 1H, OH), 6.80-7.40 (m, 7H, Ph), 8.1 (s, 1H, HC=N). MS 289.1 (M^+). Anal. calcd for $C_{16}H_{16}ClNO_2$: C, 66.32; H, 5.57; N, 4.83. Found: C, 66.27; H, 5.60; N, 4.80.

2-{[(2,4-dichlorophenethyl)imino]methyl}-6-methoxyphenol (Compound 6)

Yield 70%, yellow crystals, mp 103-104 °C. IR (KBr) $\bar{\upsilon}_{max}$ (cm^{-1}): 3005-3089 (CH, aromatic), 2831-2961 (CH, aliphatic), 1633 (C=N), 1253, 702-710, 819-867. ^{1}H-

NMR (400 MHz, DMSO-*d6*, δ): 3.1 (t, J=7.10 Hz, 2H, - CH_2-Ph), 3.84 (t, J=7.10 Hz, 2H, CH_2-N=C), 3.90 (s, 3H, O-CH_3), 5.30 (s, 1H, OH), 6.80-7.30 (m, 6H, Ph), 8.1 (s, 1H, HC=N). MS 323.1 (M^+). Anal. calcd for $C_{16}H_{15}Cl_2NO_2$: C, 59.28; H, 4.66; N, 4.32. Found: C, 59.24; H, 4.69; N, 4.30.

2-{[(3-chlorophenethyl)imino]methyl}-6-methoxyphenol (Compound 7)

Yield 90%, yellow crystals, mp 39-40 °C. IR (KBr) $\bar{\upsilon}_{max}$ (cm^{-1}): 3009-3060 (CH, aromatic), 2853-2936 (CH, aliphatic), 1633 (C=N), 1254, 780-731, 774-838. ^{1}H-NMR (400 MHz, DMSO-*d6*, δ): 2.98 (t, J=7.10 Hz, 2H, CH_2-Ph), 3.80 (t, J=7.10 Hz, 2H, CH_2-N=C), 3.88 (s, 3H, O-CH_3), 5.30 (s, 1H, OH), 6.70-7.20 (m, 7H, Ph), 8.1 (s, 1H, HC=N). MS 289.1 (M^+). Anal. calcd for $C_{16}H_{16}ClNO_2$: C, 66.32; H, 5.57; N, 4.83. Found: C, 66.28; H, 5.61; N, 4.81.

2-{[(2-fluorophenethyl)imino]methyl}-6-methoxyphenol (Compound 8)

Yield 83%, yellow crystal, mp 71-72 °C. IR (KBr) $\bar{\upsilon}_{max}$ (cm^{-1}): 3010-3053 (CH, aromatic), 2856-2931 (CH, aliphatic), 1632 (C=N), 1253, 735-790. ^{1}H-NMR (400 MHz, DMSO-*d6*, δ): 3.04 (t, J=7.10 Hz, 2H, CH_2-Ph), 3.84 (t, J=7.10 Hz, 2H, CH_2-N=C), 3.90 (s, 3H, O-CH_3), 5.30 (s, 1H, OH), 6.80-7.20 (m, 7H, Ph), 8.1 (s, 1H, HC=N). MS 273.1 (M^+). Anal. calcd for $C_{16}H_{16}FNO_2$: C, 70.31; H, 5.90; N, 5.12. Found: C, 70.28; H, 5.93; N, 5.09.

2-{[(4-fluorophenethyl)imino]methyl}-6-methoxyphenol (Compound 9)

Yield 70%, yellow oil. IR (KBr) $\bar{\upsilon}_{max}$ (cm^{-1}): 3427 (s, OH), 2941-3058 (CH, aromatic), 2771-2827 (Al. CH), 1632 (C=N), 1254, 736-780. ^{1}H-NMR (400 MHz, DMSO-*d6*, δ): 2.64 (t, J=7.10 Hz, 2H, CH_2-Ph), 3.70 (t, J=7.10 Hz, 2H, CH_2-N=C), 3.90 (s, 3H, O-CH_3), 5.30 (s, 1H, OH), 6.80-7.10 (m, 7H, Ph), 8.1 (s, 1H, HC=N). MS 273.1 (M^+). Anal. calcd for $C_{16}H_{16}FNO_2$: C, 70.31; H, 5.90; N, 5.12. Found: C, 70.29; H, 5.94; N, 5.10.

2-({[2-(dimethylamino)ethyl]imino}methyl)-6-methoxyphenol (Compound 10)

Yield 70%, yellow oil. IR (KBr) $\bar{\upsilon}_{max}$ (cm^{-1}): 3433 (s, OH), 2941 (CH, aromatic), 2772-2821 (CH, aliphatic), 1633 (C=N), 1254, 736-780. ^{1}H-NMR (400 MHz, DMSO-*d6*, δ): 2.3 (s, 6H, CH_3-N), 3.70 (t, J=7.10 Hz, 2H, CH_2-N.), 3.80 (t, J=7.10 Hz, 2H, CH_2-N=C), 3.90 (s, 3H, O-CH_3), 5.35 (s, 1H, OH), 6.80-7.10 (m, 3H, Ph), 8.1 (s, 1H, HC=N). MS 222.0 (M^+). Anal. calcd for $C_{12}H_{18}N_2O_2$: C, 64.84; H, 8.16; N, 12.60. Found: C, 64.81; H, 8.19; N, 12.58.

2-({[2-(diethylamino)ethyl]imino}methyl)-6-methoxyphenol (Compound 11)

Yield 88%, yellow oil. IR (KBr) $\bar{\upsilon}_{max}$ (cm^{-1}): 3435 (s, OH), 2968 (CH, aliphatic), 1631 (C=N), 1253. ^{1}H-NMR (400 MHz, DMSO-*d6*, δ): 1.00 (t, J=8 Hz, 6H, CH_3-CH_2-N-), 2.40 (q, J=8 Hz, 4H, CH_3-CH_2-N-), 2.72 (t, J=7.10 Hz, 2H, -CH_2-N.), 3.65 (t, J=7.10 Hz, 2H, CH_2-N=C), 3.90 (s, 3H, O-CH_3), 5.30 (s, 1H, OH), 6.40-7.10 (m, 3H, Ph), 8.1 (s, 1H, HC=N). MS 250.2 (M^+). Anal. calcd for $C_{14}H_{22}N_2O_2$: C, 67.17; H, 8.86; N, 11.19. Found: C, 67.14; H, 8.89; N, 11.18.

2-{[(2-chloroethyl)imino]methyl}-6-methoxyphenol (Compound 12)

Yield 88%, yellow oil. IR (KBr) $\bar{\upsilon}_{max}$ (cm^{-1}): 3418 (s, OH), 2965 (CH, aliphatic), 1651 (C=N), 1256. ^{1}H-NMR (400 MHz, DMSO-*d6*, δ):3.60 (t, 2H, -CH_2-Cl), 3.83 (t, 2H, -CH_2-N=C.), 3.90 (s, 3H, OCH_3), 5.30 (s, 1H, OH), 6.50-7.10 (m, 3H, Ph), 8.1 (s, 1H, HC=N). MS 213.1 (M^+). Anal. calcd for $C_{10}H_{12}ClNO_2$: C, 56.21; H, 5.66; N, 6.56. Found: C, 56.18; H, 5.70; N, 6.54.

2-methoxy-6-({[2-(piperazin-1-yl)ethyl]imino}methyl)phenol (Compound 13)

Yield 75%, yellow oil. IR (KBr) $\bar{\upsilon}_{max}$ (cm^{-1}): 3427 (s, OH), 2938 (CH, aromatic), 2830 (CH, aliphatic), 1633 (C=N), 1254. ^{1}H-NMR (400 MHz, DMSO-*d6*, δ): 2.0 (s, 1H, Ppz NH), 2.48 (t, 4H, Ppz H), 2.65 (t, 4H, Ppz H), 2.72 (t, 2H, CH_2-Ppz), 3.83 (t, 2H, J=7.10 Hz, CH_2-N=C), 3.90 (s, 3H, O-CH_3), 5.35 (s, 1H, OH), 6.50-7.90 (m, 3H, Ph), 8.1 (s, 1H, HC=N). MS 263.2 (M^+). Anal. calcd for $C_{14}H_{21}N_3O_2$: C, 63.85; H, 8.04; N, 15.96. Found: C, 63.82; H, 8.07; N, 15.93.

2-({[2-(1*H*-imidazol-2-yl)ethyl]imino}methyl)-6-methoxyphenol (Compound 14)

Yield 74%, yellow oil. IR (KBr) $\bar{\upsilon}_{max}$ (cm^{-1}): 3437 (s, OH), 3005-3089 (CH, aromatic), 2831-2961 (CH, aliphatic), 1635 (C=N), 1254. ^{1}H-NMR (400 MHz, DMSO-*d6*, δ): 2.90 (t, J=7.10 Hz, 2H, -CH_2-Imd) 3.83 (t, 2H, J=7.10 Hz, CH_2-N=C), 3.90 (s, 3H, OCH_3), 5.35 (s, 1H, OH), 6.60-7.30 (m, 5H, Ph and Imd), 8.1 (s, 1H, HC=N), 13.00 (1H, Imd. NH). MS 245.1 (M^+). Anal. calcd for $C_{13}H_{15}N_3O_2$: C, 63.66; H, 6.16; N, 17.13. Found: C, 63.63; H, 6.19; N, 17.10.

2-methoxy-6-[(phenethylimino)methyl]phenol (Compound 15)

Yield 88%, yellow crystal, mp 76-77 °C. IR (KBr) $\bar{\upsilon}_{max}$ (cm^{-1}): 3023-3085 (CH, aromatic), 2859-2996 (CH, aliphatic), 1627 (C=N), 1253. ^{1}H-NMR (400 MHz, DMSO-*d6*, δ): 3.0 (t, J=7.10 Hz, 2H, CH_2-Ph), 3.84 (t, J=7.10 Hz, 2H, CH_2-N=C), 3.90 (s, 3H, OCH_3), 5.30 (s, 1H, OH), 6.80-7.40 (m, 8H, Ph), 8.1 (s, 1H, HC=N). MS 255.1 (M^+). Anal. calcd for $C_{16}H_{17}NO_2$: C, 75.27; H, 6.71; N, 5.49. Found: C, 75.25; H, 6.74; N, 5.46.

Microbiological Screening

The following test microorganisms were obtained from LGC Standards GmbH (Wesel, Germany): *Staphylococcus aureus* (S. aureus) ATCC 25923, *Escherichia coli* (E. coli) ATCC 25922, *Pseudomonas aeruginosa* (P. aeruginosa) ATCC 27853, and *Candida albicans* (C. albicans) ATCC 60193. All the synthesized compounds were dissolved in dimethyl sulphoxide (DMSO) to prepare a stock solution at 10 mg/mL.

Agar-well diffusion method

An adapted simple susceptibility screening based on agar-well diffusion was used[50-52]. Each bacterium was suspended in a Mueller-Hinton broth (MHB) (Difco, Detroit, MI, USA) and the fungal sample, *C. albicans,* was suspended in a Sabouraud Agar Modified medium (BD 274720) for pre-incubation at 35±2 °C. Then, all the microorganisms were diluted until they approximately matched the turbidity of 0.5 McFarland standard (1-2 × 10^8 cfu/mL). Later, they were flood-inoculated onto the surface of Mueller-Hinton (MH) and Sabouraud dextrose (SD) agars and dried. Five-millimeter diameter wells were cut from the agar using a sterile cork borer, and 20 µL of the stock substances was delivered into the wells. The plates were incubated for 16-24 h at 35±2 °C. Antibacterial activity was evaluated by measuring the radius of the inhibition zone against the test organism using a digital caliper. *o*-vanillin (10 mg/mL), ampicillin (10 µg/mL) and fluconazole (5 µg/mL) were used as standards. DMSO diluted to 1:10 was used as the solvent control to ensure that it did not have any effect on bacterial growth.

Broth microdilution method

The minimal inhibition concentration (MIC) values (µg/mL) for the organisms were determined using the methods recommended by the Clinical and Laboratory Standards Institute (CLSI) guidelines[53-54]. The antimicrobial effects of the substances against the *S. aureus*, *E. coli* and *C. albicans* microorganisms were tested quantitatively in broth media using double dilution. The broth microdilution method was not performed on *P. aeruginosa* since none of the compounds showed inhibition zones with the agar well diffusion method. The antibacterial and antifungal assays were performed in an MH broth (Difco) at pH 7.3 and a buffered yeast nitrogen base (Difco) at pH 7.0, respectively. MIC was defined as the lowest concentration with no bacterial or fungal growth. Ampicillin (10 µg/mL) and fluconazole (10 µg/mL) were prepared as stocks, then diluted in a range from 10 to 0.5 µg/mL using DMSO and tested as standard antibacterial and antifungal drugs, respectively. The tested dilutions ranged from 128 to 0.5 µg/mL using DMSO as the solvent for all compounds. The control samples prepared with the amounts of DMSO used in the dilutions did not show any inhibitory activity under these conditions.

Prediction of drug-likeness, molecular and ADME properties

All the molecules were prepared in 3D using the LigPrep module of Maestro (Schrodinger Inc.). ADME properties (46 molecular descriptors) were calculated using the QikProp program (Schrödinger 2015-3) in the normal mode. QikProp generates physically relevant descriptors and uses them to perform ADME predictions. An overall ADME-compliance score, the drug-likeness parameter (indicated by #stars), was used to assess the pharmacokinetic profiles of the compounds. The #stars parameter (ranging from 0 to 5) indicates the number of property descriptors computed by QikProp that fall outside the optimum range of values for 95% of known drugs.

The predicted descriptors were: central nervous system (CNS) activity (–2 for inactive to +2 for active); octanol/water partition coefficient, logPo/w (–2.0 to 6.5); IC_{50} value for the block of HERG K^+ channels, log *HERG* (concern < –5); Caco-2 cell membrane permeability in nm s^{-1}, PCaco (: < 5 low to > 100 high);

Table 1: Antimicrobial activity of compounds using the microdilution (MIC, μg/mL) and agar well diffusion methods (diameter of inhibition zones in mm)[a]

Minimal inhibition concentration (μg/mL) and diameter of inhibition zones (mm)a

Compound	S. aureus	E. coli	C. albicans	P. aeroginosa
1	>128 (0)	>128 (1)	16 (17)	(0)
2	>128 (0)	>128 (2)	16 (17)	(0)
3	32 (11)	>128 (0)	16. (17)	(0)
4	16. (15)	32. (7)	64. (22)	(0)
5	>128 (0)	>128 (0)	64 (14)	(0)
6	>128 (0)	>128. (0)	>128. (14)	(0)
7	>128 (0)	>128 (3)	>128 (14)	(0)
8	>128 (0)	>128 (3)	16 (21)	(0)
9	32 (13)	16 (9)	8. (25)	(0)
10	32. (11)	64 (4)	16 (21)	(0)
11	32 (11)	>128 (2)	32 (17)	(0)
12	>128 (0)	64 (5)	16 (22)	(0)
13	>128 (0)	>128 (1)	32 (19)	(0)
14	>128 (0)	>128 (3)	16 (22)	(0)
15	>128 (0)	>128 (3)	16 (19)	(0)
o-Vanillin	>128 (0)	16 (8)	16 (20)	(7)
Ampicillin	2 (35)	>8 (10)	-	(18)
Fluconazole	-	-	8 (25)	-

[a]The results obtained from the agar well diffusion method are given in parentheses.

logarithm of predicted blood/brain barrier partition coefficient, log B/B (-3.0 to 1.0); apparent Madin-Darby canine kidney cell permeability (PDMCK) that mimic the blood-brain barrier for non-active transport in nm s^{-1}, PMDCK (< 25 poor to > 500 great); skin permeability, log K_p (–8.0 to –1.0); logarithm of binding constant to human serum albumin, log K_{HAS} (-1.5 to 1.2); qualitative human oral absorption, HOA (1: low, 2: medium, 3: high); percent of HOA (>80%: high, <25%: poor) (Table 2).

Table 2: Calculated drug-likeness, molecular properties and ADME predictions for Compounds 1-15 using QikProp

Name	#stars	CNS	logPo/w	logHERG	PCaco	logBB	PMDCK	logKp	logKhsa	HOA[a]	%HOA
1	0	0	3.25	-5.62	2723.09	-0.42	1460.83	-0.86	0.02	3.00	100.00
2	0	1	1.60	-5.35	841.86	0.08	454.39	-3.35	-0.45	3.00	88.66
3	0	1	2.30	-5.49	771.51	0.04	413.49	-3.43	-0.15	3.00	92.10
4	0	1	2.56	-5.70	863.10	0.07	466.79	-3.33	-0.01	3.00	94.48
5	1	0	4.19	-5.46	3553.49	-0.18	3632.38	-0.66	0.32	3.00	100.00
6	0	1	4.67	-5.54	4079.69	0.05	10000.00	-0.68	0.45	3.00	100.00
7	0	0	4.30	-5.60	3423.27	-0.15	4640.13	-0.76	0.35	3.00	100.00
8	1	0	4.23	-5.53	3421.94	-0.24	2720.15	-0.67	0.26	3.00	100.00
9	0	0	4.26	-5.55	3438.21	-0.20	3397.39	-0.72	0.27	3.00	100.00
10	0	1	1.74	-5.21	753.41	0.05	403.01	-3.45	-0.35	3.00	88.62
11	0	1	2.74	-5.42	845.05	-0.04	456.25	-3.16	-0.17	3.00	95.37
12	0	1	2.61	-4.14	3405.88	0.02	4692.47	-1.47	-0.19	3.00	100.00
13	0	1	0.98	-6.33	110.12	0.18	55.78	-5.96	-0.33	2.00	69.22
14	0	-1	2.38	-5.13	1254.71	-0.73	632.21	-1.74	-0.24	3.00	96.34
15	0	0	4.02	-5.72	3376.93	-0.33	1843.40	-0.61	0.25	3.00	100.00

[a]The assessment uses a knowledge-based set of rules, including checking for suitable values of percent human oral absorption, number of metabolites, number of rotatable bonds, logP, solubility and cell permeability.

RESULTS AND DISCUSSION

Using the conventional method, the proposed Schiff bases of *o*-vanillin were successfully synthesized giving yields between 70-90%. In the IR spectra, all the compounds had a strong C=N stretching band at 1627–1651 cm^{-1}. The ^{1}H-NMR spectra of the compounds showed that the protons belonging to the compounds in the HC=N group were exhibited at δ 8.10–8.25 ppm as a singlet, in which both the IR ^{1}H-NMR data were accepted as evidence for the formation of an imine

bond. All the other protons were observed according to the expected chemical shift and integral values. The molecular ion peaks (M^+) of the compounds were examined under electron ionization and they confirmed the molecular weights of the compounds. MIC and inhibition zones of Compounds 1-15 were evaluated for their antibacterial and antifungal activities using *o*-vanillin, ampicillin and fluconazole as a standard for the microorganisms (*S. aureus, E. coli, C. albicans and P. aeruginosa*). Throughout the experiments, the parent compound *o*-vanillin was observed to be active for *E. coli and C. albicans* but there was minimum or no activity for *S. Aureus and P. aeruginosa*. The best activity of *o*-vanillin was seen against *C. albicans* with the MIC value of 16 μg/mL. Since none of the synthesized compounds was found to be active against *P. aeruginosa* during the measurement of the diameter for inhibition zones, further analysis on the compounds was not performed for this microorganism and broth microdilution experiments were not undertaken to determine MIC. According to the results on the inhibition zones of *S. aureus*, Compounds 3, 4, 9, 10, 11 were more active compared to the parent compound *o*-vanillin; however, they were not as active as ampicillin. Similarly, for *E. coli,* Compound 9 showed similar activity to *o*-vanillin but performed worse than ampicillin. All the compounds had moderate to strong activity against *C. albicans* resulting in similar inhibition zones. In broth dilution experiments, Compounds 1, 2, 3, 8, 10, 12, 14, 15 were found to have an MIC of 16 μg/mL, which was similar to that of *o*-vanillin. Another significant result was that Compound 9 had an MIC value of 8 μg/mL presenting the same anti-fungal activity as fluconazole.

In this study, the drug-likeness, molecular and ADME properties of all compounds were promising presenting a drug-like/lead-like profile according to their #stars rankings. The combinations of HOA values being mostly around 3 (except Compound 13), %HOA values ranging from 88.62 to 100%, all PCaco values being high and log Kp values varying between -0.61 and -5.96 indicate that these compounds can be effectively used in both oral and topical preparations. It is important to note that the binding of drugs to plasma proteins (such as human serum albumin, lipoprotein, glycoprotein, α, β and γ globulins) greatly reduces the quantity of the drug in general blood circulation. In other words, the less bound a drug is, the more efficiently it can traverse cell membranes or diffuse. Furthermore, the logarithm of the predicted binding constant to human serum albumin, $\log K_{\text{HSA,}}$ values of the synthesized Schiff bases varied between -0.45 to +0.45, which showed that these derivatives might circulate freely and easily traverse cell membranes. The HERG K^+ channel, best known for its impact on the electrical activity of the heart by synchronizing beating, appears to be the molecular target responsible for the cardiac toxicity of a wide range of therapeu-

tic drugs[55]. HERG has also been found associated with modulating the functions of certain cells of the nervous system and with establishing and maintaining cancer-like features in leukemic cells[56]. Thus, HERG K^+ channel blockers are potentially toxic and the predicted IC_{50} values often provide reasonable predictions for the cardiac toxicity of drugs in the early stages of drug discovery[57]. The logHERG values of the compounds predicted with the in silico method were between -4.14 and -6.33 with only Compound 13 exhibiting a tendency for the blockage of this channel. As a basic rule, polar drugs cannot easily penetrate blood–brain barrier (BBB). The blood/brain partition coefficient (log BB), PMDCK and logPo/w values are useful to determine the penetration capacity of a compound from BBB. The values predicted for these parameters of the synthesized compounds were within the ranges defined for 95% of drugs. Moreover, the predicted CNS value of the compounds was between -1 and +1 indicating mild to medium activity.

Although the prediction results must be checked with actual experiments, the activity studies showed that the Schiff bases derived from *o*-vanillin derivatives could be considered as potential antifungal agents. Furthermore, investigations showed that the Schiff bases synthesized from the starting point of *o*-vanillin can act as a monovalent bidentate ligand, which develop antibacterial properties by combining the azomethine nitrogen and phenolic oxygen atom[58]. Based on this information, we plan to undertake further research to evaluate the metal complexes of these ligands and their antibacterial/antifungal properties.

REFERENCES

1. Shi, L.; Ge, H. M.; Tan, S. H., et al., Synthesis and Antibacterial Activities of Schiff Bases Derived from 5-Chloro-Salicylaldehyde. *Eur. J. Med. Chem.* **2007,** *42* (4), 558-564.

2. Moss, G. P.; Smith, P. A. S.; Tavernier, D., Glossary of Class Names of Organic Compounds and Reactivity Intermediates Based on Structure (Iupac Recommendations 1995). *Pure App. Chem.* 1995; Vol. 67, p 1307.

3. Kajal, A.; Bala, S.; Kamboj, S., et al., Schiff Bases: A Versatile Pharmacophore. *J. Catal.* **2013**, *2013*, 14.

4. Eliot, A. C.; Kirsch, J. F., Pyridoxal Phosphate Enzymes: Mechanistic, Structural, and Evolutionary Considerations. *Ann. Rev. Biochem.* **2004**, *73*, 383-415.

5. Hernández-Molina, R.; Mederos, A., 1.19 - Acyclic and Macrocyclic Schiff Base Ligands A2 - Mccleverty, Jon A. In *Comprehensive Coordination Chemistry Ii*, Meyer, T. J., Ed. Pergamon: Oxford, **2003**; pp 411-446.

6. Nozaki, H.; Takaya, H.; Moriuti, S.; Noyori, R., Homogeneous Catalysis in the Decomposition of Diazo Compounds by Copper Chelates. *Tetrahedron.* **1968**, *24* (9), 3655-3669.

7. Hindson, J. C.; Ulgut, B.; Friend, R. H., et al., All-Aromatic Liquid Crystal Triphenylamine-Based Poly(Azomethine)S as Hole Transport Materials for Opto-Electronic Applications. *J. Mater. Chem.* **2010**, *20* (5), 937-944.

8. Petrus, M. L.; Bein, T.; Dingemans, T. J.; Docampo, P., A Low Cost Azomethine-Based Hole Transporting Material for Perovskite Photovoltaics. *J. Mater. Chem.* **2015,** *3* (23), 12159-12162.

9. Işık, D.; Santato, C.; Barik, S.; Skene, W. G., Charge-Carrier Transport in Thin Films of Π-Conjugated Thiopheno-Azomethines. *Org. Electron.* **2012**, *13* (12), 3022-3031.

10. Sicard, L.; Navarathne, D.; Skalski, T.; Skene, W. G., On-Substrate Preparation of an Electroactive Conjugated Polyazomethine from Solution-Processable Monomers and Its Application in Electrochromic Devices. *Adv. Func. Mat.* **2013**, *23* (28), 3549-3559.

11. Uribe-Romo, F. J.; Hunt, J. R.; Furukawa, H., et al., A Crystalline Imine-Linked 3-D Porous Covalent Organic Framework. *J. Am. Chem. Soc.* **2009**, *131* (13), 4570-4571.

12. Sridhar, S. K.; Saravanan, M.; Ramesh, A., Synthesis and Antibacterial Screening of Hydrazones, Schiff and Mannich Bases of Isatin Derivatives. *Eur. J. Med. Chem.* **2001**, *36* (7-8), 615-625.

13. Mladenova, R.; Ignatova, M.; Manolova, N., et al., Preparation, Characterization and Biological Activity of Schiff Base Compounds Derived from 8-Hydroxyquinoline-2-Carboxaldehyde and Jeffamines Ed®. *Eur. Polym. J.* **2002**, *38* (5), 989-999.

14. Panneerselvam, P.; Nair, R. R.; Vijayalakshmi, G., et al., Synthesis of Schiff Bases of 4-(4-Aminophenyl)-Morpholine as Potential Antibacterial Agents. *Eur. J. Med. Chem.* **2005**, *40* (2), 225-229.

15. Walsh, O. M.; Meegan, M. J.; Prendergast, R. M.; Al Nakib, T., Synthesis of 3-Acetoxyazetidin-2-Ones and 3-Hydroxyazetidin-2-Ones with Antifungal and Antibacterial Activity. *Eur. J. Med. Chem.* **1996**, *31* (12), 989-1000.

16. Pandeya, S. N.; Sriram, D.; Nath, G.; DeClercq, E., Synthesis, Antibacterial, Antifungal and Anti-Hiv Activities of Schiff and Mannich Bases Derived from Isatin Derivatives and N-[4-(4'-Chlorophenyl)Thiazol-2-Yl] Thiosemicarbazide. *Eur. J. Pharm. Sci.* **1999**, *9* (1), 25-31.

17. Pahontu, E.; Ilies, D. C.; Shova, S., et al., Synthesis, Characterization, Crystal Structure and Antibacterial Activity of Copper(Ii) Complexes with the Schiff Base Derived from 2-Hydroxy-4-Methoxybenzaldehyde. *Molecules.* **2015**, *20* (4), 5771-5792.

18. Liu, M. C.; Lin, T. S.; Sartorelli, A. C., Synthesis and Antitumor Activity of Amino Derivatives of Pyridine-2-Carboxaldehyde Thiosemicarbazone. *J. Med. Chem.* **1992**, *35* (20), 3672-3677.

19. Hodnett, E. M.; Mooney, P. D., Antitumor Activities of Some Schiff Bases. *J. Med. Chem.* **1970**, *13* (4), 786-786.

20. Alt, G. H. C. C., MO) Plant Growth Regul. 1980.

21. Hamada, Y.; Takeuchi, I.; Ito, Y., et al., On the Antibacterial Activity and Syntheses of Salicylanilide Derivatives. *Yakugaku Zasshi.* **1981**, *101* (7), 633-641.

22. Ismail, M. M., New Derivatives of 3,5-Dichlorosalicylaldehyde as Antimycotic Agents. *Indian J. Pharm. Sci.* **1986**, *48* (5), 121-124.

23. Abbaspour, A.; Esmaeilbeig, A. R.; Jarrahpour, A. A., et al., Aluminium(Iii)-Selective Electrode Based on a Newly Synthesized Tetradentate Schiff Base. *Talanta.* **2002**, *58* (2), 397-403.

24. Mahajan, R. K.; Kaur, I.; Kumar, M., Silver Ion-Selective Electrodes Employing Schiff Base P-Tert-Butyl Calix[4]Arene Derivatives as Neutral Carriers. *Sens. Actuators B. Chem.* **2003**, *91* (1–3), 26-31.

25. Ganjali, M. R.; Golmohammadi, M.; Yousefi, M., et al., Novel Pvc-Based Copper(Ii)

Membrane Sensor Based on 2-(1'-(4'-(1"-Hydroxy-2"-Naphthyl)Methyleneamino)Butyl Iminomethyl)-1-Naphthol. *Anal. Sci.* **2003**, *19* (2), 223-7.

26. Jain, A. K.; Gupta, V. K.; Ganeshpure, P. A.; Raisoni, J. R., Ni(Ii)-Selective Ion Sensors of Salen Type Schiff Base Chelates. *Anal. Chim. Acta* **2005**, *553* (1-2), 177-184.

27. Jeong, T.; Lee, H. K.; Jeong, D.-C.; Jeon, S., A Lead(Ii)-Selective Pvc Membrane Based on a Schiff Base Complex of N,N'-Bis(Salicylidene)-2,6-Pyridinediamine. *Talanta.* **2005**, *65* (2), 543-548.

28. Gupta, V. K.; Singh, A. K.; Mehtab, S.; Gupta, B., A Cobalt(Ii)-Selective Pvc Membrane Based on a Schiff Base Complex of N,N'-Bis(Salicylidene)-3,4-Diaminotoluene. *Anal. Chim. Acta* **2006**, *566* (1), 5-10.

29. Pfeiffer, P.; Breith, E.; Lubbe, E.; Tsumaki, T., Tricyclic Ortho-Condensed Partial Valence Rings. *Ann.* **1933**, *503*, 84-130.

30. Hunter, L.; Marriott, J. A., CoöRdinated Copper and Nickel Compounds of Salicylidene Derivatives. *J. Chem. Soc.* **1937**, 2000-2003.

31. Sacconi, L.; Ciampolini, M.; Maggio, F.; Cavasino, F. P., Coordination Chemistry. Ix. Stereochemistry of Some Complex Compounds of Cobalt(Ii) with N-Substituted Salicyl-Aldimines. *J. Am. Chem. Soc.* **1962**, *84*, 3246-3248.

32. Holm, R. H.; Swaminathan, K., Nickel(Ii) Complexes. Iii. Bis-(N-Arylsalicylaldimine) Complexes. *Inorg. Chem.* **1962**, *1*, 599-607.

33. Percy, G. C.; Thornton, D. A., N-Aryl Salicylaldimine Complexes. Infrared and Pmr Spectra of the Ligands and Vibrational Frequencies of Their Metal(Ii) Chelates. *J. Inorg. Nucl. Chem.* **1972**, *34* (11), 3357-3367.

34. Cozzi, P. G., Metal-Salen Schiff Base Complexes in Catalysis: Practical Aspects. *Chem. Soc. Rev.* **2004**, *33* (7), 410-421.

35. Chandra, S.; Sangeetika, Epr and Electronic Spectral Studies on Copper(Ii) Complexes of Some N-O Donor Ligands. *J. Indian Chem. Soc.* **2004**, *81* (3), 203-206.

36. Burt, S., Essential Oils: Their Antibacterial Properties and Potential Applications in Foods - a Review. *Int. J. Food Microbiol.* **2004**, *94* (3), 223-253.

37. Davidson, P. M.; Naidu, A. S. In *Phyto-Phenols*, CRC Press LLC, Boca Raton, **2000**, pp 265-294.

38. Holley, R. A.; Patel, D., Improvement in Shelf-Life and Safety of Perishable Foods by Plant Essential Oils and Smoke Antibacterials. *Food Microbiol.* **2005**, *22* (4), 273-292.

39. Shazia, M.; Saba, M.; Jasmine, F., et al., Anti-Bacterial, Anti-Oxidant and Cytotoxic Potential of Various Extracts of Myristica Fragrans. *Int. J. Res. Ayurveda Pharm.* **2015**, *6* (5), 643-648.

40. Fitzgerald, D. J.; Stratford, M.; Gasson, M. J., et al., Mode of Antibacterial Action of Vanillin against Escherichia Coli, Lactobacillus Plantarum and Listeria Innocua. *J. Appl. Microbiol.* **2004**, *97* (1), 104-113.

41. Leifertova, I.; Hejtmankova, N.; Hlava, H., et al., Antifungal and Antibacterial Effects of Phenolic Substances. A Study of the Relation between The Biological Activity and the Constitution of the Investigated Compounds. *Acta Univ. Palacki. Olomuc., Fac. Med.* **1975**, *74*, 83-101.

42. Ohmagari, H.; Fukahori, A.; Nakaya, M., et al., Crystal Structures and Magnetic Properties of Manganese(Iii) Complexes with Tridentate Schiff Base Ligands. *J. Inc. Phenom. Macrocycl.*

Chem. **2015**, *82* (1), 213-218.

43. Petek, H.; Albayrak, C.; Iskeleli, N. O., et al., Crystallographic and Conformational Analyses of Zwitterionic Form of (E)-2-Methoxy-6-[(2-Morpholinoethylimino)Methyl]Phenolate. *J. Chem. Crystallogr*. **2007**, *37* (4), 285-290.

44. Wang, Y.-X.; Zhao, W.-L.; Bi, C.-W., et al., Synthesis and Structure-Activity Relationship of N-(2-Arylethyl) Isoquinoline Derivatives as Anti-Cancer Agents. *Yao Xue Xue Bao*. **2012**, *47* (2), 200-205.

45. Sasmal, S.; Mohanta, S., M-Phenoxo-M-Pseudohalide and M-Pseudohalide Dinuclear, Tetranuclear and One-Dimensional Complexes: Magneto-Structural Correlation and Interesting Type of Solid State Isomerism. *J. Chem. Sci. (Bangalore, India)* **2012**, *124* (6), 1353-1364.

46. Mistri, S.; Puschmann, H.; Manna, S. C., DNA/Protein Binding, Cytotoxicity and Catecholase Activity Studies of a Piperazinyl Moiety Ligand Based Nickel(Ii) Complex. *Polyhedron*. **2016**, *115*, 155-163.

47. Wang, Y.-X.; Li, Y.-H.; Li, Y.-H., et al., Synthesis, Structure-Activity Relationship and in Vitro Biological Evaluation of N-Arylethylisoquinoline Derivatives as Coxsackievirus B3 Inhibitors. *Bioorg. Med. Chem. Lett*. **2011**, *21* (19), 5787-5790.

48. Das, K.; Datta, A.; Liu, P.-H., et al., Structural Characterization of Cobalt(Ii) Complexes of an N,O Donor Schiff Base and Their Activity on Carcinoma Cells. *Polyhedron*. **2014**, *71*, 85-90.

49. Shit, S.; Sankolli, R.; Row, T. N. G., A Dinuclear Cadmium(Ii) Schiff Base Thiocyanato Complex: Crystal Structure and Fluorescence. *Acta Chim. Slov*. **2014**, *61* (1), 59-66.

50. Perez, C.; Pauli, M.; Bazerque, P., An Antibiotic Assay by Agar-Well Diffusion Method. *Acta Biol. Med. Exp*. **1990**, *15*, 113-115.

51. Ahmad, I.; Mehmood, Z.; Mohammad, F., Screening of Some Indian Medicinal Plants for Their Antibacterial Properties. *J. Ethnopharmacol*. **1998**, *62* (2), 183-93.

52. Balouiri, M.; Sadiki, M.; Ibnsouda, S. K., Methods for in Vitro Evaluating Antibacterial Activity: A Review. *J. Pharm. Anal*. **2016**, *6* (2), 71-79.

53. (CLSI), C. L. S. I., Performance Standards for Antibacterial Susceptibility Testing Twenty-Third Informational Supplement. Clsi Document. M100-S20. **2013.**

54. (CLSI), C. L. S. I., Methods for Dilution Antibacterial Susceptibility Tests for Bacteria That Grow Aerobically; Approved Standard-Ninth Edition, Clsi Document: M07-A9. **2012**.

55. Vandenberg, J. I.; Walker, B. D.; Campbell, T. J., Herg K+ Channels: Friend and Foe. *Trends Pharmacol. Sci*. **2001**, *22* (5), 240-246.

56. Chiesa, N.; Rosati, B.; Arcangeli, A., et al., A Novel Role for Herg K+ Channels: Spike-Frequency Adaptation. *J. Physiol. (Cambridge, U. K.)* **1997**, *501* (2), 313-318.

57. Aronov, A. M., Predictive in Silico Modeling for Herg Channel Blockers. *Drug Discov. Today*. **2005**, *10* (2), 149-155.

58. Anupama, B.; Sunita, M.; Shiva Leela, D., et al., Synthesis, Spectral Characterization, DNA Binding Studies and Antibacterial Activity of Co(Ii), Ni(Ii), Zn(Ii), Fe(Iii) and Vo(Iv) Complexes with 4-Aminoantipyrine Schiff Base of Ortho-Vanillin. *J. Fluoresc*. **2014**, *24* (4), 1067-1076.

(Received 14 September 2016; accepted 06 December 2016)

Acta Pharm. Sci. Vol 55 No: 1. 2017
DOI: 10.23893/1307-2080.APS.0557

Molecular Modelling and Compound Activity of The Escherichia Coli and Staphylococcus Aureus DNA Gyrase B ATPase Site

Barkın Berk[1,*], Gürmen Kaynar[2], Merve Ertaş[1], Sevde Nur Biltekin[1]

[1] İstanbul Medipol University, School of Pharmacy, 34810, İstanbul, Turkey
[2] World Medicine Corp., İstanbul, Turkey

ABSTRACT

Development of new treatment ligands that can distinguish *Escherichia coli (E. coli)* from *Staphylococcus aureus (S. aureus)* is important because of bacterium multiple drug resistance. High-throughput virtual screening (HTVS), docking-scoring and receiver operating characteristic curves are essential components of computational methods used in designing potential new ligands.

Here, we investigated the *E. coli and S. aureus* DNA gyrase B active site; amino acid, water molecule, and ligand interactions using crystallographic data and HTVS to determine potential hits.

Trial and test sets were prepared from the 5000 and 50000 compounds of the ZINC databases with known *E. coli* and *S. aureus* DNA gyrase B ATPase inhibitor molecules. Trial sets were evaluated and screened by determining the contribution of water molecules to interactions.

Data analysis led to the identification of novel interaction patterns, which were screened over a test set; 20 maximum scored compounds were identified and further tested against the novobiocin standard with gel-based *E. coli* and *S. aureus* supercoiling assays. The highest scoring N'-(1-naphthylcarbonyl)-2, 1, 3-benzothiadiazole-5-carbohydrazide structure showed selective inhibition with *E. coli* and *S. aureus* DNA gyrase B ATPases.

We determined that in terms of selectivity, some water molecules have a major impact on amino acid-ligand interactions.

Keywords: HTVS, ROC curves, Docking, *Escherichia coli, Staphylococcus aureus,* DNA gyrase B ATPase

*Corresponding author. Tel.; +90-216-6815364 Fax: +90-212-5317555.
E-mail address: bberk@medipol.edu.tr (Barkın Berk).

INTRODUCTION

Escherichia coli (*E. coli*) and *Staphylococcus aureus* (*S. aureus*) are well known gram-negative and gram-positive bacteria that are a common part of normal human flora[1]. When the normal balance of human flora is disrupted for example by immune system deficiencies such as those observed with human immunodeficiency virus (HIV), both bacteria assume opportunistic behaviour, which can subsequently lead to death[2].

In clinical practice, one of the biggest problems encountered with diseases such as HIV is multi-drug resistance. Unfortunately, over the last 40 years, no new drugs (with the exception of rifampicin and rifabutin) have been introduced and traditional drug combination treatments no longer prevent drug resistance[3].

Classically, with antibacterial compound design, when DNA replication or transcription at the cell division level is targeted, DNA gyrase enzyme and topoisomerase IV inhibitions are the first options for gram-negative and gram-positive bacteria[4].

Recently, *E. coli and S. aureus* DNA Gyrase B X-ray crystal structures (Pdb id: 3G7E and 3G7B) and binding dynamics with the inhibitors "prop-2-yn-1-yl [[5-(4-piperidin-1-yl-2-pyridin-3-yl-1,3-thiazol-5-yl)-1H-pyrazol-3-yl]methyl] carbamate" (1a) and "methyl([5-[4-(4-hydroxypiperidin-1-yl)-2-phenyl-1,3-thiazol-5-yl]-1H-pyrazol-3-yl]methyl) carbamate" (1b), were respectively released from the Protein Data Bank (PDB) (Figure 1)[5,6].

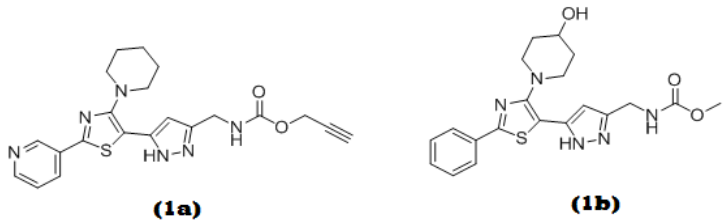

Figure 1: Chemical structure of ligands from 3G7E (1a) and 3G7B (1b)

When both amino-acid sequences were aligned and scored by a matrix adjustment composition method to verify similarities (using BlastP) entire identity alignment was 100/206 (49%), and on the basis of positives 127/206 (62%) similarity.[7] When the amino acids of both protein sequences are overlapped as pairs (in the whole chain) the pairwise root-mean-square deviation (RMSD) matrix value is 1.50, and the backbone value is 1.19.

E. coli DNA Gyrase B (Pdb id: 3G7E) and compound (1a) interactions showed that the nitrogen of the thiazole ring system is in a H bond interaction with Phe 104 and HOH 443, where one of the N atoms of the pyrazole ring system is a H

bond interaction with Ile 78, Gly 77, Thr 165, Asp 73 and HOH 408. There is a H bond bridge between the N atom of the carbamate moiety of the ligand-HOH 406 and ASP 73.

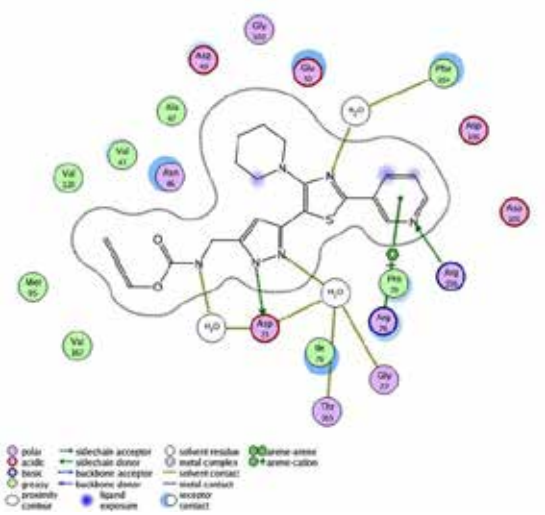

Figure 2: The active site-ligand interactions in *E. coli*

In the case of compound (1b) and the binding site of *S. aureus* (Pdb id: 3G7B), water molecules are dominantly active by setting boundaries to positioning such as HOH 263, which is trapped in the cavity. Furthermore, the H containing N atom of the pyrazole ring is oriented to Thr173, Gly85, Asp 81 amino acids by using a HOH 235 bridge.

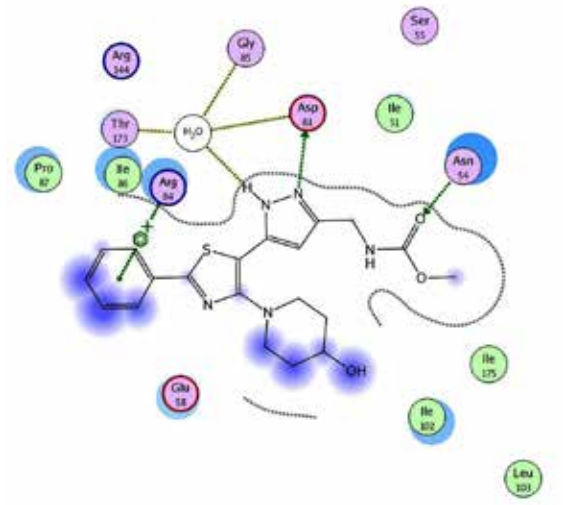

Figure 3: The active site-ligand interactions in *S. aureus*

Scorings from BlastP and ligand-active site interactions suggest that positioning of some water molecules especially HOH 408, 443 in *E. coli* and HOH 235, 263 in *S. aureus* DNA Gyrase B ATPase sites are essential for bridge and boundary functions, which might cause fractional differences among ligand designs for the both DNA Gyrase B's in terms of specific selectivity.

Molecular docking and HTVS are two basic tools, which are widely used in computer-assisted drug design[8,9]. Docking software consists of two basic elements; simulation algorithms that produce "exposure-pose" or "pose", which determine how structures such as ligand-protein or protein-protein interact with each other and scoring algorithms made of certain mathematical functions that rank these poses[9].

Usually, docking software determines poses that are responsible for the most probable interactions. However, until recently, scoring functions that were supposed to reflect the relationship between activity and pose were not useful, because many different biological parameters, including basic solvation parameters cannot sufficiently be revealed by mathematical algorithms[10-14]. In all virtual screening studies, test sets that consist of compounds selected from databanks are enriched, by using a cluster of compounds that have previously been experimentally proven to be active on the related target. When the ratio of active compounds in the test set is known and when the correct pose is determined, it is possible to measure statistically and numerically the quality of a hypothesis that is screening based by using methods such as receiver operating characteristic (ROC) curves[15-18].

In the present study, 36 *in vitro* experimental active DNA Gyrase ATPase inhibitor ligands (true positives) were added to the 5000 trial and 50000 test sets of compounds for enrichment purposes and later prepared for docking based HTVS. Subsequently, a trial set was subjected to a series of docking processes with *E. Coli* and *S. aureus* DNA Gyrase B ATPase sites. During docking processes, several GRID files called; "restricted" or "unrestricted" were prepared either by including or excluding the previously referred to water molecules. Scoring and further evaluation of ROC curves with these files identified if the interaction pattern including or excluding water molecules can be considered as "important" or "necessary" for an inhibition process. Later, the selected GRID files were similarly experimented over the enriched test set of 50000 compounds. Finally, the top 20 scoring compounds were selected and combined and subjected to gel-based supercoiling assays of both microorganisms for inhibition measurement, hypothesis testing and hit finding.

METHODOLOGY

PDB files of the "Crystal structure of *E. coli* Gyrase B co-complexed with inhibitor" and "*S. aureus* Gyrase B co-complex with inhibitor" (PDB ID; 3G7E and 3G7B) were downloaded from RCSB Protein Data Bank (2). Preparation of protein structures, trial and test sets, GRID files, docking and scoring were performed using algorithms from Maestro modules (Schrodinger Inc, USA). Special "ROC Curves SVL" of MOE (Chemical Computing Group Inc., Canada) software were used during preparation of ROC curves and interaction graphics.

After screening, compounds presumed to be active were purchased from Molport Chemicals (Letonia) with minimum 99.5 % purity and used after checking their LC-MSMS spectral and elemental analysis results. Biological activities of compounds were assessed by *E. coli* and *S. aureus* Gyrase Supercoiling Assay Kits (Inspiralis Inc. UK- Gyrase Supercoiling Assay kits-K0003 and SAS4002) using BIO-RAD (CA, USA) gel electrophoresis and imaging systems against novobiocin (CAS; 1476-53-5, AppliChem, Germany) as a reference.

Preparation of protein structures

3G7E and 3G7B PDB files were subjected to protein preparation wizard workflow (Maestro), for hydrogen insertion and rotamer adjustment, and H-bond optimization using OPLS 2005 as the energy parameters.

Preparation of trial and test sets

The process begins with the reduction of 1442716 compounds in the content Zinc data base of "clean-leads-subset (# 11)" (LogP values < 3.5, molecular weight < 350 and the number of rotational bonds <= 7) to 50000 randomly selected compounds as a test set. The trial set was evaluated by the test set with a second random selection of 5000 from this group. Later these two sets were transferred to the Lig Prep function of Maestro prepared for their tautomers and ionized forms at various pH levels (pH= 7 ± 2). Later duplicates were eliminated with an automatic script. Thirty-six activity proved ligands were prepared in the same manner and added for enrichment purposes to both sets before docking and scoring.

Preparation of grid files

Both bacterium DNA Gyrase ATPase active site GRID files were prepared using Maestro's Glide-Receptor Grid Generation tool. Receptor binding pockets were defined by picking 6 A° surrounding of both ligands existing in each PDB file. During preparation, the original ligands were excluded and a scaling factor of 1.0 and a partial charge cut-off of 0.25 were used as parameters for the Van der Walls radius-scaling factor. For *S. aureus* Gyrase B active site (PDB ID; 3G7B), three different GRID files were prepared;

- Without water molecules (without restrictions/ places the compounds considering the original ligand as centroid)
- With HOH 235 (with restrictions to make bond either with HOH 235 or define the position of ligand considering the position of HOH 235)
- With HOH 235 and 263 (with restrictions to make bond either with HOH 235 and /or HOH 263 or define the position of ligand considering the position of HOH 235 and 263)
- Similarly for *E. coli* Gyrase B (PDB ID; 3G7E), three different GRID files were prepared;
- Without water molecules (without restrictions/ places the compounds considering the original ligand as centroid)
- With HOH 408 (with restrictions to make bond either with HOH 408 or define the position of ligand considering the position of HOH 408)

With HOH 408 and 443 (with restrictions to make bond either with HOH 408 and /or HOH 443 or define the position of ligand considering the position of HOH 408 and 443)

Docking and scoring

All docking experiments were performed by using Maestro's Glide-docking tool. The basic settings for HTVS, SP and XP algorithms were set as;

- Treating receptor as rigid and ligands as flexible,
- Dock without using core pattern comparison algorithm,
- Use constrains from GRID files if needed,
- Write 1 000 000 poses per docking run and perform top 5 poses a post-docking minimization.
- In trial sets for both bacterium DNA Gyrase ATPase active site, HTVS algorithms were performed by using each GRID file stated.

With the enriched test set of *S. aureus* Gyrase B active site (PDB ID; 3G7B), restricted GRID files with HOH 235 and 263 (with restrictions to make bond either with HOH 235 and /or HOH 263 or define the position of ligand considering the position of HOH 235 and 263) was used. 50000 prepared compounds were included with their isomers and tautomers during docking with HTVS and SP algorithms whereas a cut-off of 20000 were experimented and re scored in place by XP algorithms for computational and time concerns.

For *E. coli* Gyrase B (PDB ID; 3G7E) active site, the enriched test set was docked by using a GRID file without water molecules (without restrictions/placing the compounds consider original ligand as centroid) and GRID HOH 408 and 443 (with restrictions to make bond either with HOH 408 and /or HOH 443 or define the position of ligand considering the position of HOH 408 and 443) in

HTVS mode for detailed evaluation of trial set ROC curves. Additional dockings were accomplished with GRID HOH 408 and 443 (with restrictions to make bond either with HOH 408 and /or HOH 443 or define the position of ligand considering the position of HOH 408 and 443) in SP mode and with a cut-off of 20000 scored in place by XP modes for computational and time concerns.

All dockings were ranked according to their docking score and e-model score for further evaluation of ROC curves.

ROC curve evaluation

All ranked results of docking experiments for each bacterium were transferred to the MOE software (Chemical Computing Group Inc., Canada) as SDF files and compiled as databases. Later databases were ranked according to their docking and e-model scores as active 1 and non-predicted 0 and processed with "ROC Curves SVL" using appropriate thresholds.

After assessment of the curves and poses, 20 compounds, nine of which had the highest e-model score during waters 235 and 263 included XP docking to 3G7B and 11 compounds which had highest e-model score during water 408 included XP docking to 3G7E were selected for gel based inhibition assay against standard novobiocin.

Biological evaluation

All 20 compounds were tested with the "Gel Based inhibition Assay" at 1mg/20, 50, 100 μL. concentrations both in *S. aureus* (for 3G7B) and *E. coli* (for 3G7E) with novobiocin standard for comparison purposes.

DNA gyrase supercoiling assays were performed with a Gyrase Supercoiling Assay Kit (Inspiralis) according to the manufacturer's instructions and analysed by monitoring the conversion of relaxed pBR322 plasmid to its supercoiled form using DNA gel electrophoresis. Essentially, 1 U of either *E. coli* or *S. aureus* DNA gyrase was first diluted in 5×gyrase buffer and incubated in an assay buffer (35 mM Tris HCl (pH 7.5), 24 mM KCl, 4 mM MgCl 2, 2 mM DTT, 1.8 mM spermidine, 1 mM ATP, 6.5% (w/v) glycerol, and 0.1 mg/mL BSA), with 0.5 μg of pBR322 plasmid and purchase twenty compound dilutions at 37 °C for 30 min. Reactions were stopped with the addition of stop dye (40% sucrose, 100 mM Tris HCl (pH 7.5), 1 mM EDTA, and 0.5 mg/mL bromophenol blue) and loaded onto TAE agarose gel (1%). Gels were visualized using a gel documentation system (Bio-Rad ChemiDoc). Since high levels of DMSO are known to affect DNA gyrase activity, titration was used to determine the minimum amount of DMSO to be used in the assays, and 5% DMSO (with negligible or no effect on the gyrase) was chosen to dilute the compounds[19].

RESULTS AND DISCUSSION

The trial set (randomly selected 5000 compounds) and the test set (randomly selected 50000 compounds) both enriched with 36 active ligands, were docked to *S. aureus* Gyrase B (PDB ID: 3G7B) and *E. coli* Gyrase B (PDB ID: 3G7E) ATP binding sites by using Glide-docking HTVS, SP, XP protocols (as detailed in methodology section).

During docking processes the novobiocin structure was bound to its original position with an RMSD range of 0.83-0.94 A°. This revealed similar interactions with original crystallographic data in both cases.

A weakness of a docking program is its scoring functions. In this study we used maximum docking and e-model scores for ROC curves to evaluate accuracy powers in discriminating interaction patterns. ROC curves used in these experiments are plots of the true positive rate (sensitivity) against the false positive rate (1-specificity) for the different possible cut points. They show the trade-off between sensitivity and specificity where any increase in sensitivity will be accompanied by a decrease in specificity. The closer any curve follows the left-hand border and then the top border of the ROC space, the higher the accuracy. The accuracy of our tests depends on how the groups being tested are separated into those with and without experimental activity. Accuracy is measured by the area under the ROC curve. An area of 1 represents a perfect test; an area of 0.5 represents a poor test during evaluation.

Trial set docking, scoring and ROC curves evaluation

The ROC curves of HTVS dockings for the *S. aureus* Gyrase B (PDB ID: 3G7B) trial set without water molecules, with HOH 235, with HOH 235 and HOH 263 are shown in Figure 4.

The highest AUC score obtained from all dockings of the trial set using the HTVS protocol was the one scored/ranked according to an e-model score with bond restrictions, either with HOH 235 and/or HOH 263 or those, which defined ligand position considering the position of HOH 235 and 263. Results paralleled our expectations, as ligand 1b also used these water molecules in interacting with the active site. In general e-model score reflected solvation parameters more accurately compared to maximum docking score (Table 1). GRID files with bond restrictions either with HOH 235 and /or HOH 263 or those that defined the position of ligand considering the position of HOH 235 and 263 were selected and used for SP and XP dockings.

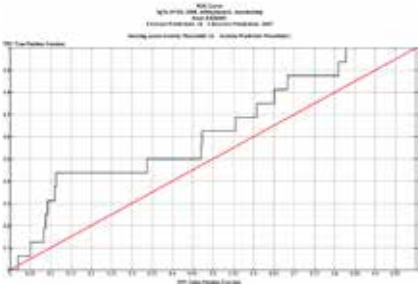

3G7B docked without waters, selected and ranked according to maximum docking score

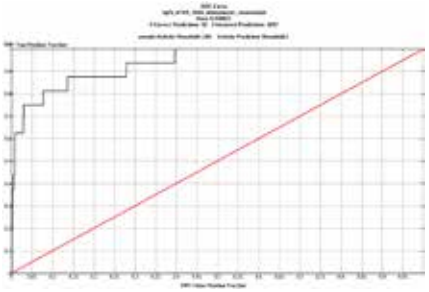

3G7B docked without waters, selected and ranked according to maximum e-model score

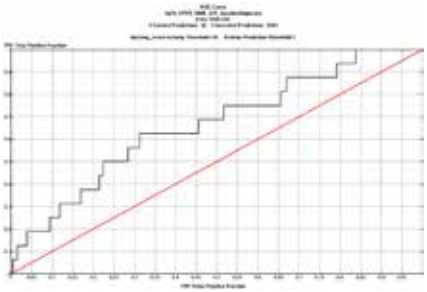

3G7B docked with water 235, selected and ranked according to maximum docking score

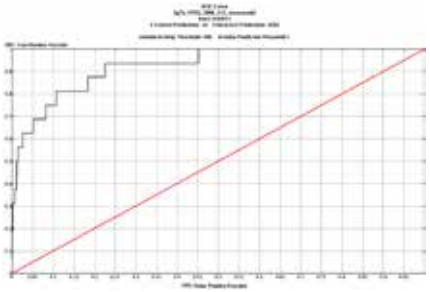

3G7B docked with water 235, selected and ranked according to maximum e-model score

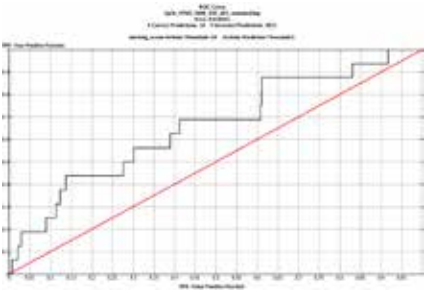

3G7B docked with waters 235 and 263, selected and ranked according to maximum docking score

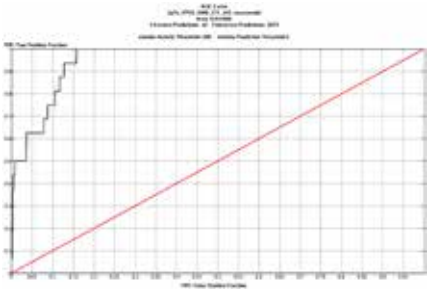

3G7B docked with waters 235 and 263, selected and ranked according to maximum e-model score

Figure 4: ROC curves of trial set docked to *S. aureus* Gyrase B (PDB ID: 3G7B) ATP binding site by using HTVS protocol with different GRID files

Table 1: AUC scores of *S. aureus* Gyrase B (PDB ID: 3G7B) trial Set with different GRID files and scoring functions

***S. aureus Gyrase* B (PDB ID: 3G7B) Trial Set**		
	Max. docking score	**Max. e-model score**
HTVS without water (without restrictions/ places the compounds considering the original ligand as centroid)	0.6268	0.9388
HTVS with water 235 (with restrictions to make bond either with HOH 235 or define the position of ligand considering the position of HOH 235)	0.6625	0.9265
HTVS with water 235 and 263 (with restrictions to make bond either with HOH 235 and /or HOH 263 or define the position of ligand considering the position of HOH 235 and 263)	0.658	0.952

The ROC curves for HTVS docking of the *E. coli* Gyrase B (PDB ID: 3G7E) trial set without water, with HOH 408, with HOH 408 and HOH 443 are combined in Figure 5.

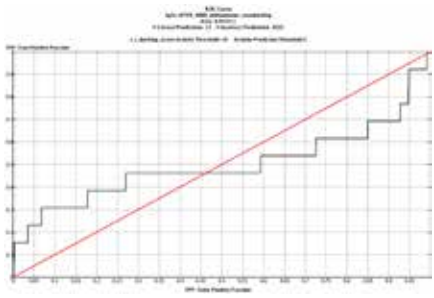

3G7E docked without waters, selected and ranked according to maximum docking score

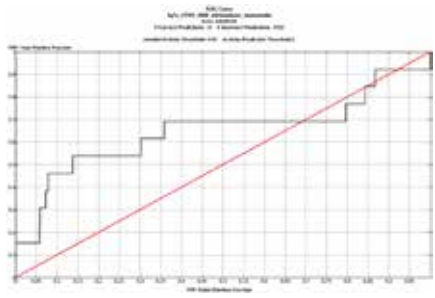

3G7E docked without waters, selected and ranked according to maximum e-model score

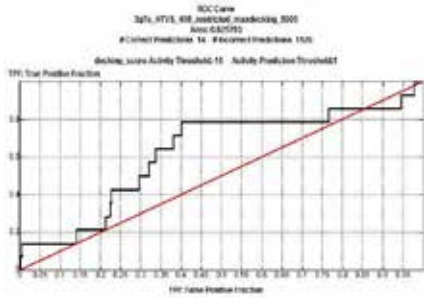

3G7E docked with water 408, selected and ranked according to maximum docking score

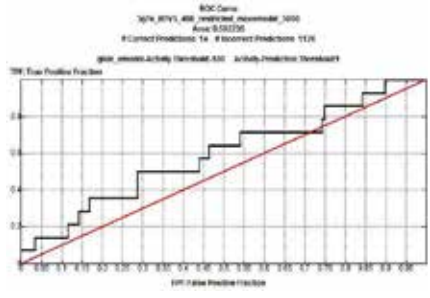

3G7E docked with water 408, selected and ranked according to maximum e-model score

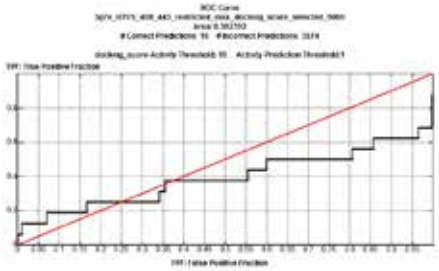

3G7E docked with waters 408 and 443, selected and ranked according to maximum docking score

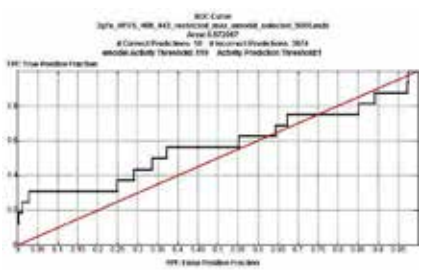

3G7E docked with waters 408 and 443, selected and ranked according to maximum e-model score

Figure 5: ROC curves of trial set docked to *E. coli* Gyrase B (PDB ID: 3G7E) ATP binding site by using HTVS protocol with different GRID files

Conflicting and poor AUC results led to repeat test set experiments. From the ligand 1a-binding site interactions it seemed that at least HOH 408 was used by ligand 1a for the H-bond bridging purposes with active site amino acids Ile 78, Gly 77, Thr 165 and Asp 73. Therefore, in further experiments, we used GRID files without water molecules (without restrictions/ places the compounds considering the original ligand as centroid) and with HOH 408 (with restrictions to make bond either with HOH 408 or define the position of ligand considering the position of HOH 408) to dock the test set of *E. coli* Gyrase B (PDB ID: 3G7E) ATP binding sites by using Glide-docking HTVS, SP, XP protocols. AUC scores of *E. coli* Gyrase B (PDB ID: 3G7E) trial set with different GRID files and scoring functions are detailed in Table 2.

Table 2: AUC scores of *E. coli* Gyrase B (PDB ID: 3G7E) trial set with different GRID files and scoring functions

***E. coli* Gyrase B (PDB ID: 3G7E) Trial Set**		
	Max. docking score	**Max. e-model score**
HTVS without water (without restrictions/ places the compounds considering the original ligand as centroid)	0.4974	0.6585
HTVS with water 408 (with restrictions to make bond either with HOH 408 or define the position of ligand considering the position of HOH 408)	0.6257	0.5922
HTVS with water 408 and 443 (with restrictions to make bond either with HOH 408 and /or HOH 443 or define the position of ligand considering the position of HOH 408 and 443)	0.3923	0.572

Test set docking, scoring and ROC curves evaluation

The test set evaluations for *S. aureus* Gyrase B (PDB ID: 3G7B), GRID file with water 235 and 263 (with restrictions to make bond either with HOH 235 and /or HOH 263 or define the position of ligand considering the position of HOH 235 and 263) was used. ROC curves were produced both with rankings according to HTVS, using maximum docking and e-model scores then SP and XP protocols were run only based on e-model scoring functions with a cut-off of maximum scoring 20000 compounds. (Figure 6).

An AUC value decrease was an expected outcome while changing sets from trial to test set as the number of compounds increased ten times. Also changing the docking algorithm from HTVS to more complex parametric SP and XP algorithms contribute to this outcome. However, results were still promising for selection of active ligands with e-model scoring functions (Table 3).

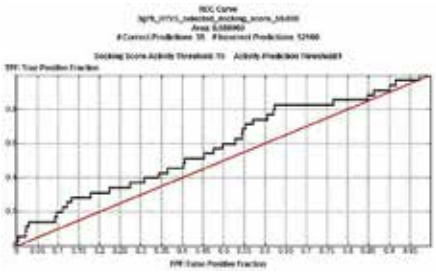

3G7B docked with waters 235 and 263 in HTVS algorithm, selected and ranked according to maximum docking score

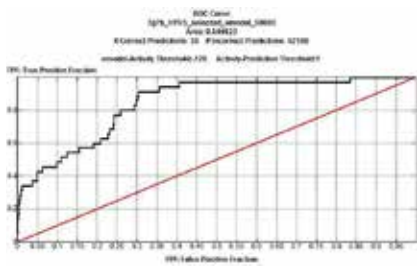

3G7B docked with waters 235 and 263 in HTVS algorithm, selected and ranked according to maximum e-model score

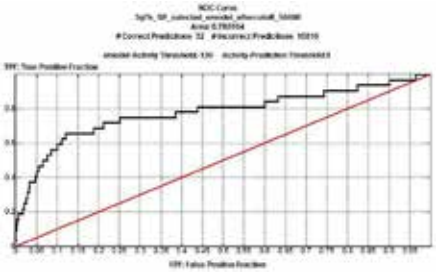

3G7B docked with waters 235 and 263 in SP algorithm after a cut off of 20000 compounds, selected and ranked according to maximum e-model score

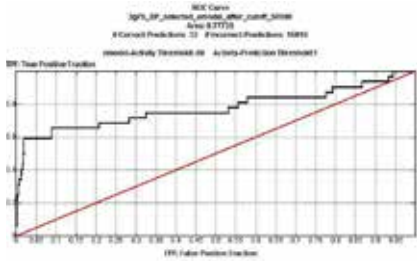

3G7B docked with waters 235 and 263 in XP algorithm after a cut off of 20000 compounds, selected and ranked according to maximum e-model score

Figure 6: ROC curves of test set docked to *S. aureus* Gyrase B (PDB ID: 3G7B) ATP binding site by using HTVS, SP and XP protocols with HOH 235 and 263 (with restrictions to make bond either with HOH 235 and /or HOH 263 or define the position of ligand considering the position of HOH 235 and 263) GRID file

Table 3: AUC scores of *S. aureus* Gyrase B (PDB ID: 3G7B) test set with different docking algorithms and scoring functions

***S. aureus* Gyrase B (PDB ID: 3G7B) Test Set with water 235 and 263**		
	Max. docking score	**Max. e-model score**
HTVS	0.588	0.8468
SP		0.7805
XP		**0.7773**

In trial and test set HTVS experiments of *S. aureus* (PDB ID: 3G7B), with HOH 235 and 263 there was a high AUC result of 0.952 and 0.8468, respectively in the e-model score ROC curve evaluation, which means that ligands that bind to these sites has to make an H-bond with HOH 235 and must bind a space that is restricted to these waters. All results for *S. aureus* (PDB ID: 3G7B) were very consistent with an average 30% difference between the docking score and e-model score, which means the ROC curves separate the true positives with very high frequency if the e-model scores were taken as a base. For further SP algorithm analysis the test set of 50000 compounds were assessed for at least 10 poses in the active site. An evaluation score by XP mode dockings with a cut-off of 20000 compounds was preferred to reduce computational load and time.

Given results with the trial set of *E. coli* Gyrase B (PDB ID: 3G7E) were contradictory, we ran HTVS of the test set with/without water (without restrictions/placing the compounds considered original ligand as centroid) and with HOH 408 (with restrictions to make bond either with HOH 408 or define the position of ligand considering the position of HOH 408) GRID files were again used to see if results were affected by the random selected compounds of the trial set. The results were then evaluated for both scoring algorithms for judgment and decision making with SP and XP algorithms. (Figure 7 and table 4).

3G7E docked without waters, using HTVS algorithm, selected and ranked according to maximum docking score

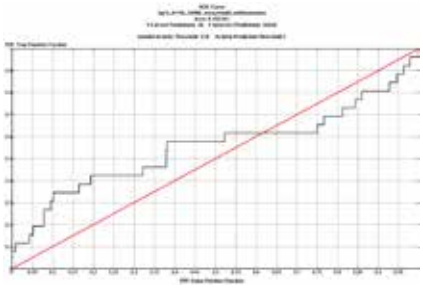

3G7E docked without waters, using HTVS algorithm, selected and ranked according to maximum e-model score

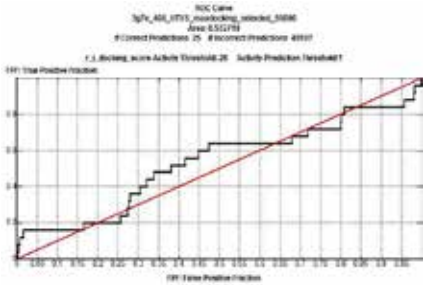

3G7E docked with water 408, using HTVS algorithm, selected and ranked according to maximum docking score

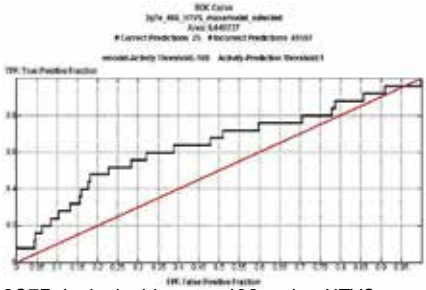

3G7E docked with water 408, using HTVS algorithm, selected and ranked according to maximum e-model score

Figure 7: ROC curves of test set docked to *E. coli* Gyrase B (PDB ID: 3G7E) ATP binding site by using HTVS protocol with without waters and with water 408 GRID files.

The results for HOH 408 GRID file scoring with the e-model were consistent with previous experiments and algorithm logic. This file was used for further SP and re-scoring XP docking experiments were performed under the same conditions previously described for time and computational concerns. (Figure 8)

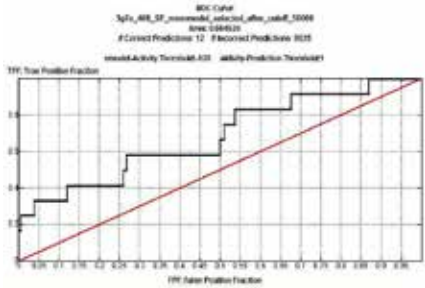

3G7E docked with water 408 in SP algorithm, selected and ranked according to maximum e-model score

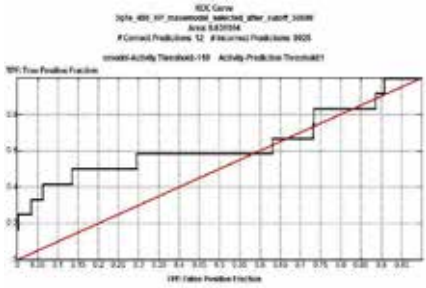

3G7E docked with water 408 in XP algorithm after a cut off of 20000 compounds, selected and ranked according to maximum e-model score

Figure 8: ROC curves of test set docked to *E. coli* Gyrase B (PDB ID: 3G7E) ATP binding site by using HTVS protocol with without waters and with water 408 GRID files

In all HTVS experiments that were run according to these GRID files, the e-model score process separated true from false positives more successfully than when compared to docking scores, except for *E. coli*'s with the HOH 408 GRID file where the docking score had an AUC of 0.6257.

E. coli's unrestricted file scored better with HOH 408 and with HOH 408 and 443 files in general. This is of interest as e-model score algorithms are designed in such a manner for reflecting solvation parameters perfectly to docking score by calculating the positions of the incidental waters.

Random compound selection in the trial set may have been the reason for this unpredicted result. We therefore repeated HTVS dockings of the test set with higher scoring, unrestricted and with HOH 408 GRID files. A number increase from 5000 to 50000 resulted in inconsistency disappearance and the e-model score of HOH 408 GRID file AUC was 0.6407. Further SP and XP simulations for *E. coli* by using this file were warranted.

During these processes, although ROC AUCs decreased from HTVS to XP algorithms gradually, a combination of the top 20 scoring compounds in the context of each set were selected for in-vitro *E. coli* and *S. aureus* DNA Gyrase gel based supercoiling assay against, novobiocin standard.

Table 4: AUC scores of *E. coli* Gyrase B (PDB ID: 3G7E) test set with different GRID files and scoring functions

***E. coli* Gyrase B (PDB ID: 3G7E) test set**		
	Max. docking score	**Max. e-model score**
HTVS without water (without restrictions/places the compounds considering the original ligand as centroid)	0.4489	0.5523
HTVS with water 408 (with restrictions to make bond either with HOH 408 or define the position of ligand considering the position of HOH 408)	0.5327	0.6407
SP with water 408 with restrictions to make bond either with HOH 408 or define the position of ligand considering the position of HOH 408)		0.6846
XP with water 408 with restrictions to make bond either with HOH 408 or define the position of ligand considering the position of HOH 408)		**0.6319**

High scoring compounds of *S. aureus* and *E. coli* test sets selected with XP algorithms with HOH 235 and 263 and with HOH 408 GRID files for further supercoiling assays are listed in descending order in Tables 5 and 6.

Biological activity

After screening, 11 compounds from the *E. coli* test set, and nine compounds from the *S. aureus* were tested against standard novobiocin using *E. coli* and *S. aureus* Gyrase Supercoiling Assay Kits (Inspiralis). All compounds were applied in a range of 1 mg/20µL, 1 mg/50µL and1 mg/100µL (w/v) dilutions to gel electrophoresis according to instructions of manufacturer. Post run staining was completed using ethidium bromide solution. All results are combined in Figures

9 -14. The first nine compounds (*S. aureus* 1-9 test set) followed by the next 11 (*E. coli* 1-11). All numbering and structures are matched with Tables 5 and 6 and are aligned with descending order maximum e-model scores.

Table 5: Compounds which received highest e-model score during waters 235 and 263 included XP docking to 3G7B and selected for "Gel Based Supercoiling Assay"

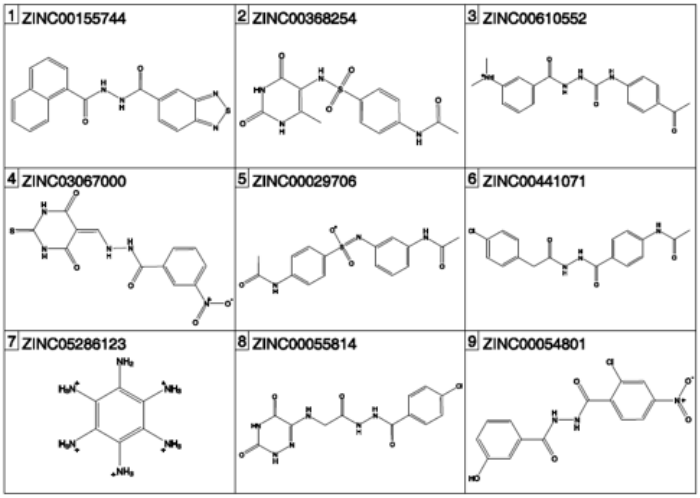

Table 6: Compounds which received highest e-model score during water 408 included XP docking to 3G7E and selected for "Gel Based Supercoiling Assay"

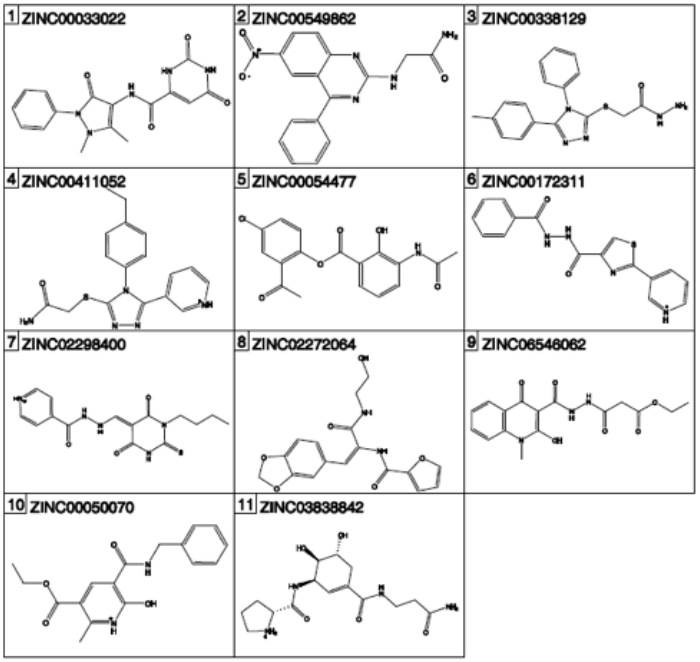

Figure 9: 1 mg/20µL (w/v) dilusion *E. coli* DNA Gyrase gel electrophoresis results, super-coiled (r. plasmid+gyrase), relaxed (r. plasmid), novobiocin (r. plasmid+gyrase+novobiocin)

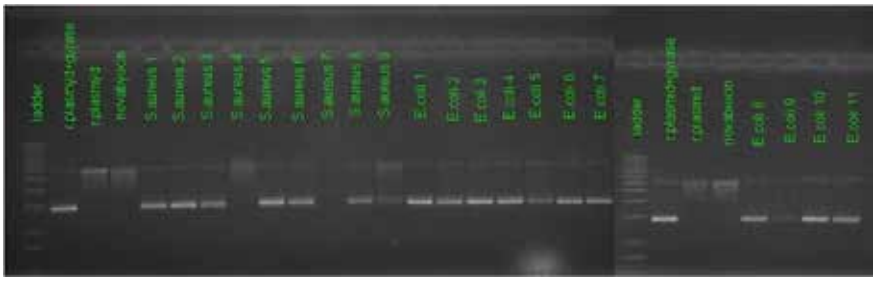

Figure 10: 1 mg/50µL (w/v) dilusion *E. coli* DNA Gyrase gel electrophoresis results, super-coiled (r. plasmid+gyrase), relaxed (r. plasmid), novobiocin (r. plasmid+gyrase+novobiocin)

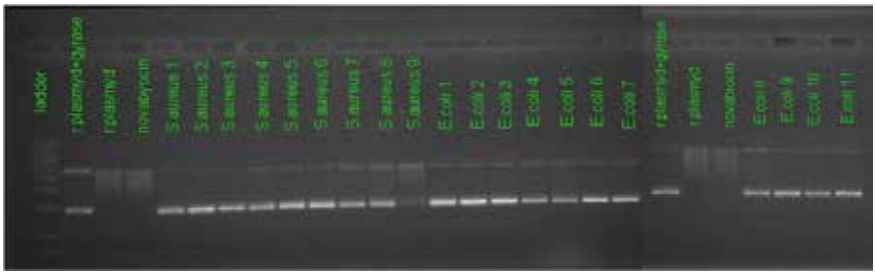

Figure 11: 1 mg/100µL (w/v) dilusion *E. coli* DNA Gyrase gel electrophoresis results, super-coiled (r. plasmid+gyrase), relaxed (r. plasmid), novobiocin (r. plasmid+gyrase+novobiocin)

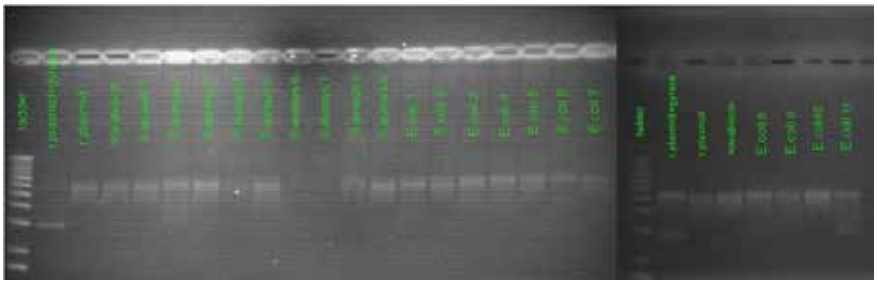

Figure 12: 1 mg/20µL (w/v) dilusion *S. aureus* DNA Gyrase gel electrophoresis results, super-coiled (r. plasmid+gyrase), relaxed (r. plasmid), novobiocin (r. plasmid+gyrase+novobiocin)

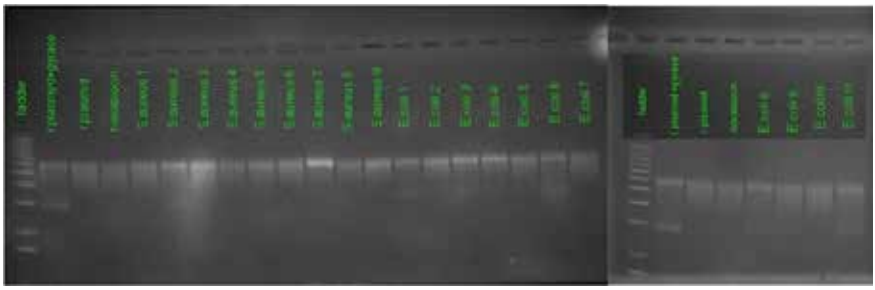

Figure 13: 1 mg/50µL (w/v) dilusion *S. aureus* DNA Gyrase gel electrophoresis results, super-coiled (r. plasmid+gyrase), relaxed (r. plasmid), novobiocin (r. plasmid+gyrase+novobiocin)

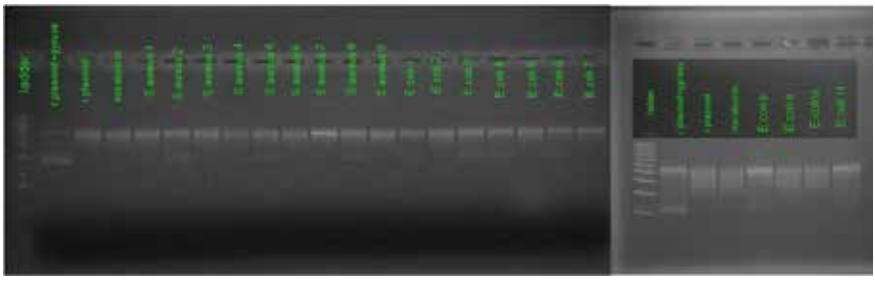

Figure 14: 1 mg/100µL (w/v) dilusion *S. aureus* DNA Gyrase gel electrophoresis results, super-coiled (r. plasmid+gyrase), relaxed (r. plasmid), novobiocin (r. plasmid+gyrase+novobiocin)

Eleven compounds from the test set of *E. coli*, except compound 7 at a 1/20 mg/µL. dilution, showed no activity over *E. coli* DNA gyrase supercoiling whereas compounds 2, 5, 7 and 10 showed promising inhibitory activity in a *S. aureus* DNA gyrase supercoiling assay.

In contrast, except for compound 2 and 3 of *S. aureus* of the test set all compounds in all concentrations showed remarkable activity in *S. aureus* DNA gyrase supercoiling assay. Compound 4 and 7 showed a moderate activity in *E. coli* DNA gyrase supercoiling.

Table 7 shows detailed activities for compounds in *E. coli* and *S. aureus* DNA Gyrase supercoiling assays.

Aside from the highest scoring compounds; 1 and 5 from the *S. aureus* test set, *E. coli* test set compounds 2, 5, and 10 selectively inhibited *S. aureus* DNA Gyrase supercoiling without effecting *E. coli*.

In vitro results are of interest because they show that the ROC curve evaluation was efficient and consistent for either separating actives from inactivity or determining the type of interaction. In addition, the evaluation results of at least 90%

Table 7: Zinc codes and activities of selected compounds during *E. coli* and *S. aureus* DNA Gyrase supercoiling assays in different concentrations

		E. coli Supercoiling Assay			*S. aureus Supercoiling Assay*		
Compound No	**Zinc Code**	**1/20**	**1/50**	**1/100**	**1/20**	**1/50**	**1/100**
***S. aureus* 1**	**ZINC00155744**	-	-	-	+	+	+
2	**ZINC00368254**	-	-	-	-	-	-
3	**ZINC00610552**	-	-	-	-	-	-
4	**ZINC03067000**	+	+	-	+	+	+
5	**ZINC00029706**	-	-	-	+	+	-
6	**ZINC00441071**	+	-	-	+	+	+
7	**ZINC05286123**	+	+	-	+	+	+
8	**ZINC00055814**	+	-	-	+	+	-
9	**ZINC00054801**	+	-	-	+	+	+
***E. coli* 1**	**ZINC00033022**	-	-	-	-	-	-
2	**ZINC00549862**	-	-	-	+	+	+
3	**ZINC00338129**	-	-	-	-	-	-
4	**ZINC00411052**	-	-	-	-	-	-
5	**ZINC00054477**	-	-	-	+	+	+
6	**ZINC00172311**	-	-	-	+	-	-
7	**ZINC02298400**	+	-	-	+	+	+
8	**ZINC02272064**	-	-	-	-	-	-
9	**ZINC06546062**	-	-	-	+	-	-
10	**ZINC00050070**	-	-	-	+	+	+
11	**ZINC03838842**	-	-	-	-	-	-

or more were processed for further testing.

Water molecules not only have an important impact on positioning but contribute to ligand selectivity by inhibiting the DNA Gyrase ATPase binding site.

CONCLUSION

Multiple drug resistance is an important and major issue in immune deficiency cases. Normally simple and common human flora bacterium, such as *E. coli and S. aureus,* can cause serious complications during treatment. In this study, with the help of X-ray crystallographic structures of *E. coli and S. aureus* DNA gyrase B, we attempted to combine the use of ROC curves with docking-scoring algorithms to verify the role of water molecules over ligand-active site interactions for identifying selective target structures.

Our study results show that water molecules HOH 235 and 263 in the *S. aureus* DNA gyrase B active site play a crucial role during ligand active site interactions. This must be taken into consideration in molecular modeling studies of *S. aureus* DNA gyrase B because 8/9 ligands showed activity during the gel based inhibition assay and ROC curve AUC scores were high.

ROC curves successfully determined true positives from false positives during docking-scoring studies, if AUC scores were greater than 0.70.

In gel-based gyrase assays and docking studies, the maximum e-model scores of the N'-(1-naphthylcarbonyl)-2, 1, 3-benzothiadiazole-5-carbohydrazide structure was validated as having selective activity at all concentrations tested.

Further study of these selective ligands and additional extensive review of binding modes with other water molecules warrants future study. Studies to synthesize more effective derivatives using other facilitating computational tools such as molecular interaction are warranted.

REFERENCES

1. Ryan KJ, Ray CG, Sherris JC. Sherris Medical Microbiology. 5th ed. New York: McGraw Hill Medical; **2010** xiv, pp. 1026.

2. Kayser FH. Medical Microbiology. Stuttgart ; New York, NY: Georg Thieme Verlag; **2005** xxvi, pp.698.

3. Tomioka, H.; Namba, K. Rifampin and Their Analogs: A Development of Antitubercular Drugs. *Kekkaku* **2006**, *81*, 753-774.

4. Lewis, R.J.; Tsai, F.T.; Wigley D.B. Molecular Mechanisms of Drug Inhibition of DNA Gyrase. *Bioessays* **1996**, *18*, 661-671.

5. Ronkin, S.M.; Badia, M.; Bellon, S.; Grillot, A.L.; Gross, C.H.; Grossman, T.H. et al. Discovery of Pyrazolthiazoles As Novel And Potent Inhibitors of Bacterial Gyrase. *Bioorg. Med. Chem. Lett.* **2010**, *20*, 2828-2831.

6. Berman, H.M.; Westbrook, J.; Feng, Z.; Gilliland, G.; Bhat, T.N.; Weissig, H. et al. The Protein Data Bank. *Nucleic Acids Res.* **2000**, *28*, 235-242.

7. Altschul, S.F.; Wootton, J.C.; Gertz, E.M.; Agarwala, R.; Morgulis, A.; Schaffer, A.A. et al. Protein Database Searches Using Compositionally Adjusted Substitution Matrices. *FEBS J.* **2005**, *272*, 5101-5109.

8. Lengauer, T.; Rarey, M. Computational Methods For Biomolecular Docking. *Curr. Opin. Struct. Biol.* **1996**, *6*, 402-406.

9. Alvarez J, Shoichet B. Virtual screening in drug discovery. Boca Raton: Taylor & Francis; **2005**, pp. 470.

10. Rester, U. From Virtuality to Reality - Virtual Screening in Lead Discovery and Lead Optimization: A Medicinal Chemistry Perspective. *Curr. Opin. Drug Discov. Devel.* **2008**, *11*, 559-568.

11. McInnes, C. Virtual Screening Strategies in Drug Discovery. *Curr. Opin. Chem. Biol.* **2007**, *11*, 494-502.

12. Willett, P. From Chemical Documentation to Chemoinformatics: 50 Years of Chemical Information Science. *J. Inf. Sci.* **2008**, *34*, 477-499.

13. Kromer, R.T. Structure-Based Drug Design: Docking and Scoring. *Curr. Protein Pept. Sci.* **2007**, *8*, 312-328.

14. Cavasotto, C.N.; Orry, A.J. Ligand Docking and Structure-based Virtual Screening in Drug Discovery *Curr. Top. Med. Chem.* **2007**, *7*, 1006-1014.

15. Triballeau, N.; Acher, F.; Brabet, I.; Pin, J.P.; Bertrand, H.O. Virtual Screening Workflow Development Guided by the "Receiver Operating Characteristic" Curve Approach. Application to High-Throughput Docking on Metabotropic Glutamate Receptor Subtype 4. *J. Med. Chem.* **2005**, *48*, 2534-2547.

16. Rizzi, A.; Fioni, A. Virtual Screening Using PLS Discriminant Analysis and ROC Curve Approach: An Application Study on PDE4 Inhibitors. *J. Chem. Inf. Model.* **2008**, *48*, 1686-1692.

17. Langer, T.; Hoffmann, R.; Bryant, S.; Lesur, B. Hit Finding: Towards 'Smarter' Approaches. *Curr. Opin. Pharmacol.* **2009**, *9*, 589-593.

18. Jacoby, E.; Schuffenhauer, A.; Popov, M.; Azzaoui, K.; Havill, B.; Schopfer, U. et al. Key Aspects of The Novartis Compound Collection Enhancement Project for The Compilation of A Comprehensive Chemogenomics Drug Discovery Screening Collection. *Curr. Top. Med. Chem.* **2005**, *5*, 397-411.

19. Maxwell, A.; Burton, N.P.; O'Hagan, N. High-Throughput Assays for DNA Gyrase and Other Topoisomerases. *Nucleic Acids Res.* **2006**, *34*, e104.

(Received 14 September 2016; accepted 06 December 2016)